Characterizing the Role of Polyacrylamide Additives in Copper Electrowinning

by

Christiaan Coetzee

Thesis presented in partial fulfilment
of the requirements for the Degree

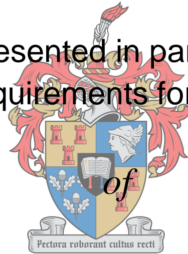

of

MASTER OF ENGINEERING
(EXTRACTIVE METALLURGICAL ENGINEERING)

UNIVERSITEIT
iYUNIVESITHI
STELLENBOSCH
UNIVERSITY
100
1918 · 2018

in the Faculty of Engineering
at Stellenbosch University

Supervisor
Dr. Margreth Tadie

Co-Supervisor
Prof. Christie Dorfling

December 2018

Stellenbosch University https://scholar.sun.ac.za

DECLARATION

By submitting this thesis electronically, I declare that the entirety of the work contained therein is my own, original work, that I am the sole author thereof (save to the extent explicitly otherwise stated), that reproduction and publication thereof by Stellenbosch University will not infringe any third-party rights and that I have not previously in its entirety or in part submitted it for obtaining any qualification.

Date: December 2018

Copyright © 2018 Stellenbosch University
All rights reserved

Stellenbosch University https://scholar.sun.ac.za

PLAGIARISM DECLARATION

1. Plagiarism is the use of ideas, material and other intellectual property of another's work and to present is as my own.
2. I agree that plagiarism is a punishable offence because it constitutes theft.
3. I also understand that direct translations are plagiarism.
4. Accordingly, all quotations and contributions from any source whatsoever (including the internet) have been cited fully. I understand that the reproduction of text without quotation marks (even when the source is cited) is plagiarism.
5. I declare that the work contained in this assignment, except where otherwise stated, is my original work and that I have not previously (in its entirety or in part) submitted it for grading in this module/assignment or another module/assignment.

Student number: 16976770

Initials and surname: C. Coetzee

Signature: ……………………………………..

Date: 08 November 2018……………………………………..

Stellenbosch University https://scholar.sun.ac.za

ACKNOWLEDGEMENTS

I wish to express my appreciation to the following people:

- My supervisors, Dr. Margreth Tadie and Prof. Christie Dorfling for their guidance and support throughout the project, and for their willingness to listen to ideas and theories.
- South African Minerals to Metals Research Institute (SAMMRI), for funding this project as well as providing technical advice.
- SENMIN for providing the organic additives (Guar and Polyacrylamides) for the experimental work of this study.
- The staff at the Department of Process Engineering of Stellenbosch University for providing administrative and technical support.
- My parents Mr Louis Coetzee and Mrs Debbie Coetzee for their emotional support. Especially to my mother for listening to countless presentation rehearsals and encouraging me when I doubted myself.
- A special thanks to my wife Leani Coetzee who has believed in me from the beginning, and for her continuous love and support through the ups and downs.

Stellenbosch University https://scholar.sun.ac.za

ABSTRACT

Additives have been used for many years in the copper electrowinning process to improve cathode morphology. The industry has leaned towards polysaccharides in the form of Guar. Polyacrylamides however have been considered as possible alternatives. To get more value from the functionality of these additives it is necessary to understand the influence of structural chemistry on the resulting performance during electrowinning.

This project investigated structurally different polyacrylamides (PAMs) and compared them to Guar and characterized their effect on copper electrodeposition. Cyclic voltammetry (CV) and electrochemical impedance spectroscopy (EIS) techniques were used to characterize the effect of molecular weight (MW) and ionic charge of polyacrylamides on electrodeposition. The findings were compared against results from a Guar product, utilized in the industry. During EIS and CV experiments copper was electrodeposited onto a platinum surface from a synthetic electrolyte containing 35 g/L copper (Cu^{2+}), 160 g/L sulfuric acid (H_2SO_4), and 25 mg/L chloride (Cl^-) at 45°C. The EIS and CV experimental work were conducted at additive concentrations of 2 mg/L and 10 mg/L.

EIS equivalent circuit modelling results indicate that an increase in polyacrylamide concentration and a decrease in additive molecular weight cause an increase in the overall system resistance. The charge transfer resistance (R_{CT}) values at 2 mg/L additive concentration gradually increased from 3.36 Ω to approximately 7 Ω as the PAM additive MW decreased from very high to low. CV results of additives at 2 mg/L show that there was no significant effect on nucleation overpotential. However, significant plating polarization was observed for lower molecular weight additives, decreasing in significance as the molecular weight of the additive increased. The measured average current density at 0.22 V vs. SHE on the return sweep during CV experimental work systematically increased from 277.35 A/m^2 for the Low MW PAM additive to 326.39 A/m^2 for the Very High MW additive. At the same experimental conditions, an average current density of 337.00 A/m^2 was measured in the absence of any additives. CV results at 10 mg/L additive show that there was significant nucleation polarization and plating polarization, correlating well with the EIS results. The industry standard organic additive Guar had no significant impact on the charge transfer resistance or the polarization behaviour at both 2 mg/L and 10 mg/L concentration. No correlation between the ionic content of the additives and system polarization were observed.

Scanning electron microscopy (SEM) micrographs of copper deposits after 10 s and 30 s of electroplating on stainless-steel cathode tips at 2 mg/L additive concentration provided strong qualitative validation for the polarization trends observed on a fundamental level. The effect of polarization or increased charge transfer resistance was identified in the structure of the deposits. A spiky, dendrite like crystal structure was observed due to fast unrestricted deposition when no additives were added to the system, while smoother spherical 3-D crystal structures were obtained when using Guar. The polyacrylamide additives systematically produced a flatter 2-D compact crystal growth structure with a decrease in additive molecular weight.

Electrowinning experiments on stainless steel plates in a laboratory (capacity) scale setup at 300 A/m^2 and 40 °C for 24 hours of electrodeposition were conducted to determine if microscale deposit structures will be sustained after multi-layers of deposition have occurred. Bench scale electrowinning results showed that PAM additives acted to radically reduce localized growth compared to copper cathode plates produced in the absence of any additive and in the presence of Guar. The copper plate in the absence of any additives developed abundant localized growth and dendrite structures. The mean surface deviation

Stellenbosch University https://scholar.sun.ac.za

(S_a) value, which is a measure of surface roughness, was calculated for all copper plates that was produced in the presence of each organic additive. The calculated S_a value for the copper plate in the absence of any additive and in the presence of Guar was 82.22 µm and 32.87 µm respectively. The Low MW PAM additive produced the smoothest, brightest copper deposit of all the deposits and had the lowest calculated S_a value of 18.18 µm. The Very High MW PAM additive was the only additive to show inconsistency between the polarization behaviour trends, and the predicted deposit structure obtained in the bench scale experimental work. Current efficiency (CE) values between each electrowinning experiment varied with less than 1%. Such insignificant variation indicates that the organic additives had minor impact on the CE of the electrowinning experiments. It was concluded that both qualitative and quantitative analyses are necessary to evaluate the performance of organic additives in copper electrowinning and that they should be used in conjunction with one another.

In future work, it is recommended that a molecular weight range should be proposed for optimal additive performance by determining the numerical molecular weights of the additives. Varying the most significant operating conditions like current density, temperature, and impurity type and concentration in the presence of the selected organic additives will provide insight into ideal operational ranges in the presence of these organic additives. SEM micrographs of cross sections of the resulting cathode plates in bench scale electrowinning work will aid in further characterization of the crystal structure that developed in the presence of each organic additive respectively.

Stellenbosch University https://scholar.sun.ac.za

OPSOMMING

Bymiddels word al vir baie jare in die koper elektroherwinning proses gebruik om katode morfologie te verbeter. Die industrie het na polisakkariedes in die vorm van guar geneig. Poliakrielamiede word egter as moontlike alternatiewe oorweeg. Om meer waarde uit die funksionaliteit van hierdie bymiddels te kry, is dit noodsaaklik om die invloed van die strukturele chemie op die resulterende werksverrigting tydens elektroherwinning te verstaan.

Hierdie projek het struktureel verskillende poliakrielamiede ondersoek en dit vergelyk met guar en hul effek op koper elektroneerslag gekarakteriseer. Sikliese voltammetrie (SV) en elektrochemiese impedansie spektroskopie (EIS) tegnieke is gebruik om die effek van molekulêre gewig en ioniese lading van poliakrielamiede op elektroneerslag te karakteriseer. Die bevindinge is vergelyk met die resultate van ’n guarproduk wat in die industrie gebruik word. Tydens EIS en SV eksperimente is koper neergeslaan op ’n platinum oppervlak vanuit ’n sintetiese elektroliet by 45 °C wat 35 g/L koper (Cu^{2+}), 160 g/L swaelsuur (H_2SO_4), en 20 mg/L chloried (Cl^-) bevat het. Die EIS en SV eksperimentele werk is uitgevoer by bymiddelkonsentrasies van 2 mg/L en 10 mg/L.

EIS ekwivalent stroombaan modellering resultate dui aan dat ’n verhoging in poliakrielamied-konsentrasie en ’n afname in bymiddel molekulêre gewig ’n verhoging in die algehele stelsel weerstand veroorsaak. Die ladingoordrag-weerstand (R_{CT}) waardes by 2 mg/L bymiddelkonsentrasie het geleidelik van 3.36 Ω na ongeveer 7 Ω verhoog soos wat die poliakrielamied bymiddel molekulêre gewig verlaag het van baie hoog na laag. SV resultate van bymiddels by 2 mg/L het gewys dat daar geen beduidende effek op kernvorming oorspanning is nie. Beduidende platering polarisering is egter waargeneem vir laer molekulêre gewig bymiddels, wat verminder in beduidendheid soos die molekulêre gewig van die bymiddel afgeneem het. Die gemete gemiddelde stroomdigtheid by 0.22 V (teen standaard waterstof elektrode) op die terug veeg gedurende SV eksperimentele werk het sistematies verhoog van 277.35 A/m^2 vir die lae molekulêre gewig poliakrielamied bymiddel na 326.39 A/m^2 vir die baie hoë molekulêre gewig bymiddel. By dieselfde eksperimentele kondisies is ’n gemiddelde stroomdigtheid van 337.00 A/m^2 gemeet in die afwesigheid van enige bymiddels. SV resultate by 10 mg/L bymiddel wys dat daar ’n beduidende kernvorming polarisering en platering polarisering was, wat goed korreleer met die EIS resultate. Die industrie standaard organiese bymiddel, guar, het geen beduidende impak op die ladingoordrag-weerstand of die polarisering gedrag by beide 2 mg/L en 10 mg/L konsentrasies gehad nie. Geen korrelasie tussen die ioniese inhoud van die bymiddel en stelsel polarisering is waargeneem nie.

Skandeerelektronmikroskopie (SEM) mikrograwe van koperneerslae na 10 s en 30 s van elektroplatering op vlekvrye staal katodepunte by 2 mg/L bymiddelkonsentrasie het die polarisering tendens wat op ’n fundamentele vlak waargeneem is kwalitatief gestaaf. Die effek van polarisering of verhoogde ladingoordrag-weerstand is geïdentifiseer in die struktuur van die neerslag. ’n Spitsige, dendrietagtige kristalstruktuur is waargeneem as gevolg van die vinnige onbeperkte neerslag toe geen bymiddels tot die stelsel bygevoeg is nie, terwyl gladder sferiese 3-D kristalstrukture verkry is toe guar gebruik is. Die poliakrielamied bymiddels het sistematies ’n platter 2-D kompakte kristal-groeistruktuur geproduseer met ’n afname in bymiddel molekulêre gewig.

Elektroherwinning eksperimente op vlekvrye staalplate in ’n laboratorium (kapasiteit) skaal opset, by 300 A/m^2 en 40 °C vir 24 uur van elektroneerslag, is gedoen om te bepaal of mikroskaal neerslagstrukture gehandhaaf sal word na veelvuldige lae van neerslag plaasgevind het. Banktoetsskaal elektroherwinning resultate het gewys dat poliakrielamied bymiddels gelokaliseerde groei radikaal verlaag het in vergelyking

Stellenbosch University https://scholar.sun.ac.za

met koper katode plate geproduseer in die afwesigheid van enige bymiddel en in die teenwoordigheid van guar. Die koperplate in die afwesigheid van enige bymiddels het oorvloedige gelokaliseerde groei- en dendrietstrukture ontwikkel. Die gemiddelde oppervlak afwyking (S_a) waarde, wat ’n mate van oppervlak grofheid is, is bereken vir alle koperplate wat geproduseer is in die teenwoordigheid van elke organiese bymiddel. Die berekende S_a-waarde vir die koperplaat in die afwesigheid van enige bymiddel en in die teenwoordigheid van guar is 82.22 µm en 32.87 µm onderskeidelik. Die lae molekulêre gewig poliakrielamied bymiddel het die gladste, helderste koperneerslag van al die neerslae geproduseer en het die laagste berekende S_a-waarde van 18.18 µm. Die baie hoë molekulêre gewig poliakrielamied bymiddel was die enigste bymiddel om inkonsekwentheid te wys tussen polariseringgedrag tendense en die voorspelde neerslagstruktuur verkry in die banktoetsskaal eksperimentele werk. Stroomrendement (SR) waardes tussen elke elektroherwinning eksperiment het gevarieer met minder as 1%. Sulke onbeduidende variasies toon aan dat die organiese bymiddels ’n geringe impak op die SR van die elektroherwinning eksperimente gehad het. Die gevolgtrekking was dat beide kwalitatiewe en kwantitatiewe analises nodig is om die werkverrigting van organiese bymiddels in koper elektroherwinning te evalueer, en dat hulle in medewerking met mekaar gebruik moet word.

In toekomstige werk word dit voorgestel dat ’n molekulêre gewig bestek voorgestel moet word vir optimale bymiddel werkverrigting deur die numeriese molekulêre gewigte van die bymiddels vas te stel. Om die mees beduidende operasionele kondisies te wissel, soos stroomdigtheid, temperatuur, onsuiwerheid tipe, en konsentrasie in die teenwoordigheid van die gekose organiese bymiddels, sal insig verskaf in die ideale operasionele bestek in die teenwoordigheid van hierdie organiese bymiddels. SEM mikrograwe van deursnitte van die resulterende katode plate in banktoetsskaal elektroherwinning werk sal verdere hulp verleen in die karakterisering van die kristalstruktuur wat ontwikkel in die teenwoordigheid van elke organiese bymiddel, onderskeidelik.

Stellenbosch University https://scholar.sun.ac.za

TABLE OF CONTENTS

Declaration .... **i**
Plagiarism declaration .... **ii**
Acknowledgements .... **iii**
Abstract .... **iv**
Opsomming .... **vi**
Table of Contents .... **viii**
List of Figures .... **xi**
List of Tables .... **xiv**
Nomenclature .... **xv**
1 Introduction **1**
1.1 PROBLEM STATEMENT 1
1.2 RESEARCH AIM AND OBJECTIVES 1
1.3 KEY QUESTIONS 2
1.4 RESEARCH APPROACH AND PROJECT SCOPE 2
1.5 THESIS STRUCTURE 3
2 Literature Review **4**
2.1 BACKGROUND AND PROCESS OVERVIEW 4
2.2 ELECTRODEPOSITION PROCESS FUNDAMENTALS 6
2.3 TRANSPORT THEORY IN ELECTROLYTIC PROCESSES 7
2.3.1 Mass Transfer 7
2.3.2 Nucleation and growth in electrocrystallization 8
2.4 ELECTROCHEMICAL CELL THERMODYNAMICS 10
2.4.1 Basic concepts 10
2.4.2 Interfacial potential differences 11
2.4.3 Electrode potential 12
2.4.4 Polarization and reaction kinetics 12
2.4.5 Diffusion limited current 14
2.5 COPPER ELECTROWINNING WITH ORGANIC ADDITIVES 15
2.5.1 Organic additive hydrolysis and adsorption characteristics 16
2.5.2 Polyacrylamides in electrowinning 18
2.5.3 Classification 19
2.5.4 Effect of organic additives on copper nucleation and growth 20
2.6 ELECTROCHEMICAL TECHNIQUES 23

Stellenbosch University https://scholar.sun.ac.za

2.6.1 Voltammetry....23
2.6.2 Electrochemical Impedance Spectroscopy (EIS)....24
2.6.3 Chronopotentiometry....26
2.7 Effects of operating parameters in copper electrowinning....26
2.7.1 Temperature....26
2.7.2 Concentration of copper ions....27
2.7.3 Concentration of electrolyte....27
2.7.4 pH....27
2.7.5 Cathode and anode material....27
2.7.6 Flowrate of electrolyte....28
2.7.7 Current density....28
2.7.8 Chloride Ions....29
2.7.9 Organic additives....29
2.8 Summary....30
3 Experimental....31
3.1 Electrochemical experiments....33
3.1.1 Materials....33
3.1.2 Equipment....34
3.1.3 Methods....35
3.2 Electrowinning experiments....36
3.2.1 RDE Electrowinning....36
3.2.2 Bench Scale Electrowinning....37
3.3 Experimental conditions....41
4 CV and EIS Results and discussion....43
4.1 Electrochemical Impedance Spectroscopy....43
4.1.1 EIS results....43
4.1.2 Equivalent circuit modeling results....44
4.1.3 EIS result discussion....46
4.2 Cyclic Voltammetry....48
4.2.1 Result interpretation of Base Case scenario....48
4.2.2 CV results....49
4.2.3 CV results discussion....57
5 Electrowinning studies....60
5.1 Fundamental electrowinning studies....60
5.1.1 Base Case....60
5.1.2 Guar....62

Stellenbosch University https://scholar.sun.ac.za

5.1.3 Low MW PAM ... 63
5.1.4 Medium MW PAM ... 64
5.1.5 High MW PAM ... 65
5.1.6 Very High MW PAM ... 66
5.2 RDE results conclusions presented on Winand's Diagram ... 67
5.3 Bench scale electrowinning results ... 71
5.3.1 Qualitative analysis ... 71
5.3.2 Quantitative analysis ... 76
6 Conclusions & Recommendations ... 81
6.1 Conclusions ... 81
6.2 Recommendations ... 82
7 References ... 84
8 Appendices ... 87
8.1 Appendix A – Derivations and supporting equations ... 87
8.1.1 Mass transfer ... 87
8.1.2 Nucleation and growth in electrocrystallization ... 87
8.1.3 Electrode potential ... 87
8.2 Appendix B – Stepwise methodology ... 88
8.3 Appendix C – Sample calculations ... 90
8.3.1 Concentration calculations ... 90
8.3.2 Current efficiency calculations ... 92
8.4 Appendix D -Bench scale electrowinning supportive results ... 94
8.4.1 Qualitative ... 94
8.4.2 Quantitative ... 97

Stellenbosch University https://scholar.sun.ac.za

LIST OF FIGURES

Figure 2.1: Schematic diagram of conventional copper processing through SX and electrowinning (adapted from Schlesinger et al., 2011)...... 4

Figure 2.2: Schematic diagram of a simplified electrowinning cell setup (adapted from Lee (2012) and Bard & Faulkner (2000))...... 5

Figure 2.3: Molecular structure of guar adapted from (Fabian et al. 2007) 17

Figure 2.4: Non-ionic polyacrylamide molecular structure...... 18

Figure 2.5: Anionic or hydrolyzed polyacrylamide molecular structure 18

Figure 2.6: Proposed schematic diagram model of the double layer region under conditions where certain anions are specifically adsorbed adapted from Bard and Faulkner (2000). 21

Figure 2.7: Simplified diagram illustrating different polycrystalline deposit types as a function of inhibition intensity and J/J_d adapted from Winand (1992)...... 23

Figure 2.8: Switching linear potential sweep during a CV test...... 24

Figure 2.9: A typical Nyquist plot showing the electrochemical impedance spectra of copper electrodeposition in an electrolytic solution. 25

Figure 3.1:Schematic diagram of standard three electrode setup with a platinum tipped RDE. 35

Figure 3.2: a) Polished GAMRY platinum cathode tip on left and stainless-steel cathode tip on the right. b) Self-made stainless-steel cathode tip set in epoxy resin, screwed into the Teflon RDE mount...... 37

Figure 3.3: Electrowinning cell with circulating electrolyte to achieve steady state before an experimental run. 38

Figure 3.4: Schematic diagram of electrowinning cell and setup configuration/process...... 38

Figure 3.5: Example of surface topography analysis of a copper plate using VGStudioMax 3.1, presenting the 6 selected regions of interest with their respective geometry and mesh elements...... 40

Figure 4.1: Nyquist plots showing the electrochemical impedance data for copper electrodeposition. Conditions: 35 g/L copper, 160 g/L H_2SO_4 and 25mg/L Cl at 45 °C in a RDE setup at 500 rpm, copper electrodeposited for 6 minutes prior to EIS, DC potential of 0.23V vs. SHE with AC rms potential of 5 mV. Additive concentration: a) 2 mg/L b) 10 mg/L. 44

Figure 4.2:Equivalent circuit model with reference electrode (RE), solution resistance (RS), charge transfer resistance (RCT), constant phase element (CPE_1), capacitance (CPE_2), Resistance (R2), and working electrode (WE)...... 45

Figure 4.3: Typical voltammogram of copper deposition on a platinum surface, 35 g/L copper, 160 g/L H_2SO_4 and 25mg/L Cl^- at 45 °C in a RDE setup at 500 rpm. Voltage sweep between 0.319 and 0.2 V vs. SHE at a scan rate of 1 mV/s...... 49

Figure 4.4: Voltammograms for Guar additive at 2 mg/L and 10 mg/L concentration compared to the base case scenario. 50

Figure 4.5: Voltammograms for the Low MW PAM additive at 2 mg/L and 10 mg/L concentration compared to the base case scenario...... 50

Figure 4.6: Voltammograms for the Medium MW PAM additive at 2 mg/L and 10 mg/L concentration compared to the base case scenario...... 51

Figure 4.7: Voltammograms for the High MW PAM additive at 2 mg/L and 10 mg/L concentration compared to the base case scenario...... 51

Stellenbosch University https://scholar.sun.ac.za

Figure 4.8: Voltammograms for the Very High MW PAM additive at 2 mg/L and 10 mg/L concentration compared to the base case scenario. 52

Figure 4.9: Voltammograms of all additives at 2 mg/L used during CV experimental work plotted on one graph. 53

Figure 4.10: Voltammograms of all additives at 10 mg/L used during CV experimental work plotted on one graph. 53

Figure 4.11: Effect of organic additives on current density measured on the return sweep at a potential of 0.22 V vs. SHE at additive concentrations of 2 mg/L and 10 mg/L. 55

Figure 4.12: Method for calculating nucleation overpotential values. 56

Figure 4.13: Effect of organic additives on the nucleation overpotential at additive concentrations of 2 mg/L and 10 mg/L. 57

Figure 5.1:SEM micrographs of copper crystal deposit on stainless steel surface in a Base Case electrolyte at 300 A/m2. a-b) After 10 s deposition. c-d) After 30 s deposition. 60

Figure 5.2: SEM micrographs of copper crystal deposit on stainless steel surface in the presence of guar at 300 A/m2. a-b) After 10 s deposition. c-d) After 30 s deposition. 62

Figure 5.3: SEM micrographs of copper crystal deposit on stainless steel surface in the presence of a Low MW PAM at 300 A/m2. a-b) After 10 s deposition. c-d) After 30 s deposition. 63

Figure 5.4: SEM micrographs of copper crystal deposit on stainless steel surface in the presence of a Medium MW PAM at 300 A/m2. a-b) After 10 s deposition. c-d) After 30 s deposition. 64

Figure 5.5: SEM micrographs of copper crystal deposit on stainless steel surface in the presence of a High MW PAM at 300 A/m2. a-b) After 10 s deposition. c-d) After 30 s deposition. 65

Figure 5.6: SEM micrographs of copper crystal deposit on stainless steel surface in the presence of a Very High MW PAM at 300 A/m2. a-b) After 10 s deposition. c-d) After 30 s deposition. 66

Figure 5.7:First interpretation of simplified diagram for predicting the crystallographic structure based on CV, EIS, and RDE electrowinning results for copper deposited for 10s in the presence of various additives, ranging in MW and ionic content by utilizing the diagram adapted from Winand, 1992. 68

Figure 5.8: Second interpretation of simplified diagram for predicting the crystal growth type based on CV, EIS, and RDE electrowinning results for copper deposited for 10s in the presence of various additives, ranging in MW and ionic content by utilizing the diagram adapted from Winand, 1992. 70

Figure 5.9: Colour image of resultant copper plate achieved in a) Base Case scenario; b) 2 mg/L Guar; c) 2 mg/L Low MW PAM; d) 2 mg/L Medium MW PAM; e) 2 mg/L High MW PAM; f) 2 mg/L Very High MW PAM. 72

Figure 5.10: Cathode surface topography delivered in a; a) Base Case; b) 2mg/L Guar; c) 2 mg/L Low MW PAM ; d) 2 mg/L Medium MW PAM; e) 2 mg/L High MW PAM; f) 2 mg/L Very High MW PAM; electrolyte, with a surface height colour scale indicating ± 0.3 mm deviation on the six selected regions of interest. 75

Figure 5.11: Average total surface elements (area) deviation from the flattest surface plane (normalized) for each plate achieved in the presence of its unique additive. 77

Figure 5.12: Calculated arithmetic meant surface deviation (Sa value) of copper deposit during electrowinning experiments at 300 A/m^2 & 40 °C in the presence of various organic additives – considering both negative and positive deviations. 78

Figure 5.13: Calculated arithmetic meant surface deviation (Sa value) of copper deposit during electrowinning experiments at 300 A/m^2 & 40 °C in the presence of various organic additives – considering only positive deviations. 79

Stellenbosch University https://scholar.sun.ac.za

Figure 8.1: Cathode surface topography delivered in an electrolyte containing no additive with a surface height colour scale indicating ± 1 mm deviation on the six selected regions of interest. 94

Figure 8.2: Cathode surface topography delivered in an electrolyte containing 2mg/L Guar additive with a surface height colour scale indicating ± 1 mm deviation on the six selected regions of interest. 94

Figure 8.3: Cathode surface topography delivered in an electrolyte containing 2mg/L Low MW PAM additive with a surface height colour scale indicating ± 1 mm deviation on the six selected regions of interest. 95

Figure 8.4: Cathode surface topography delivered in an electrolyte containing 2mg/L Medium MW PAM additive with a surface height colour scale indicating ± 1 mm deviation on the six selected regions of interest. 95

Figure 8.5: Cathode surface topography delivered in an electrolyte containing 2mg/L High MW PAM additive with a surface height colour scale indicating ± 1 mm deviation on the six selected regions of interest. 96

Figure 8.6: Cathode surface topography delivered in an electrolyte containing 2mg/L Very High MW PAM additive with a surface height colour scale indicating ± 1 mm deviation on the six selected regions of interest. 96

Figure 8.7: Average total surface elements (area) deviation from the flattest surface area (normalized) for each plate achieved in the presence of its unique... 97

Figure 8.8: Average total surface area deviation from the flattest surface area (best fit plane) for each plate achieved in the presence of its unique additive by taking only the average positive deviation values of the 6 regions of interest for each plate into account – with focused view of total area of high positive deviation from flat surface. 98

Stellenbosch University https://scholar.sun.ac.za

LIST OF TABLES

Table 2.1: Summary of copper electrodeposition organic additives by category from Moats et al, (2016). 20

Table 3.1: Summary of the experimental approach........ 32

Table 3.2: List of chemicals used to prepare the synthetic electrolyte for all experimental work........ 33

Table 3.3: Summarized information on Guar........ 34

Table 3.4: Polyacrylamides selected for this study with SENMIN MW classification. 34

Table 3.5: Experimental conditions for RDE experimental work. 41

Table 3.6: Experimental conditions for bench scale electrowinning experimental work........ 42

Table 4.1: Summary of the parameters with their errors obtained from equivalent circuit model and model fitting. 46

Table 4.2: Collection of charge transfer values and conditions obtained from similar previous studies. . 46

Table 5.1: The amount and average rate of copper deposited during 24 hours of electrowinning at 300 A/m^2 & 40 °C in the presence of various organic additives with the corresponding calculated CE values. 80

Table 8.1: Presentation of relevant chemicals densities at 25 °C, and their respective molecular weights. 91

Stellenbosch University https://scholar.sun.ac.za

NOMENCLATURE

Symbol	Unit	Meaning
a	Dimensionless	Chemical activity
C^b	mol/L	Bulk concentration of additive
C_{DL}	mS.s	Double layer capacitance
C_i	mol/dm^3	Concentration of species i
D_i	cm^2/s	Diffusion coefficient of species i
E	V	Electrode potential
E^o	V	Standard electrode potential
F	C/mol	Faradays constant
G	J/mol or kJ/mol	Gibbs free energy
G^o	J/mol or kJ/mol	Gibbs free energy at steady-state
I	A	Electrical current
i	A/m^2	Current density
I_a	A	Anodic current
I_c	A	Cathodic current
i_0	A/m^2	Exchange current density
i_L	A/m^2	Limiting current density
N_i	Mol/cm^2.s	Molar flux density
Q	Coulomb	Charge
R	J/mol.K	Gas constant
R_{CT}	Ω	Charge transfer resistance
R_S	Ω	Solution resistance
S_a	µm	Mean surface deviation

Stellenbosch University https://scholar.sun.ac.za

t	s, min or h	Time
T	˚C or K	Temperature
μ	Da	Dalton
u_i	$cm^2/s.V$	Ion mobility
v_i	cm/s or m/s	Mass-average velocity
ν	cm^2	Kinematic viscosity
σ	N/m or N/cm^2	Surface tension
η	V	Overpotential

Stellenbosch University https://scholar.sun.ac.za

Acronym	Meaning
APAM	Activated polyacrylamide
CE	Current efficiency
CPE	Constant phase element
CV	Cyclic voltammetry
DLC	Diffusion limited current
EIS	Electrochemical impedance spectroscopy
IHP	Inner Helmholtz plane
LSV	Linear sweep voltammetry
MW	Molecular weight
OHP	Outer Helmholtz plane
PAM	Polyacrylamide
ppm	Parts per million
RDE	Rotating disk electrode
RE	Reference electrode
rms	Root mean square
rpm	Revolutions per minute
SEM	Scanning electron microscopy
SHE	Standard hydrogen electrode
SX	Solvent Extraction

Stellenbosch University https://scholar.sun.ac.za

1 INTRODUCTION

1.1 Problem statement

The recovery of copper follows one of two major processing routes namely hydrometallurgical or pyrometallurgical processing. Copper-sulfide orebodies conventionally follow a pyrometallurgical route where the ore is typically crushed, floated, smelted, and finally the copper is electrochemically extracted by means of an electrorefining process step. Oxide ores favor a hydrometallurgical process route, where the ores usually undergo crushing, leaching, solvent extraction (SX), and finally electrochemical extraction of the copper in an electrowinning stage. Hydrometallurgical processing of copper has seen much growth over the past few decades with its contribution to the world's total copper production rising from 3% in 1980 to 20% in 2005 (Moats & Free 2007). This growth can be attributed to many factors like lower capital investments, lower energy consumption per copper cathode, and reduced environmental impact compared to pyrometallurgical processing (Dresher 2001). The most significant growth factor for hydrometallurgical processing is its ability to create high quality copper cathodes.

To produce high quality copper cathodes, the growth and structure of the depositing metal must be controlled. The factor that is most influential in controlling the growth and structure of the deposit is the real current distribution over the cathode surface. Real current distribution is primarily determined by cell design, cell layout, and the selection of construction materials. Even with rigorous cell and tankhouse design procedures, current maldistribution still occurs in tankhouses. The detrimental effect of current maldistribution on cathode quality can be reduced by adding an organic smoothing agent to the electrowinning cell to produce smoother, denser, and brighter copper cathodes.

Guar has traditionally been used as an organic additive in copper electrowinning because of its compatibility with the SX stage, and because of its ability to reduce short-circuiting by limiting dendrite growth on the cathode surface. Recent studies have shown a shift in the application of Guar as the mainstream smoothing agent for copper electrowinning. Robinson et al. (2003) conducted a survey which indicated that 34 copper electrowinning facilities were using Guar/similar additives and only 8 were using alternative organic additives. A similar study in 2013 revealed that a modified polysaccharide (trading as "HydroStar") was being used by more copper electrowinning facilities than Guar (Robinson et al. 2013). It was also reported that other modified polysaccharide and polyacrylamide products were being used successfully on various active copper electrowinning facilities due to their ability to produce brighter, smoother, more compact and pure copper deposits compared to Guar (Bernu et al. 2010; Fabian et al. 2007; Moats et al. 2016). Consequently, much work has been done to compare the performance of these alternative organic additive products with each other and with the industry standard, Guar (Moats et al. 2014; Moats et al. 2016; Luyima et al. 2016). There however exists very little information which describes the adsorption mechanisms and molecular characteristics of the organic additives.

1.2 Research aim and objectives

This project aims to relate polysaccharide and polyacrylamide molecular characteristics (e.g. molecular weight, functional group, and ionic charge) to process outputs, specifically cathode morphology. Smoother copper cathode plating leads to enhanced plant productivity in terms of current efficiency (Fabian (2005)). The effect that these additives have on the deposit morphology and current efficiency involved in the electrowinning process will therefore be investigated and potentially quantified. The aim of this study will be achieved by fulfilling the following project objectives:

- Determine the effect of two types of polymers namely a polysaccharide (Guar) and polyacrylamides on the polarization behaviour of the electrodeposit on the cathode surface.

Stellenbosch University https://scholar.sun.ac.za

- Determine the effect of two types of polymers namely a polysaccharide (Guar) and polyacrylamides on the nucleation mechanisms and structures of copper deposit on the cathode surface during electrodeposition.
- Determine the effect of a polysaccharide (Guar) and polyacrylamides on the morphology, brightness, and integrity of the copper cathode plate in a macro/bench scale setup.
- Investigate how current density and current efficiency are affected by nucleation mechanisms in the presence of organic additives.

1.3 Key questions

The key question that this study aims to answer can be formulated in the following manner:

'How do polyacrylamides and Guar (polysaccharide) interact with nucleating/depositing copper to influence the crystal growth and structure (morphology) on the cathode surface during copper electrowinning?'

The following questions will help to guide the researcher into answering the core question of this study:

- How is the over-potential of the electrolytic cell affected by the presence of various polymeric additives in the electrowinning cell?
- What is the relationship between the polymeric structure of the organic additive and the polarization behaviour exhibited at the cathode surface?
- What is the relationship between the concentration of the organic additive and the polarization behaviour experienced at the cathode surface?
- What is the relationship between cathode morphology and the structure/characteristics of the organic smoothing agent used in the copper electrowinning process?
- Will the type of additive influence the current efficiency of the copper electrowinning system?

1.4 Research approach and project scope

The experimental approach incorporated two phases. The first phase involved fundamental studies on a rotating disk electrode (RDE) and the second phase involved applied studies on a RDE and a bench scale electrowinning cell. By using electrochemistry, more specifically cyclic voltammetry (CV) and electrochemical impedance spectroscopy (EIS), the polarization behaviour and mechanisms of polyacrylamides and Guar interaction at the surface were investigated during the copper electrodeposition process.

RDE electrowinning experimental work investigated nucleation and growth structures of copper via scanning electron microscopy (SEM) micrograph interpretation of deposits after 10 s and 30 s of electrodeposition in the presence of the various additives. The bench scale electrowinning experimental work allowed for a qualitative analysis of the eventual cathode morphologies obtained respectively by using the organic additives as smoothing agents. A hand-held Artec Spider surface scanner was used to generate 3D images of the cathode plates. The high-quality 3D volumetric data of each scanned plate were then imported and analyzed on Volume Graphics VGStudioMax 3.1 (a 3D data viewing and analysis software program) to attribute a mean surface deviation (surface roughness factor) to each plate. This allowed for a qualitative and quantitative analysis of the surface morphology of all the plates that were generated in the presence of the different organic additives. Finally, the copper electrowinning current efficiency values in the presence of each organic additive respectively were calculated and compared. The calculation of the current efficiency was based on the actual mass of copper plated.

Stellenbosch University https://scholar.sun.ac.za

These sequential analysis methods did not only enable the author to propose possible interaction mechanisms of the various organic additives with the electrode surface but also allowed for the evaluation of additive performance during copper electrowinning. Additive performance was primarily evaluated in terms of the quality of the resultant cathode morphology.

The research did not include upstream or downstream processing of the copper and focused only on the electrowinning stage.

1.5 Thesis structure

Chapter 1 provides an introduction of the project including the problem statement, aim and objectives, key questions, and research approach. Chapter 2 provides an overview of the copper electrowinning process with specific focus on the fundamentals of electrochemistry, the use of organic additives in copper electrowinning, and the effect of various operating conditions on electrowinning. A short literature history on the existing knowledge concerning the use of alternative organic additives in the electrowinning process is also presented.

Chapter 3 contains the experimental approach and methodology. Experimental work is divided into two major phases. The first stage being fundamental studies (EIS and CV) on a RDE electrode, and the second stage being electrowinning studies on a RDE and a bench scale electrowinning setup. This chapter gives a description of the materials, methods, and equipment that were utilized to conduct this study.

Chapter 4 presents the results and discussion of the EIS and CV experimental work. Chapter 5 follows the fundamental work and gives a presentation of the results and discussion of the three-electrode (RDE) and bench scale electrowinning experimental work. The conclusions and recommendations are included in Chapter 6, followed by Chapter 7 which includes the reference list of all the sources utilized during research of this topic. Finally, Chapter 8 provides the supplementary information to this document in the form of attached Appendices.

Stellenbosch University https://scholar.sun.ac.za

2 LITERATURE REVIEW

2.1 Background and process overview

Electrometallurgy is the final process in the recovery of copper from the mining industry. Electrometallurgy can be divided into two sub-categories namely electrorefining and electrowinning, depending on whether the copper is extracted from its ore through a pyrometallurgical or hydrometallurgical process. Around 80% of the world's copper-from-ore is extracted via the process of smelting and refining, with the remaining 20% produced from leaching/solvent extraction (SX)/electrowinning processes (Schlesinger et al. 2011). Copper recovery via electrowinning therefore contributes to a substantial portion of the global copper commodity supply. The process of copper production through conventional hydrometallurgical methods can be seen schematically in Figure 2.1.

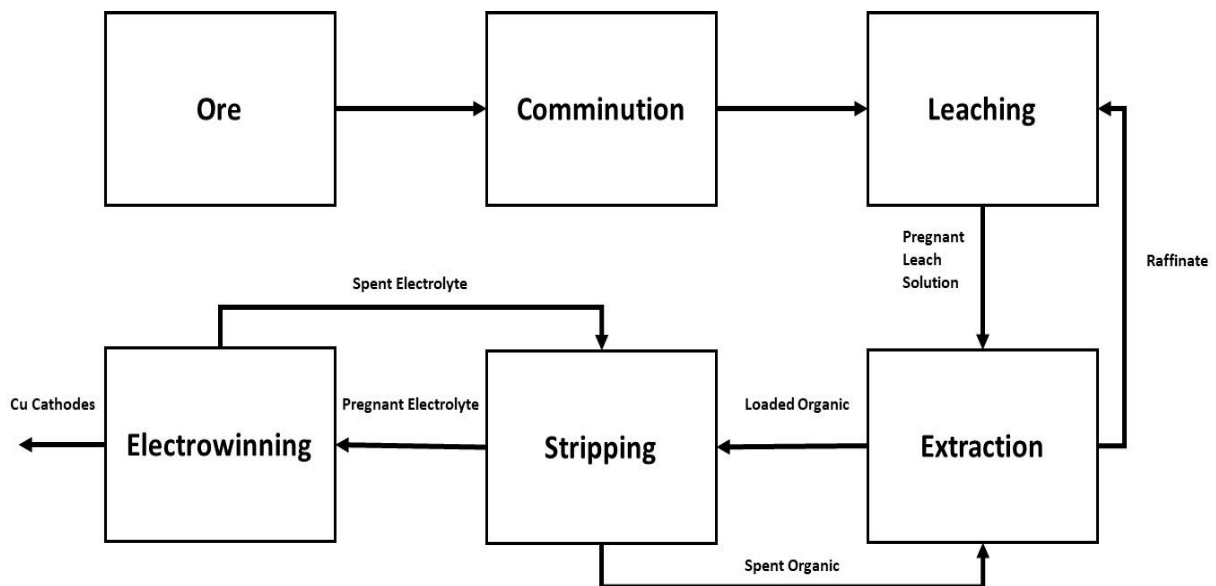

Figure 2.1: Schematic diagram of conventional copper processing through SX and electrowinning (adapted from Schlesinger et al., 2011).

There are three methods for mining copper namely: underground, open pit, and solution mining. Open pit mining is the most widely used method for extracting low grade ore from the ground. Open pit mining is safer and usually less expensive than underground mining. Copper is usually hosted by sulfide or oxide orebodies, and it is the characteristics of the hosting orebody that determine the specific method most suitable for liberating the copper. Sulfide ores are conventionally floated, smelted and then purified by the process of electrorefining. Oxide ores are predominantly processed by leaching the ore to extract the copper into solution, followed by a purification and concentration, SX stage where the copper is sequentially recovered by, and stripped from an organic phase. The copper is stripped from the organic phase with an acidic electrolyte and then sent to an electrowinning circuit.

Electrowinning is a term used to describe the selective deposition of a specific metal onto a surface in an electrolytic cell. The electrolyte loaded with copper ions (advance electrolyte) from the SX stage enters an acid resistant electrowinning cell located in the cellhouse/tankhouse of the plant. A tankhouse is made up of multiple cells in series and parallel depending on configuration. Many anode and cathode electrode pairs are immersed into each cell and an electrical current is passed through the electrodes to reverse the process of metal dissolution.

A simplified schematic diagram of a cathode-anode pair is given in Figure 2.2. Water decomposes via an oxidation reaction at the anode, producing oxygen and hydrogen ions according to the following anodic reaction seen in Equation 2.1 (Lee 2012):

$$H_2O \rightarrow 0.5\ O_2 + 2H^+ + 2e^- \qquad E^\circ = -1.229V \qquad 2.1$$

The oxygen escapes to the atmosphere and the electrons released by the decomposition reaction flows through the anode to the negatively charged cathode. Here the electrons are donated to the Cu^{2+} ions in the electrolytic solution to form a Cu deposit on the cathode surface according to the following cathodic reduction reaction seen in Equation 2.2 (Lee 2012):

$$Cu^{2+} + 2e^- \rightarrow Cu \qquad E^\circ = 0.337\ V \qquad 2.2$$

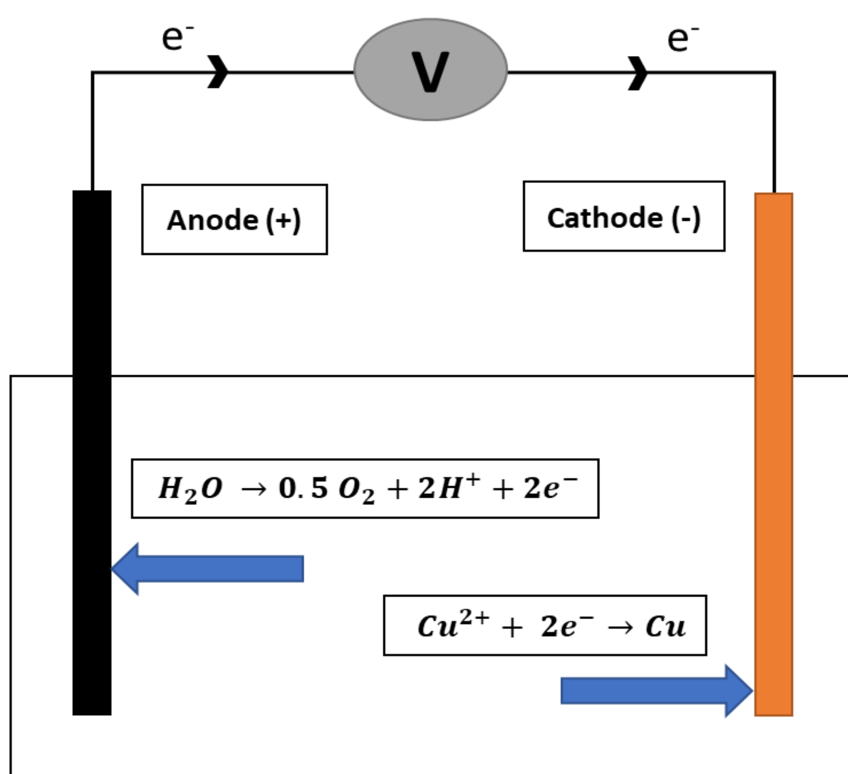

Figure 2.2: Schematic diagram of a simplified electrowinning cell setup (adapted from Lee (2012) and Bard & Faulkner (2000)).

The highly conductive electrolyte in an electrowinning cell usually contains 40-50 g/L Cu^{2+}, 160-180 g/L H_2SO_4, and 1-3 g/L Fe (Beukes & Badenhorst 2009; Schlesinger et al. 2011; Cui 2014; Moats et al. 2016). Reactions 2.1 and 2.2 described above take place in the electrolyte environment, leading to the overall electrowinning reaction illustrated in Equation 2.3 (Schlesinger et al. 2011):

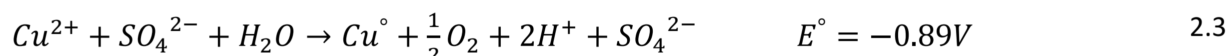

$$Cu^{2+} + SO_4{}^{2-} + H_2O \rightarrow Cu^\circ + \frac{1}{2}O_2 + 2H^+ + SO_4{}^{2-} \qquad E^\circ = -0.89V \qquad 2.3$$

The conditions in the cell should be controlled to optimize product quality, schedule, and cost. The most important characteristics/aspects to consider in the copper electrowinning optimization process include: cell design and maintenance, temperature, cell potential, current density, current efficiency, pH, concentration of impurities, and the concentration and type of additives added to the cell (Beukes & Badenhorst 2009). Electrowinning cells are mostly made from an acid resistant polymer concrete with

Stellenbosch University https://scholar.sun.ac.za

fiberglass lining (Beukes & Badenhorst 2009). The cathodes are made from 316L stainless steel because of its good balance between being inert, robust, and cost effective. The cold rolled Pb-Sn-Ca alloy anodes are spaced in between the cathode plates (Mirza et al. 2016). Cathodes are large square plates packed into the cell with a minimum spacing of 95 mm between cathode centers. The large cathode area is specifically designed to increase the deposition area. Copper is typically electrowon for a period of 5-10 days at a temperature of between 45 ^{o}C and 55 ^{o}C (Moats & Free 2007; Beukes & Badenhorst 2009).

The additives used in electrowinning can be classified as inorganic and organic. The most important inorganic additives added to electrowinning cells are cobalt and chloride. Cobalt is added to the advanced electrolyte in a concentration range of between 90-250 mg/L to protect the anode by promoting oxygen evolution rather than lead oxidation (Robinson et al. 2013). Cobalt addition reduces lead contamination on the cathode surface, thereby also extending the life of anode. Chloride ions serve as grain refiners and facilitate the promotion of smoother and denser cathode deposits. It is suggested that chloride levels should however be kept below 30 mg/L to prevent pitting corrosion on the top of the cathode surface at the air-electrolyte interface (Cui 2014).

2.2 Electrodeposition process fundamentals

Electrodeposition is a process in which a solid phase forms on a substrate which is immersed in an ionic conducting electrolyte in contact with an electrical field (Fabian 2005c). Electrodeposition is a process that takes place in electrochemical systems. An electrochemical system, in short, involves the transport of charge from one interface to another. During metal deposition, charge is transferred at the interface of an electronic conductor (electrode) and an ionic conductor (electrolyte) (Bard & Faulkner 2000). The interface between these chemical phases is the focal point of electrodeposition and for that matter a very important aspect of this study.

When a potential difference is induced between the electrolyte and the electrode surface the flow of charge is promoted. Oxidation at the anode (negative electrode) is balanced by reduction at the cathode through the flow of electrons. An electrical circuit is completed providing the energy for the process of electrocrystallization to take place. In this process, metal ions in the solution are used in conjunction with free electrons to produce the building bricks of the solid crystal structure formation that develops on the face of the working electrode. The working electrode is the electrode on which the reaction of interest is occurring. The reaction process of transferring mass from one phase to the next can be explained in three steps (Fabian 2005):

i. Mass transfer of the reactant (metal) from the electrolyte or the bulk solution to the electrolyte/electrode interface area through three mechanisms namely diffusion, convection, and migration (Beukes & Badenhorst 2009; Bard & Faulkner 2000).
ii. Formation of metal adatoms through adsorption on the surface of the same metal species or a different substrate.
iii. Metal phase formation on the cathode. The type of growth is dependent on process conditions and can be described as two -dimensional (2D) or three-dimensional (3D) growth.

The following sections will describe some of the fundamental laws governing mass transfer from a bulk solution to an electrode surface. Faraday's Law, the Nernst equation, and Fick's Law describe some of the governing principles in electrochemistry and will be investigated in the following sections to gain further insight into this phenomenon. The existing theory on crystal nucleation and growth will be discussed as well as the process kinetics involved during electroplating of copper.

Stellenbosch University https://scholar.sun.ac.za

2.3 Transport theory in electrolytic processes

2.3.1 Mass Transfer

Mass transfer is the first step in the reaction process and involves three possible mechanisms namely: diffusion, convection, and migration. Diffusive mass transfer can be attributed to a concentration gradient from the borders of the bulk solution to the solution layer in contact with the electrode interface. The species will diffuse from a region of high concentration to a region of low concentration. Convective mass transfer can either be forced or natural and occurs because of hydrodynamics or density/temperature gradients. Lastly, the transfer of mass through the mechanism of migration will occur if there is a notable gradient in electrical potential.

Fick's first law describes the process of two-dimensional diffusion in Equation 2.4.

$$N_i = -D_i \nabla c_i \qquad 2.4$$

Where

N_i diffusion flux vector of species *i.*

D_i Diffusivity or the diffusion constant.

∇c_i Concentration gradient of species *i*.

When Fick's first law is expanded to include both migration and convection. Equation 2.4 is converted into Equation 2.5 (Fabian 2005c).

$$N_i = -D_i \nabla c_i - z_i u_i \mathrm{F} c_i \nabla \Phi + c_i \mathrm{v}_i \qquad 2.5$$

Where

z_i Charge number of the ion.

u_i Ion mobility.

F Faraday's constant.

$\nabla \Phi$ Electric field gradient

c_i Concentration of species *i*.

v_i Bulk velocity

The first term on the right-hand side (RHS) of Equation 2.5 accounts for mass transport via diffusion. The second term represents the mass flux due to electric field migration. The third term on the RHS embodies the convection flux, where v_i is the bulk velocity of the solution. In the presence of a highly conductive electrolyte like sulfuric acid, the electrical field is sufficiently decreased to assume that mass flux due to migration is negligible. Equation 2.5 can therefore be simplified appropriately to Equation 2.6 to only include the effects of diffusion and convection.

$$N_i = -D_i \nabla c_i + c_i \mathrm{v}_i \qquad 2.6$$

If the effects of migration are neglected, and electroneutrality allows for the electric field to be eliminated, the known convective diffusion Equation 2.7 is formulated by doing a transient mass balance. This implies that mass transfer in the system is primarily governed by diffusion and convection (Fabian 2005c). A

Stellenbosch University https://scholar.sun.ac.za

physiochemical model can be developed for copper electrodeposition by using Equation 2.7. The full derivation of Equation 2.7, along with the transient mass balance can be seen in Appendix A – Derivations and supporting equations (Equations 8.1-8.3).

$$\frac{\partial c_i}{\partial t} + \mathrm{v}_i \nabla c_i = D_i \nabla^2 c_i \qquad 2.7$$

Where

c_i Concentration of species *i*.

D_i Diffusivity or the diffusion constant.

v_i Average mass velocity in cm/s.

2.3.2 Nucleation and growth in electrocrystallization

Electrocrystallization necessitates the formation of nuclei and crystal growth on a surface under the influence of an electrical field. The first step of electrocrystallization is the formation of new nuclei of the depositing metal on the surface of the same metal or a foreign material. The evolution of nucleation is initiated when cations in the bulk migrate towards the electrode surface via mass transfer (described in Section 2.3.1). An electron transfer step then follows where the copper cation is transformed into an adatom on the surface of the electrode. The charge transfer step usually occurs very fast and therefore the formation of adatoms is limited to the rate of mass transfer from the bulk to the electrode surface. The adatom then travels into a nucleation site, usually a surface imperfection, via surface diffusion where it encounters other already diffused adatoms to form a nucleus (Pasa & Munford 2006). Nuclei are formed in these nucleation sites, followed by grain formation and eventually cathode growth.

The competition between nucleation and crystal growth is what determines the granularity of the deposit (Budevski et al. 2000). Higher nucleation rates promote the formation of smaller crystal sizes. On the other hand, the shape of the growing crystals determines the structure and physical appearance of the metal deposit (Fabian 2005). Consequently, if a higher growth rate of the crystal grains normal to the substrate surface is observed a more fibrous crystal structure will develop. A brightening effect of the metal deposit can be achieved if the crystal grows parallel to the substrate.

Nucleation is therefore the first stage of crystal growth and can be divided into two main sub-categories, namely primary and secondary nucleation (Gebbie 2013). When there are no previously formed crystalline material on the depositing surface and a nucleus forms on the surface, primary nucleation is said to occur. Primary nucleation is reported to take place via homogenous or heterogenous nucleation. Homogenous nucleation occurs when small clusters of molecules or atoms are formed spontaneously without the aid of a foreign substrate or a defect on the depositing surface. Energy is required for the formation of a nucleus by a cluster of atoms on a substrate surface. This energy is known as the Gibbs excess free formation energy and is given in Equation 2.8 (Durai et al. 1987). Equation 2.8 is specially adapted for the process of electrocrystallization from its original form developed for physical crystallization.

$$\Delta G = -nze|\eta| + An^{\frac{1}{2}}\sigma \qquad 2.8$$

Where

n number of atoms or molecules

Stellenbosch University https://scholar.sun.ac.za

z	number of electrons
e	electronic charge
η	overpotential
A	constant depending on shape and nature of electrode
σ	surface tension

The first term on the RHS of Equation 2.8 is associated with the transfer of *n* ions from the bulk to the electrode surface which is driven by the overpotential (Budevski et al. 2000). This term always adopts a negative value. The concept of overpotential is discussed in Section 2.4.4 of this report. The second term considers energy contributions derived from the deviation of the new phase from the bulk phase (Budevski et al. 2000). The free energy related to the presence of grains and strain are neglected for simplicity.

Minimum energy conditions for the formation of a nucleus are given in Equation 2.9. At the conditions where Equation 2.9 holds, a critical number of atoms, n_{crit} is required for a nucleus to form.

$$\left[\frac{d\Delta G}{dn}\right]_{\eta} = 0 \qquad 2.9$$

By inserting Equation 2.9 into Equation 2.8 and by assuming the surface tension is independent of the number of atoms, the size of the critical 2-D nucleus (n_{crit}) can be calculated. The number of critical sized 2-D nuclei formed per unit area in a unit time, known as the nucleation rate, can be determined by plotting the free energy of formation of a 2-D critical nucleus as a function of overpotential for different values of interfacial tension (Durai et al. 1987). The nucleation rate can be calculated with Equation 2.10. See Appendix A – Derivations and supporting equations, Section 8.1.2 for Equations 8.4-8.5 to calculate n_{crit} and ΔG_{crit}.

$$J = A_J exp\left(-\frac{\Delta G_{crit}}{kT}\right) \qquad 2.10$$

Where A_J is a constant of proportionality and k is the Boltzmann constant with a value of 1.38×10^{-23} JK^{-1}.

Heterogenous nucleation is the second form of primary nucleation and involves nucleation in the presence of an aiding foreign substrate (Gebbie 2013). Not all foreign substrates act to promote nucleation and may in fact inhibit nucleation. Heterogenous nucleation requires a lower overpotential (energy), since both Equation 8.4 & 8.5 depend on the surface free energy. It is known that the presence of a growth promoting foreign substrate will lower the surface free energy, resulting in lower n_{crit} and ΔG_{crit} values at a constant overpotential. Accordingly, it can be reasoned that heterogenous nucleation is more favorable than homogenous nucleation. A smaller overpotential is needed which translates to less energy required to promote nucleation on the depositing surface.

Secondary nucleation is the growth of a crystal structure on a seed crystal introduced to the system. The seed crystal acts as a surface on which secondary nucleation and growth can occur. For the same reason that heterogenous nucleation is preferred above homogenous nucleation, secondary nucleation is preferred above primary nucleation. Less energy is needed due to the lower surface free energy value related to nucleation on an already existing growth surface.

The process of nucleation can be described as either instantaneous or progressive (Berlic et al. 2014). Instantaneous nucleation occurs when the rate of nucleation is rapid in comparison with the rate of crystal

Stellenbosch University https://scholar.sun.ac.za

growth. Nuclei will form at all possible nucleation sites in a very short space of time. Progressive nucleation occurs when the rate of nucleation is much slower and occurs in conjunction with crystal growth. It is said that organic additives or smoothing agents are used during electrowinning to promote progressive nucleation rather than the more erratic process of instantaneous nucleation (Winand 1994).

2.4 Electrochemical cell thermodynamics

2.4.1 Basic concepts

2.4.1.1 Faraday's Law

In the case of a copper electrowinning cell water undergoes an oxidation reaction at the anode and the copper undergoes a reduction reaction at the cathode. Faraday's Law presented in Equation 2.11 gives the amount of charge (Q) spent to reduce M moles of the oxidizing agent, which in this case is the cupric ions (Beukes & Badenhorst 2009).

$$Q = n.F.M \tag{2.11}$$

Where F is Faraday's constant of 96 487 Coulombs. This constant accounts for the passage of 96 487 Coulombs of charge for every equivalent chemical change in the system (Lee 2012). The charge spent per unit time can be determined by differentiating Equation 2.11 with relation to time to produce Equation 2.12:

$$\frac{dQ}{dt} = I = n.F.\frac{dM}{dt} \tag{2.12}$$

In electrochemistry, it is often useful to relate current with the area that the current is subjected to. This is termed the current density. Faraday's equation can be expressed in terms of current density (Equation 2.13) by normalizing Equation 2.12 with the total area.

$$i = \frac{I}{A} = n.F.\frac{1}{A}.\frac{dM}{dt} \tag{2.13}$$

The implication of Equations 2.11 to 2.13 is that the quantity of electricity transferred at an electrode surface is proportional to the mass of a substance altered at the electrode surface during electrolysis.

2.4.1.2 Current efficiency

When two or more faradaic reactions can proceed simultaneously at an electrode surface, the fraction of the current being spent on the relevant reaction (i_r) is called the instantaneous current efficiency (Bard & Faulkner 2000). See Equation 2.14.

$$Instantaneous\ CE = \frac{i_r}{i_{total}} \tag{2.14}$$

In a copper rich electrolytic cell, the current efficiency is a ratio between the current producing the copper and the total current applied to the system. In practical terms, the current efficiency is the ratio between the charge spent on plating the actual amount of copper, and the total charge spent for a theoretical amount of copper that was expected to plate at a 100% efficiency. Equation 2.15 represents this ratio (Beukes & Badenhorst 2009).

Stellenbosch University https://scholar.sun.ac.za

$$\varepsilon = \frac{\frac{dM_{Cu}}{dt}}{I \cdot \frac{t}{nF}} = \frac{Q_r}{Q_{total}} \qquad 2.15$$

A current efficiency of 100% is desired, since this means that no applied current was wasted on side reactions. It is however nearly impossible to achieve this ideal current efficiency because of numerous prevailing factors like the presence of impurities, materials of construction etc. In copper electrowinning processes side reactions with water and iron are mainly to blame for a drop in overall current efficiency. The cyclic oxidation and reduction of iron reduces current efficiency significantly and there exist several implementation methods to address this problem. According to Beukes & Badenhorst (2009), current efficiencies can be as low as 65% for direct electrowinning operations and as high as 95% for electrowinning operations with an intermediate SX stage because it eliminates most impurities in the electrolyte before the electrowinning circuit.

2.4.2 Interfacial potential differences

An interface is created when a metal electrode is submerged in an electrolyte. This interface becomes electrified because of the transfer of electrons across the interface from the solution to the electrode, and vice versa. The charge transfer over the electrified interface leads to a redistribution of mobile ions near the electrode interface region, and a potential difference develops between the electrode and the electrolyte. The chemical potential of a component *i*, present in two mixtures that are in contact and in chemical equilibrium across the interface is given in Equation 2.16.

$$\mu_i(I) = \mu_i(II) \qquad 2.16$$

If Equation 2.16 does not hold it implies that a spontaneous reaction will take place across the interface. Metal M is in contact with its ions M^{z+} in solution and therefore the following equilibrium reaction is expected in Equation 2.17.

$$M^{\circ}{}_{(s)} \leftrightarrow M^{z+}{}_{(aq)} + ze_m \qquad 2.17$$

The direction of the reaction in Equation 2.17 is determined by the chemical potential on either side of the equation. If the chemical potential of the left-hand side (LHS) of Equation 2.17 is larger than that of the RHS of the equation, the metal will dissolve into cations and free electrons at a faster rate than the reverse reaction. More M^{z+} ions flow from the metal crystal lattice compared to what enters the metal lattice. This renders the metal surface more negatively charged (q_M^-) and the region around the metal more positively charged (q_M^+), creating an electrical double layer around the metal surface. This reaction will proceed forward until the potential difference over the interface acquires a dynamic equilibrium value that prevents further dissolution at that point. The exact same logic is followed for the reverse reaction of Equation 2.17, where the chemical potential on the RHS of the reaction is larger than the LHS of the equation. The metal-solution interface region has a neutral charge at the dynamic equilibrium as presented in Equation 2.18.

$$q_m = -q_s \qquad 2.18$$

Chemical reactions on both sides of the reaction in Equation 2.17 are needed to create an equal potential for both phases. These reactions will consume or generate electrical charge which ultimately creates a potential difference over the interface. The metal-solution interface potential, Ø(M,S), is equal to the

Stellenbosch University https://scholar.sun.ac.za

difference between the potential of the metal, $\emptyset_M$ and the potential of the solution $\emptyset_S$ as shown in Equation 2.19.

$$\emptyset(M,S) = \emptyset_M - \emptyset_S \quad 2.19$$

2.4.3 Electrode potential

The standard electrode potential is the potential that naturally arises in the system without external energy input. In other words, it is the potential difference between the energy states of the product and the reactant present in the system, which is a manipulation of the Gibbs free energy reaction. Reaction thermodynamics describe the following relationship for the Gibbs free energy for a single electrode in Equation 2.20 (Lee 2012).

$$G = G^{\circ} + RTln\frac{aRed^n}{aOx^m} \quad 2.20$$

Where

G	Gibbs free energy.
G°	Gibbs free energy at standard-state.
R	Ideal gas constant (8.31 J°K^{-1}mol^{-1}).
T	Temperature (K).
a^n	Chemical activity of the product species.
a^m	Chemical activity of the reactant species.

It is very difficult to measure the Gibbs free energy of an electrochemical system and therefore it is desired to translate the Gibbs free energy into cell potential values. Potential can be measured more easily and is the equivalent measure of existing energy in an electrochemical system. Equation 2.20 is transformed into the well-known Nernst equation seen in Equation 2.21 (derivation shown in Appendix A – Derivations and supporting equations, Section 8.1.3).

$$E_{half-cell} = E^{\circ} + \frac{RT}{nF}ln\ \frac{aOx^m}{aRed^n} \quad 2.21$$

Equation 2.21 is significant for distinct reasons. It enables the calculation of the required potential (energy) needed for the desired reaction to take place. By studying Equation 2.21 it can be deduced that the overall reaction potential of the cell can be expressed in terms of the half-cell potential values of the electrode reactions. Equation 2.22 illustrates this.

$$E_{cell} = E_{right} - E_{left} \quad 2.22$$

Where E_{right} and E_{left} refers to the two half-cell potentials calculated by the Nernst equation independently. E_{cell} refers to the overall resultant cell potential.

2.4.4 Polarization and reaction kinetics

The equilibrium potential of a cell is an important reference point of a system. The departure of the cell potential from this equilibrium potential due to the passage of faradaic current is termed polarization (Bard & Faulkner 2000). Overpotential is described to be the extra energy required to promote the

Stellenbosch University https://scholar.sun.ac.za

forward reaction at the intended rate (Moats et al. 2016). This is an important term in the realm of electrochemistry and much information about electrode reactions can be derived from the occurrence of electrode polarization. The overpotential (ɳ) measures the extent to which the polarization takes place in the system. Overpotential can be calculated by using Equation 2.23.

$$\eta = E_{cell} - E_{eq} \quad 2.23$$

Copper is predominantly present as a divalent cation (Cu^{2+}) in the acidic electrolyte. During copper electrowinning, the copper (II) or cupric ions migrate towards the negative cathodes primarily via diffusion and convection. Once at the cathode surface the cupric ion undergoes a series of reactions before it is transformed into a solid copper deposit. Equation 2.24 depicts the rate limiting step where the cupric ion is reduced to the cuprous state by transferring a single electron (Hinatsu & Foulkes 1991). The cuprous ion then undergoes a reaction where it gains another electron to form a neutral copper atom either via the process presented in Equation 2.25 or by disproportionation as given in Equation 2.26. Disproportionation is a chemical reaction where a compound of intermediate oxidation state converts to two different compounds of the same element. The two compounds that form will have a higher and lower oxidation state than the original compound.

$$Cu^{2+}{}_{(aq)} + e^- \rightarrow Cu^+{}_{(aq)} \quad 2.24$$

$$Cu^+{}_{(aq)} + e^- \rightarrow Cu^{\circ}{}_{(s)} \quad 2.25$$

$$2Cu^+{}_{(aq)} \rightarrow Cu^{\circ}{}_{(s)} + Cu^{2+}{}_{(aq)} \quad 2.26$$

Because of the slow reaction kinetics observed in Equation 2.24 and the relatively fast kinetics observed in Equation 2.25 a negligible concentration of cuprous ions is present at the cathode surface, but due to the equilibrium achieved in Equation 2.26 the cuprous ion concentration becomes significant. To achieve copper deposition on the cathode, the reactions of Equations 2.24 to 2.26 must be driven away from the equilibrium state. This is achieved by the application of energy in the form of applied potential, and the additional energy required to drive these reactions away from their equilibrium state is called the overpotential. The rate of the reaction is measured in terms of current density. It is therefore convenient to have equations that relate the overpotential with current density. The equation that fundamentally relates current density with the overpotential is known as the Butler-Volmer equation represented in Equation 2.27.

$$i = i_0 \left(e^{\frac{\alpha_{Ox} nF(\eta)}{RT}} - e^{\frac{-\alpha_{Red} nF(\eta)}{RT}} \right) \quad 2.27$$

Where

i	Current density
i_0	Exchange current density
ɳ	Overpotential
α	Transfer coefficient
n	Number of electrons transferred
F	Faraday’s constant

Stellenbosch University https://scholar.sun.ac.za

R Gas constant

T Temperature

The Tafel equation is derived from the B-V equation, where it is assumed that the system is non-mass transfer limiting, that there is equal surface to bulk concentrations, and that dominant forward or reverse reactions are present (Beukes & Badenhorst 2009). The Tafel equation presented in Equation 2.28 provides a way of linearizing the relationship between overpotential and current density (rate of reaction).

$$\eta = a + b \cdot log(i) \qquad 2.28$$

Where a and b are empirical constants.

The overpotential required to drive a reaction at the desired rate depends on many factors like the metal and electrolyte concentration, and the surface characteristics upon which the plating occurs. Vereecken et al. (2005) found that copper deposited faster in cuprous rich solutions than in cuprous-depleted solutions at the same applied potential. The study also established that additives affect the activity of the cuprous ions by either deactivating or activating these ions which in turn leads to the polarization or de-polarization of copper deposition (Vereecken et al. 2005). This phenomenon speaks directly to one of the objectives of the present study. Smoothing agents can facilitate in the process of polarization or de-polarization of copper deposition, which directly affects cathode morphology and energy consumption (Adcock et al. 2002).

2.4.5 Diffusion limited current

Two equations describing the reaction rate have been derived. The first being the convective-diffusion Equation 2.7 from Fick's law describing mass transfer, and the second being the B-V Equation 2.27 which describes heterogenous electron transfer. It was further established that by increasing the overpotential the reaction rate can be increased. If all the species that reach the electrode surface are oxidized or reduced it indicates that the system is limited by mass transfer to the electrode. When a system is limited by mass transfer there exists a certain current limit where no increase in potential will increase the rate of reaction. This is termed the diffusion limited current (DLC). The DLC should be determined to optimize and design of an electrochemical cell, since much energy can be lost if the system is run above its DLC. At the DLC the concentration of the plating species at the electrode surface is equal to zero, meaning that the species is consumed at the same rate as it is supplied to the electrode. Equation 2.29 describing the DLC is given by Beukes and Badenhorst (2009).

$$i_L = nFk_d\left(C_{ox(bulk)}\right) \qquad 2.29$$

Beukes and Badenhorst (2009) further point out two important observations:

i. By increasing the concentration of the relevant species (Cu^{2+}) in the bulk the DLC is also increased.
ii. By increasing the mass transfer coefficient (k_d) the DLC is also increased.

The mass transfer coefficient is a function of both the hydrodynamics and physical properties of the system. The hydrodynamics of the system influence the general bulk motion and are the most effective way of increasing the mass transfer coefficient (Beukes & Badenhorst 2009). Bulk movement allows for the passage of fresh solution to the electrode surface, thereby enhancing the value of the transfer coefficient which in turn allows for a higher DLC.

Stellenbosch University https://scholar.sun.ac.za

2.4.5.1 Rotating Disk Electrode

The hydrodynamics of a system play a vital role in the overall energy consumption of a system. It is therefore necessary to present the hydrodynamic movements inside a rotating disk electrode (RDE), since all fundamental studies of this project will be conducted with a RDE. The RDE setup has achieved much experimental success for various reasons (Gabe & Walsh 1983). Firstly, the RDE is normally used in laminar flow regimes which give it flow stability over a wide range of rotation speeds. This characteristic makes it preferable for use in electrode kinetic studies. Secondly, a rigorous solution for the mass transfer equation has been derived from theoretical and experimental studies. Thirdly, the moderately low rate of mass transfer to the electrode surface restricts the current requirements and consequently a modest power supply can be used for full operation.

Convective currents are induced by the rotation of the electrode in the electrolytic solution. The rotation of the electrode drags fresh solution upwards and then the centrifugal forces created by the rotating electrode disperse the solution radially outward. The unique flow patterns of a RDE affects the mass transfer coefficient describing the system. These effects have been accounted for in the adjusted limiting equation for a RDE that has been derived and developed in literature. This Equation is also known as the Levich equation and is represented in Equation 2.30 (Lu 2011).

$$i_L = 0.62nFAD_i^{\frac{2}{3}}\omega^{\frac{1}{2}}\nu^{-\frac{1}{6}}C_0^{\ *} \qquad 2.30$$

Where

n	number of electrons
F	Faraday's constant
A	Area of cathode
D_i	Diffusivity or the diffusion constant.
ω	Angular velocity of RDE (rad/s)
v	Kinematic viscosity of the electrolyte
C_0	Concentration of the ion in the bulk of the solution

The Levich equation can be used to determine the DLC of the RDE experiment. In the case of an industrial electrowinning cell, Equation 2.29 can be used instead. The mass transfer coefficient can be solved by using empirical correlations which is made up by various dimensionless numbers like the Reynolds number and the Schmidt number.

2.5 Copper electrowinning with organic additives

A literature review revealed several publications concerning the use of organic additives in copper electrowinning processes. Guar gum became the standard organic additive in copper electrowinning, mainly because of its compatibility with solvent extraction introduced in 1968 (Moats & Free 2007; Moats et al. 2016). Recently, a decrease in the popularity of Guar products has been observed due to seasonality and high prices of the product (Robinson et al. 2013). Increasingly more tankhouses are using alternative modified polysaccharides and polyacrylamides because these products are less expensive and are also reported to deliver a higher purity copper cathode. Studies suggest that modified polysaccharides and polyacrylamides are more economic and sustainable than Guar as an additive in copper electrowinning (Robinson et al. 2013). Furthermore, it was shown that an improved cathode deposit morphology can be

Stellenbosch University https://scholar.sun.ac.za

achieved by using alternative modified organic additives (Fabian et al. 2007; Moats et al. 2016). These relatively recent findings are in contrast with what Vereecken and Winand found in 1976; that various non-ionic and cationic polyacrylamide additives delivered less desirable copper deposits compared to when Guar was used (Vereecken & Winand 1976). This finding was challenged by Fabian (2005) where a high molecular weight, non-ionic, polyacrylamide was found to deliver a smoother surface roughness compared to Guar as a copper electrowinning additive. Fabian et al. (2007) state that Vereecken and Winand used outdated methods in their study of 1976 and that is why it was found that polyacrylamides delivered a less desirable cathode deposit.

In a previous study it was found that a PAM additive, "Superfloc N100", was more efficient at minimising lead (Pb) contamination of the copper cathodes during electrowinning compared to other polysaccharide based products like Guarfloc 64 and Jaguar M50 (Tshimwanga et al. 2011). Helsten and Moats (2012) found that a polyacrylamide product was more effective at low concentrations (2 mg/L) than HydroStar or a HydroStar/Guar mixture to produce smooth copper electrodepositions. The experimental work of both Fabian et al. (2007) and Helsten and Moats (2013) were conducted in a laboratory bench scale electrowinning cell.

Modified polysaccharide products have also been compared to Guar in previous studies. A plant trial revealed that a denser cathode with less sulphur contaminant was achieved by using HydroStar, a modified polysaccharide, as opposed to three different Guar products it was compared with (Bernu et al. 2010). Sulphur contamination is primarily related to the density of the deposit, since more porous deposits will lead to increased electrolyte entrapment. Furthermore, 44% more HydroStar product was used than the normal Guar dosage and it was still considered cheaper due to its lower cost. It is reported that the oligosaccharide product, DXG-F7 is becoming very popular in Chile and other global operations due to the previously mentioned advantages related to using modified polysaccharides (Robinson et al. 2013). A decrease in sulfur contamination of the copper cathodes was also reported when using the DXG-F7 product.

Very little literature was found on characterizing the behavior of Guar as an organic additive in copper electrowinning. The important contributions to literature on polyacrylamide organic agents in the copper electrowinning process are however more numerous and are presented in Section 2.5.2 of the literature study.

2.5.1 Organic additive hydrolysis and adsorption characteristics

2.5.1.1 Polysaccharides

The traditional additive used in the electrowinning circuit is Guar, and has been utilized as a smoothing agent in copper electrowinning for more than 40 years (Cui 2014; C P Fabian et al. 2007). Guar is a polysaccharide, more specifically, a galactomannan polymer which occurs naturally and is used extensively as a flocculant or a coagulant in various processes. Guar is a linear D-mannose sugar with an attached D-galactose chain on every other mannose chain as shown in Figure 2.3 (Fabian et al. 2007). The reported molecular weight of Guar ranges extensively from 0.25 to 5 million Da depending on the method of analysis (Mudgil et al. 2014). Mudgil et al. (2014) further report that more recent results indicate that the average molecular weight of Guar is between 1 and 2 million Da. This average molecular weight range was obtained with the techniques of size exclusion chromatography and low angle laser light scattering.

Stellenbosch University https://scholar.sun.ac.za

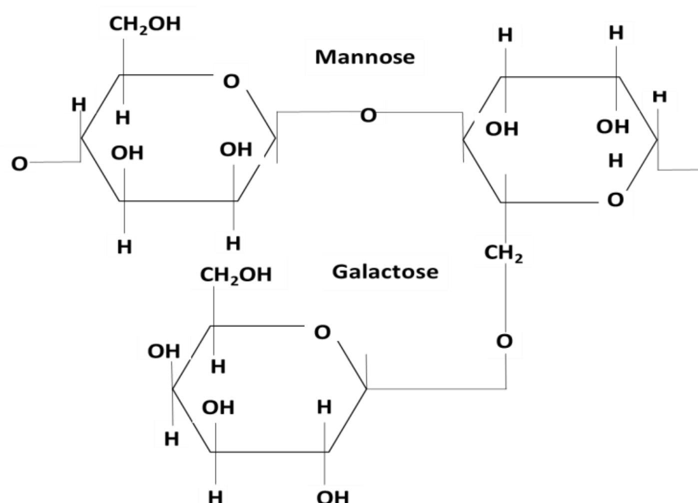

Figure 2.3: Molecular structure of guar adapted from (Fabian et al. 2007)

Very little information on the hydrolysis of Guar and modified polysaccharides in sulfuric acid was obtained from the literature. It is however reported that Guar gum solutions are stable over a pH range of 1-10.5 due to their non-ionic nature (Mudgil et al. 2014). Fabian (2005) state that Guar forms colloidal suspensions when hydrated with chilly water and this is confirmed by Mudgil et al. (2014). Guar gum also shows a high level of hydrogen bonding activity, especially with cellulosic material and hydrated minerals because of the presence of the hydroxyl group on the molecule (Mudgil et al. 2014).

2.5.1.2 Polyacrylamides

Polyacrylamides are highly soluble in water just like polysaccharides and are used in a diverse range of industrial applications due to their adsorption properties. Polyacrylamides are used most extensively as flocculant or coagulant additives. The higher molecular weight polyacrylamides are typically used as flocculants, while the lower weight, shorter chain, polyacrylamides are used as coagulants and mud stabilizers. Fabian (2005) list the following possible interactions involved individually or simultaneously during the adsorption of polyacrylamides onto solid surfaces.

- Chemical short distance interactions e.g. hydrogen bonding and covalent bonding.
- Physical longer-range bonding in the form of electrostatic bonding, London-Van der Waals bonding and dipole attractions.
- Hydrophobic associations e.g. surface hydrophobicity
- Chemical nature of the surface, functional groups in the polymer and the presence of solutes.

Polyacrylamides are stable under neutral conditions as represented in Figure 2.4 but undergo hydrolysis in acidic conditions. The molecular structure of the hydrolyzed polyacrylamide is shown in Figure 2.5 (Fabian et al. 2006). According to Fabian et al. (2006) adsorption of non-ionic polyacrylamides occur due to chemical short distance bonding interactions in the form of hydrogen bonding from the polyacrylamide function group (-$CONH_2$).

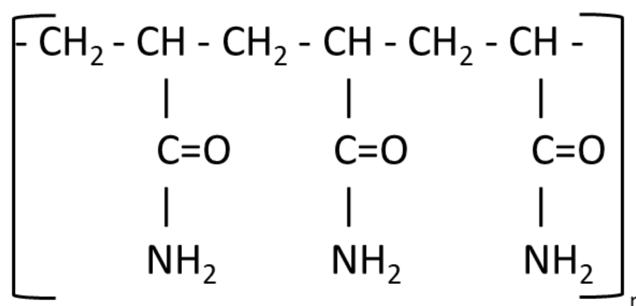

Figure 2.4: Non-ionic polyacrylamide molecular structure

Hydrolysed polyacrylamide is also referred to as anionic polyacrylamide and consists of acrylamide-acrylic acid co-polymers.

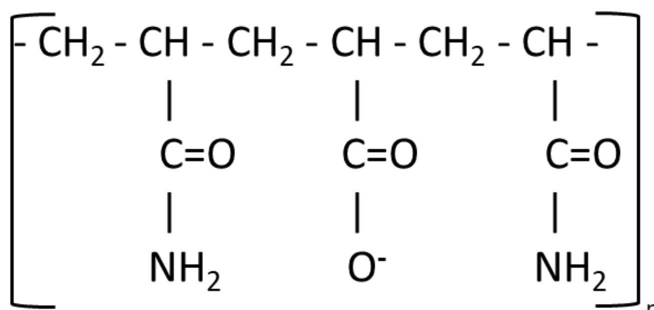

Figure 2.5: Anionic or hydrolyzed polyacrylamide molecular structure

In a previous study Grchev et al. (1991) concluded that the adsorption of non-ionic polyacrylamide in 0.5 M sulfuric acid solution on gold and mild steel is strongly dependent on the molecular weight (MW) of the polymer, electrode potential, and temperature. Major highlights drawn from that work were:

- The maximum surface coverage in the temperature range of 20 to 80 °C for a concentration of 20 mg/L polyacrylamide remained unaffected by the MW of the polymer.
- The surface coverage of dissolved polyacrylamide at concentrations ranging between 2-3 mg/L decreased from about 0.52 to 0.02 as the MW of the polyacrylamide increased from 5 x 10^3 Da to 1.5 x 10^6 Da.

These results significantly indicate that increased adsorption was observed with a decrease in the polyacrylamide molecular weight.

2.5.2 Polyacrylamides in electrowinning

It was proposed for the first time by Pye and Schurz (1957) that polyacrylamides can be used as organic smoothing agents during copper electrowinning. Pye and Schurz (1957) reported that an acrylamide polymer can be used in both zinc and copper electrowinning processes to obtain smooth bright copper cathodes. The concentration of the acrylamide polymer was between 25-150 mg/L and the copper concentration between 20-70 g/L. The strong electrolyte was claimed to be essentially chloride free and bright smooth deposits was achieved after 5, 13, and 16 hours of electrowinning at 25 °C and at a current density of 172 A/m^2. It was also reported that the polyacrylamide can be dissolved in electrolyte or water, or just be added in solid form to the electrolyte.

Vereecken and Winand (1976) conducted a study to compare the copper cathode quality of electrowinning experiments where non-ionic polyacrylamides, cationic polyacrylamides, and Guar were used as organic additives. Industrial quality copper sulphate was used in the electrolyte with a

Stellenbosch University https://scholar.sun.ac.za

concentration of 50 g/L copper and 50 g/L sulfuric acid. The copper was electrowon at a current density of 200 A/m^2 and a temperature of 50 °C for a total of 48 hours where 1 mg/L polyacrylamide was added every 12 hours. Vereecken and Winand (1976) neglect to mention in what media the polyacrylamides were prepared. The conclusion of the study was that polyacrylamide did not deliver smoother, higher quality copper cathodes compared to when Guar was used. It is important to note that no chloride ions were added to the electrolyte and the sulfuric acid concentration was below the current industry concentration levels.

A comprehensive study was conducted by Fabian et al. (2006) where the effect of the organic additive preparation on the surface roughness of the copper deposit was assessed. Polyacrylamide was prepared at 50 °C for 2 hours in full strength and systematically half strength electrolyte as well as water and alkaline solutions. The prepared polyacrylamide was then dosed to an electrolyte prior to electrowinning for 6 hours in a rotating cylinder electrode. The full-strength electrolyte contained 36 g/L copper, 160 g/L sulfuric acid and 25 mg/L chloride. A statistical analysis revealed that by preparing the polyacrylamide in a 16-fold diluted electrolyte the lowest surface roughness was achieved. It was proposed that the polyacrylamide prepared in the 16-fold diluted electrolyte produced a block polymer hydrolysis product termed activated polyacrylamide (APAM).

In the same work, Fabian et al. (2007) studied the effect of current density, deposition time, diffusion layer thickness, temperature, Guarfloc66, and APAM on the surface roughness of electrodeposited copper. The level of these variables was chosen to approximate the current operation conditions on an electrowinning plant. The low-level concentration of organic additive was set at 0.5 mg/L electrolyte, while the high-level factor was set at 1 mg/L. Electrowinning tests (up to 6 hours) on a rotating cylinder electrode revealed that a more uniform electrode surface was obtained when APAM was used as additive instead of Guar. Regression models suggested that a significant reduction of deposit surface roughness can be expected by using APAM at an electrowinning temperature of 65 °C. Fabian et al. (2007) continued with bench scale continuous electrowinning tests at 50°C for 44.6 hours using a parallel plate electrode setup. The experimental results showed that by using APAM, smoother and brighter copper cathodes were produced. Porous copper deposits were achieved when Guar was used compared to the slightly columnar copper deposit when APAM was used as the additive.

Helsten and Moats (2012) found that a polyacrylamide product was more effective at low concentrations (2 mg/L) than HydroStar or a HydroStar/Guar mixture to produce smooth copper electrodepositions. Electrowinning was conducted in a laboratory scale setup at 40°C for a duration of 1 hour of electrodeposition (Moats et al. 2016).

2.5.3 Classification

Smoothing agents can act to either polarize or de-polarize the copper electrodeposition by increasing or decreasing the activity of the cuprous ions close to the cathode surface (Moats et al. 2016). Organic additives polarize the copper electrodeposition when they initiate a decrease in the rate of reaction at a fixed potential. The copper electrodeposition will be de-polarized if the organic additive enhances the rate of reaction at a fixed potential. Fabian et. al (2009) found that Guarfloc66 acted to slightly de-polarize the copper deposition, while PAM additives consistently acted to polarize the deposit (Alex Luyima et al. 2016; Moats et al. 2014). Additives that inhibit or polarize the copper electrodeposit are believed to adsorb onto the surface of the working electrode, thereby decreasing the area available for plating and increasing *effective* current density resulting in an increase of the overpotential. This manifestation is indicated by the Tafel equation, Equation 2.28. Clearly, certain additives affect the properties,

Stellenbosch University https://scholar.sun.ac.za

electrochemistry, and morphology of the copper deposit on the cathode. Table 2.1 gives a summary of the organic additives and their respective classifications. A description of the various classifications of organic additives follows thereafter.

Table 2.1: Summary of copper electrodeposition organic additives by category from Moats et al, (2016).

Brightener	Leveler	Carrier/suppressor/inhibitor
Thiourea	Polyacrylamides	Polyethylene glycol (PEG)
Bis (sodium sulfopropyl) disulfide (SPS)	Glue	Polyalkylene glycol (PAG)
	Thiourea	Glue
	Benzotriazole (BTA)	Gelatin
	Janus Green B (JGB)	Polyacrylamides

2.5.3.1 Levelers

Levelers are typically added to the electrowinning process to achieve a geometric change on the copper cathode. Levelers are nitrogen containing compounds and usually produce a smoother surface with less protrusions or edges. It is stated that levelers and brighteners usually work well with each other as in copper electrorefining where glue and thiourea are often used together.

2.5.3.2 Brighteners

Brighteners aid in orientating the grain structure of the deposit which affects the deposit appearance, making it appear brighter and shinier. Generally, they are sulfur bearing compounds that interact with the copper on the surface of the cathode to form Cu-S bonds (Moats et al. 2016). Brighteners often refine the copper deposit structure by acting to catalyze the deposition reaction and by promoting the formation of new nuclei.

2.5.3.3 Carriers

Carriers are also known as suppressors or inhibitors. Carriers are known as polarizing agents and are believed to affect both the copper dissolution and deposition process. These additives interact with the surface to produce tighter packed deposits.

2.5.3.4 Chloride ion

Chloride ions are classified as inorganic but serve as a perfect example of a de-polarizing agent that enhance the rate of copper plating. Chloride ions are essential in any copper electrowinning circuit that use organic additives as they assist with the surface interactions between the organic additives and the copper (Shao et al. 2007).

2.5.4 Effect of organic additives on copper nucleation and growth

It is known from literature that organic additives play a significant role in the relationship between the current and the potential of the electrical system (Moats et al. 2014; Luyima et al. 2016; C P Fabian et al. 2007). The reason for their influence on the current/potential is due to the competition for surface

coverage with chloride ions and other species present in the electrolyte system (Fabian et al. 2007). The control of the metal nucleation and growth onto the electrode surface during the deposition process is a strong function of the type and quantity of organic additive added to the system.

The competition for surface coverage between the various ions present in the system is represented in Figure 2.6 (Bard & Faulkner 2000). Figure 2.6 illustrates the region near the surface of the electrode known as the electrical double layer which comprises the whole array of orientated dipoles and charged species close to the electrolyte/electrode interface. The double layer is thought to be made up of many layers, with the layer closest to the electrode called the inner Helmholtz plane (IHP). This layer is said to contain solvent molecules and other ions which are specifically adsorbed. Non-specifically adsorbed solvated ions can approach the electrode only to a distance x_2 in the outer Helmholtz plane (OHP). The interaction of the non-specifically adsorbed solvated ions and the electrode surface is therefore only via long-range electrostatic forces and independent of the chemical properties of the solvated ion. Literature indicates that the presence of organic additives changes the interaction of the solvated copper cations and the specifically adsorbed anions in this electrical double layer region on the cathode surface (Fabian 2005c; Bard & Faulkner 2000). The presence of diverse types of organic additives lead to distinct types of specifically adsorbed ions in the inner Helmholtz layer contributing to the different nucleation and growth mechanisms observed respectively.

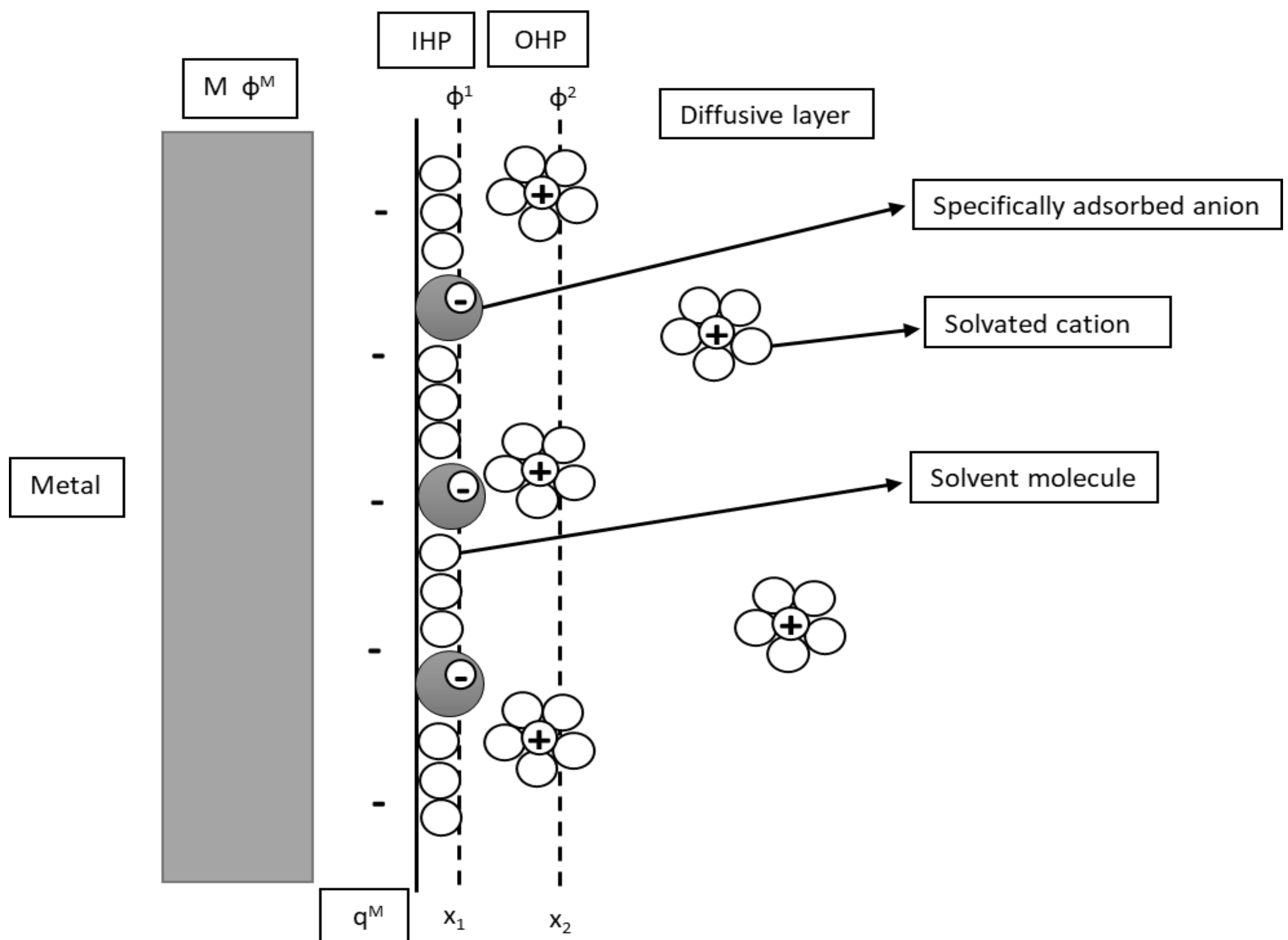

Figure 2.6: Proposed schematic diagram model of the double layer region under conditions where certain anions are specifically adsorbed adapted from Bard and Faulkner (2000).

Winand conducted an extensive study on the theory and application of electrocrystallization in 1992. In this study Winand's Diagram is introduced and can be seen in Figure 2.7. Winand's Diagram was

Stellenbosch University https://scholar.sun.ac.za

developed to exhibit the relationship between the type of electrodeposit growth and structure, the ratio between current density and the DLC density, and the inhibition intensity. The identification of the growth type of polycrystalline electrodeposits that was used by Winand was first described by Fisher in 1969 and can be classified into 5 main categories (Winand 1992; Fischer 1969):

i. Field-oriented isolated crystals type (FI)
ii. Basis-oriented reproduction type (BR)
iii. Twinning intermediate type (Z)
iv. Field-oriented texture type (FT)
v. Un-oriented dispersion type (UD)

Before the 5 main growth types can be discussed, the term *inhibition* must first be explained. According to Fischer (1969) inhibition occurs when there are substances (ions, molecules etc.) present other than M^{z+} or the corresponding adatom in the electrical double layer or diffusion layer as seen in Figure 2.6. These substances are called inhibitors because they act to hinder the cathodic process. Inhibitors do not cover the entire cathode surface area but favor active high energy sites and are physically or chemically adsorbed (Winand 1992). Inhibitors can be:

- Poisonous/impurity substances that cause the cathodic reaction to occur at an increased overpotential and thereby wasting energy unnecessarily.
- A substance that reduces simultaneously with M^{z+}, thereby reducing the current density and lowering the current efficiency.
- A substance that changes the metallographic structure and texture of the deposit.
- A substance that changes the overpotential value by affecting the diffusion/rate constants.

Organics in solution have various effects on the electrodeposition of the copper. Winand (1992) further gives 4 possible ways in which an organic substance will behave/not behave as an inhibitor:

i. Strong inhibition can be expected from an organic that has no affinity for water and adsorbs onto the metal surface.
ii. Little inhibition can be expected from organic compounds that have an affinity for water and adsorb onto the metal surface.
iii. Organic additives will act to slightly activate the reduction process if the organic does not adsorb onto the metal surface but has an affinity for water.
iv. No effect can be expected from organic additives with no affinity for water and no adsorption on the metal surface.

In Figure 2.7 the level of inhibition and the magnitude of the ratio between current density and the DLC density (J/J_d or i/i_{DLC}) is related to the type of growth that can be expected.

Stellenbosch University https://scholar.sun.ac.za

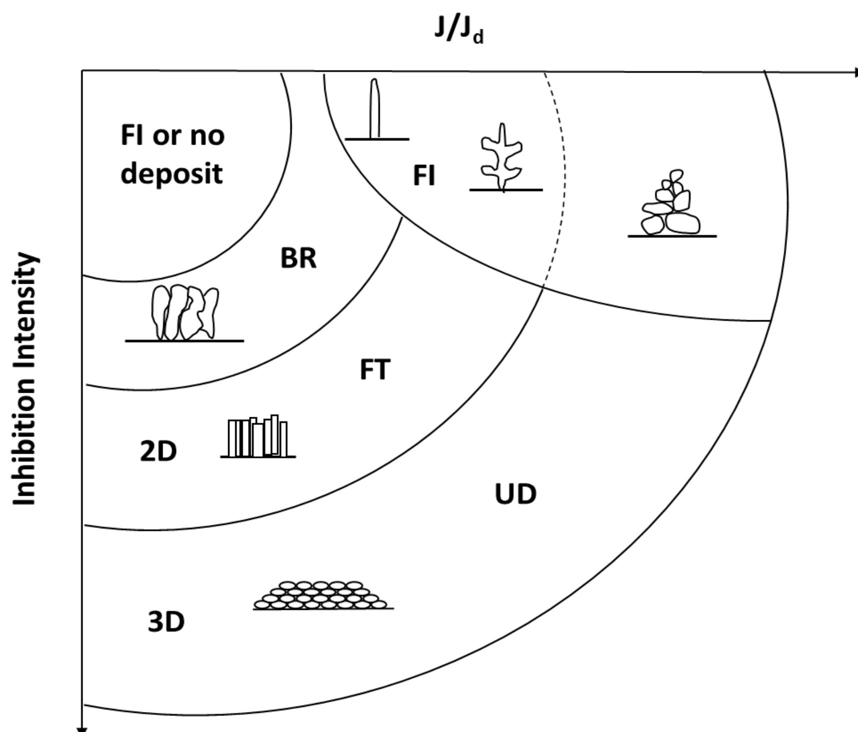

Figure 2.7: Simplified diagram illustrating different polycrystalline deposit types as a function of inhibition intensity and J/J_d adapted from Winand (1992).

FI growth type can be expected at low inhibition levels with whiskers, then dendrites, and finally powder forming when the current density is increased. At moderate inhibition intensity and current density BR type crystal growth is observed. Here, sufficient time is available for good lateral growth, though the crystal may become so large that it entraps electrolyte in the crystal structure. BR type growth can degrade to FI type growth if the electrolysis period becomes too long. Type Z growth is described by Fischer (1969) as a mixture between growth types BR and FT. FT crystal growth is characterized by elongated crystals that grow perpendicular to the cathode surface and is observed at relatively high inhibition and current density levels. This type of growth is usually desired in copper electrowinning processes due to the coherent deposit morphology achieved. UD crystal growth is achieved at very high inhibition intensity and current density and is characterized by a dispersion type, uniform, small grain structure deposit. Promoting this type of crystal growth is most expensive due to the cost of the excessive amount of additive and energy related to drive the reaction. When running at these extreme levels of current density and inhibition level, one also runs the risk of producing a powder like deposit which is not desirable. Even though Figure 2.7 only gives a qualitative relationship between crystal growth type, inhibition intensity, and current density it still serves as an effective tool in the design and understanding of electrocrystallization experiments.

2.6 Electrochemical techniques

2.6.1 Voltammetry

Voltammetry is an electrochemical technique that involves a potential scan to observe variations in current as a function of voltage. Voltammetry has the advantage that it has few limitations and can be used for a wide variety of electrochemical investigations. The two most common methods are linear sweep voltammetry (LSV) and cyclic voltammetry (CV). The difference in these two methods resides in the way in which the potential is controlled during the experiments. LSV encompasses the continuous

Stellenbosch University https://scholar.sun.ac.za

variation of potential with time between the working and reference electrode, while the current is measured as a function of the varied potential. CV is essentially the same process, except that the potential is varied between two set potential values. The cycle of sweeping the potential from an initial to a final potential and then back to the initial potential can be repeated numerous times to determine how the reaction in the cell is affected.

CV is perhaps the most versatile of the two electrochemical methods and can be used to obtain valuable information about the electroactive species. In conventional CV experiments the current is measured as a response to a linear potential sweep, which has a triangular waveform shown in Figure 2.8. The potential is swept linearly between E_1 and E_2, and while the variation in current is recorded at the working electrode.

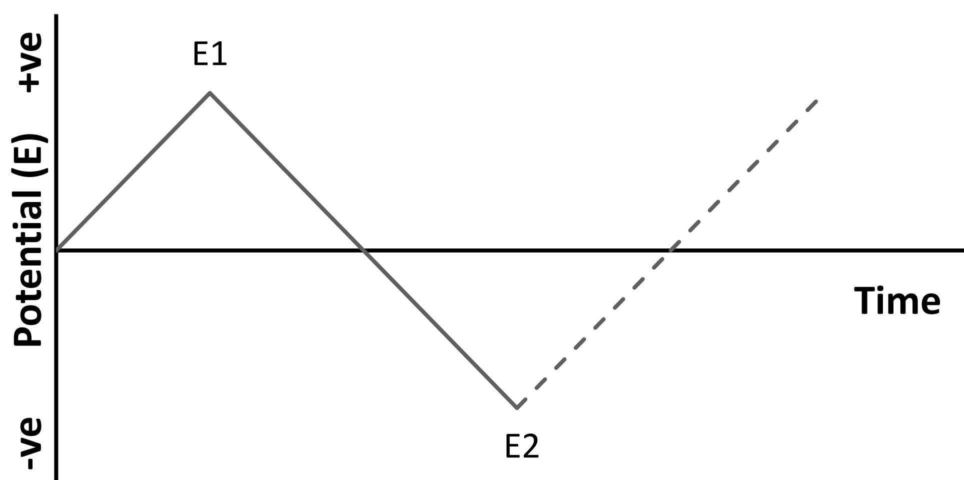

Figure 2.8: Switching linear potential sweep during a CV test.

When the potential is swept in the negative direction from E_1 to E_2 a cathodic current is achieved. The negative potential sweep is labelled the cathodic sweep where electrons migrate from the electrodes to the solution promoting reduction of oxidized species at the surface of the working electrode. The anodic sweep encourages oxidation rather than reduction and an anodic current is observed which is often related with a positive current value. The electrochemical technique of cyclic voltammetry has been used by numerous researchers to study the effect that organic additives have on the behavior of copper deposition during electrowinning (Fabian et al. 2006; C P Fabian et al. 2007; Cui 2014; Moats et al. 2014; Luyima et al. 2016).

2.6.2 Electrochemical Impedance Spectroscopy (EIS)

Electrochemical impedance spectroscopy (EIS) is an electrochemical technique used to effectively characterize electrode processes. EIS experiments involve the response analysis of a system that was exposed to periodic small amplitude AC signals. A sinusoidal potential (current) is applied at a set frequency and the response is measured to compute the impedance at that frequency. The process is then repeated for a wide range of frequencies and the data is usually presented as Nyquist or Bode plots for analysis and interpretation. Impedance is the frequency dependent resistance to current flow of a circuit element. Resistance as defined by Ohm’s law is the impedance at a limit of zero frequency. Resistance is therefore a type of impedance, and the equivalent equation to calculate impedance is given in Equation 2.31

Stellenbosch University https://scholar.sun.ac.za

$$Z_\omega = \frac{E_\omega}{I_\omega} \quad 2.31$$

Where

Z_w Impedance

E_w Frequency – dependent potential

I_w Frequency – dependent current

EIS is used as a tool to gain insight into the kinetics of the electrochemical system, and it specifically relays information about the charge transfer resistance (R_{CT}), solution resistance (R_S), and double layer capacitance (C_{DL}) of the electrochemical system (Cui 2014). The values of these various measured resistances can be used to model the electrochemical cell as a network of passive circuit elements. R_{CT} is also known as the polarization resistance (Fabian et al. 2009). R_S relays information about the solution characteristics especially in terms of its conductivity. C_{DL} relays information of the specific system's ability to store electrical energy by means of the electrical double layer effect (as discussed in Section 2.5.4). Often the double layer region does not behave as a perfect capacitator in which case a constant phase element (CPE) is modelled instead of a capacitator (C_{DL}), to model the double layer as an imperfect capacitator.

Figure 2.9 presents a typical Nyquist plot on a complex plane, with the imaginary and real impedance values as a function of frequency. Each data point represents a measurement at a specific frequency, ranging from high frequencies (left side) to low frequencies (right side). The intercept on the x-axis at the high frequency region of the curve represents the solution resistance (R_S) of the specific experimental run. The intercept at the end of the first semicircle is the sum of the solution resistance and the charge transfer resistance (R_{CT}). The horizontal semicircle (arc) diameter is therefore equal to the R_{CT}. The double layer capacitance (C_{DL}) can be calculated by using the frequency at the peak of the semi-circle.

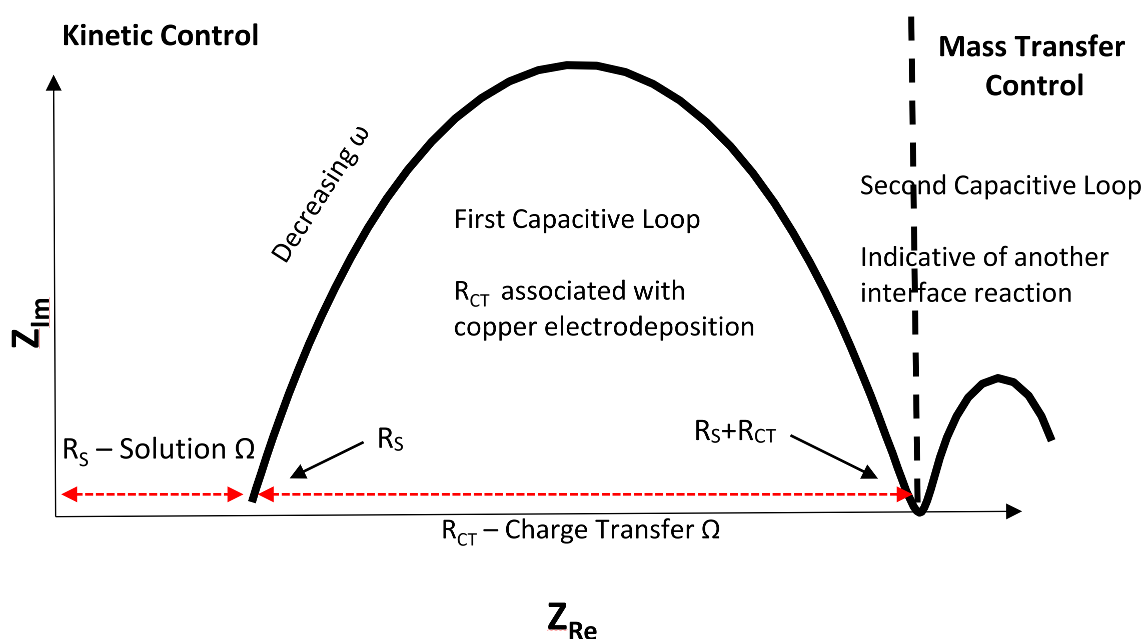

Figure 2.9: A typical Nyquist plot showing the electrochemical impedance spectra of copper electrodeposition in an electrolytic solution.

Stellenbosch University https://scholar.sun.ac.za

Many researchers have used the technique of EIS to determine the effects of organic additives on the resistance/polarization behaviour during the copper deposition process (Gabrielli et al. 2006; Fabian et al. 2009; Moats et al. 2014; Luyima et al. 2016). This technique will allow for characterization and comparison of the tested organic additives during the electrodeposition process in terms of their unique interaction with the cathode surface in the double layer region.

2.6.3 Chronopotentiometry

Chronopotentiometry (CP) is described to be the most basic constant current experiment (Bott 2000). In CP, a current pulse is induced over an electrochemical cell and the resulting potential is then measured against a reference electrode as a function of time. The interaction between current and potential is used to relay information to the researcher. CP is an electrochemical method used to gain further insight into the kinetics and mechanisms governing the system. CP can also be used to determine diffusion coefficients of ions present in the bulk.

2.7 Effects of operating parameters in copper electrowinning

The main process variables influencing the surface roughness of the copper deposit onto the cathode are: current density, electrolyte fluid flow as described by the diffusion layer thickness (δ), temperature, deposition time, chloride ions, and organic additives (Fabian et al. 2006; Cui 2014). Dini & Snyder (2011) state that the character of copper deposits is influenced by free acid, additives, concentrations of copper, cathode current density and the nature and degree of agitation in the electrowinning cell. These overlapping parameters obtained from literature are therefore considered and discussed in the following sub Sections 2.7.1 to 2.7.9.

2.7.1 Temperature

The temperature of the electrolyte is usually controlled by a heat exchanger setup before the electrowinning cells. The optimum electrolyte conductivity is achieved at an operating temperature of between 45 ℃ and 55 ℃ (Beukes & Badenhorst 2009). Dini & Snyder (2011) reported that the common temperature range for copper electrowinning is between 32℃ and 43℃. This temperature range reported by Dini and Snyder (2011) is supported by Cui (2014). The SX organic phase will degenerate if it is brought into contact with a spent electrolyte with a temperature above 40℃ (Beukes & Badenhorst 2009).

The physicochemical properties and mass transfer of the electrolyte are affected by temperature and therefore, ultimately the energy efficiency of the electrowinning cell is also affected by temperature. An increase in temperature reduces the viscosity of the electrolyte resulting in an increased diffusion coefficient of ions in the solution, thereby improving mass transfer in the system. Ehsani et al. (2016) showed that by increasing the temperature of an electrowinning cell a beneficial effect on the deposition rate, current efficiency, and energy consumption is achieved. A reduction of approximately 10% in energy consumption was observed when increasing the electrolyte temperature from 20℃ to 50℃ (Ehsani et al. 2016). It was hypothesized that the reduction in energy consumption due to the increase in electrolyte temperature could be attributed to the significant increase in the number of high energy collisions with the increase in temperature. In this work of Ehsani et al. (2016) the improved kinetics in the cell lead to a reduced cell voltage of approximately 0.09V. The study of Ehsani et al. (2016) did however also indicate that the surface roughness of the copper cathodes increased with an increase in temperature. The findings of Ehsani et al. (2016) suggest that effective control of temperature should be implemented to establish a balance between the deposition rate and the deposition quality of the copper in the electrowinning cell.

Stellenbosch University https://scholar.sun.ac.za

2.7.2 Concentration of copper ions

Copper sulfate pentahydrate ($CuSO_4 \cdot 5H_2O$) and sulfuric acid are the main constituents of a synthetic electrowinning electrolyte solution. Panda et al. (2001) studied how a change in copper concentration influenced the cell voltage, anode potential and current efficiency. The copper concentration was varied between 10-50 g/L and it was found that the copper concentration had little to no effect on either one of the three independent variables that were tested. This supports the assertion of Dini & Snyder (2011) that copper concentration is not a critical parameter in the process of electroplating.

2.7.3 Concentration of electrolyte

Variation in sulfuric acid concentration influences anode and cathode polarization. Dini & Snyder (2011) report that cathode de-polarization is observed with an increase of sulfuric acid concentration up until a sulfuric acid concentration of 38 g/L. A further increase in sulfuric acid concentration from 38 g/L causes cathode polarization. A drastic cathodic overpotential is observed when excess sulfuric acid is added to the electrolyte solution, prompting a smaller ratio of level plane electrodeposits. Excess sulfuric acid addition also increases the surface overpotential which encourages three-dimensional nucleation (Dini & Snyder 2011). Dini & Snyder (2011) further report that the specific conductivity of the electrolyte doubles when the concentration of sulfuric acid is raised from 50 g/L to 100 g/L.

Panda et al. (2001) measured how the concentration of sulfuric acid influenced cell voltage, anode potential and current efficiency. Sulfuric acid concentrations were varied between values of 30 g/L and 150 g/L and a marginal decrease in cell voltage, anode potential and power consumption were observed for an increase in sulfuric acid concentration. The slight decrease in power consumption with an increase in sulfuric acid concentration observed in the results of Panda et al. (2001) is attributed to a decrease in electrolyte resistivity with an increase in sulfuric acid concentration.

Cooper and Mishra (1987) electrowon copper at sulfuric acid concentrations of 20 and 100 g/L, and their study revealed that an increase in surface roughness was observed at higher sulfuric acid concentrations (Cooper & Mishra 1987).

These previous studies suggest that only major variations in sulfuric acid concentration have an influence on the electrowinning process. It is however apparent that a tradeoff exists between decreasing resistivity of the system and increasing surface roughness of the depositing metal by increasing the sulfuric acid concentration.

2.7.4 pH

The pH of the electrolyte plays a significant role during the electrowinning process. In a sulfate electrolyte, the primary anode reaction is the breakdown of water into oxygen and hydrogen ions, otherwise known as electrolysis. This reaction promotes the formation of H^+ ions, steadily causing a more acidic environment. The pH of the electrolyte in the electrowinning cell has a significant influence on current efficiency, hydrogen evolution and the precipitation of hydroxides (Ngandu 2016).

2.7.5 Cathode and anode material

2.7.5.1 Cathode

Copper ions migrate towards the negative terminal (cathode) were they gain electrons and form a copper deposit on the cathode surface. Stainless steel 316 is the material of choice for the construction of cathodes in the industry (Robinson et al. 2013). Stainless steel cathodes are re-useable, less labor

Stellenbosch University https://scholar.sun.ac.za

intensive and a 3% increase in current efficiency can be achieved by using stainless steel compared to using copper as the material of construction (Owais et al. 2015). The minimum spacing from cathode center to cathode center is 95 mm. Any values lower than this is unacceptable because of the risk of short circuiting due to nodular growth (Beukes & Badenhorst 2009).

2.7.5.2 Anode

Lead based alloys are most used as the anode in electrowinning circuits containing a sulfate-based electrolyte. The material of choice for anodes has evolved over the past years migrating from pure lead and lead-antimonial alloys to anodes based on an alloy of lead, calcium (0.05 to 0.08%) and tin (1.2-1.5%) (Mirza et al. 2016; Beukes & Badenhorst 2009). New electrowinning operations almost exclusively use cold-rolled lead anodes to achieve a higher dimensional stability in the cell. Lead is preferred because it is inert and lead has the capacity to form a regenerative oxide layer (PbO_2) on its surface, impeding corrosion and cathode degeneration (Mirza et al. 2016). Cobalt (100-200 mg/L) is usually added to the electrowinning cell to prevent lead anode corrosion. Co^{2+} ions promote oxygen evolution, rather than lead oxidation at the anodes (Robinson et al. 2013). The life expectancy of the new rolled lead-calcium-tin alloy anodes is 7-9 years (Beukes & Badenhorst 2009). The life cycle of anodes is however subject to tank house operating conditions and maintenance of the anodes, including straightening and cleaning.

2.7.6 Flowrate of electrolyte

Najminoori et al. (2015) did a study to compare actual experimental conditions of an industrial electrowinning cell with a CFD simulation model. After validation of the model, the effects of electrical current density, volumetric flowrate of the feed and the distance between electrodes on cell efficiency were studied. Flowrate of the feed electrolyte was varied between 8-11 m^3/h while other parameters were held constant. It was found that an increase in electrolyte flowrate caused an increase in the vertical velocity near the cathode surface. Due to a change in the electrolyte hydrodynamic behaviour, a 0.2% increase in concentration of copper ions between cells was measured at a flowrate of 11 m^3/h compared to 8 m^3/h. The current density remained the same for varying flowrates and therefore according to Faraday's Law the rate of deposition remained the same. The conclusion was drawn that to further improve the deposition rate of copper from the electrolyte to the cathodes at an increased flowrate, the electrical current density should also be increased. At an increased flowrate, the Nernst boundary layer thickness decreases which in turn increases the limiting current density (Najminoori et al. 2015).

2.7.7 Current density

Current density is perhaps the most important electrowinning parameter when it comes to cathode morphology and energy efficiency. Faraday's law of electrolysis states that the rate of metal reduction is proportional to the electrical current applied to the system. The amount and quality of the copper deposited onto the cathodes is therefore immensely dependent on the consistency of the applied current over the cathode surface.

According to Beukes and Badenhorst (2009) the typical current density in an industrial electrowinning cell ranges in value between 200 – 375 A/m^2. Most electrowinning tank houses following a SX circuit operate in the range of 250 – 300 A/m^2, given that coalescing units and filters are installed to remove organics and solids before the electrolyte enters the electrowinning tank house (Beukes & Badenhorst 2009).

The limiting current density (i_L) of the system is the current density at which the deposit will become powdery and hydrogen gas will start to evolve (Winand 1992). According to Winand (1992) it is possible to achieve acceptable deposit morphology at operating conditions between 80-90% of i_L. Electrowinning

Stellenbosch University https://scholar.sun.ac.za

tank houses are however operated at around 50% of its estimated i_L value because of unevenly distributed current and the tendency to form dendrites and nodules in large scale operation.

2.7.8 Chloride Ions

Chloride ions are often not added to the electrowinning circuit but transferred from the SX circuit. It is important to understand the effect of chloride ions on the deposition process, especially since chloride mostly exists naturally in the electrolyte. Most electrowinning operations operate with a chloride concertation of between 20-30 mg/L (Robinson et al. 2013). The reason for this being that chloride levels of above 30 mg/L lead to pitting corrosion on top of the stainless-steel cathode surface at the air-electrolyte interface.

Chloride ions are known to act as de-polarizers (accelerators) and grain refiners and in the copper deposition process (Moats et al. 2016; Dini & Snyder 2011; Cui 2014). Sun and O' Keefe (1992) reported that the rate of reaction is increased when 40 mg/L of chloride is present in the electrolyte, possibly because of copper-chloride complexes formation. It was also found that an increase of chloride ions enhanced surface roughness and impurity levels on the cathode. Chloride ions should be used in conjunction with a polarizing organic additive to benefit from its reaction accelerating benefits without compromising on cathode quality as was proved by Fabian (2005).

2.7.9 Organic additives

Organic additives promote the plating of more uniform and dense copper cathodes, while they also assist to minimize physical entrapment of electrolyte impurities (Robinson et al. 2013). The type of organic additive that is chosen for the electrowinning circuit is largely dependent on its compatibility with the SX stage. Without the use of an organic additive it becomes impossible to regulate the growth of nodules and dendrites on the cathode surface. Organic smoothing agents are essential to the copper electrowinning process because they drastically reduce the manifestation of short-circuiting on plants resulting in a higher, more consistent copper product throughput. Section 2.5 of this report gives an in-detail analysis of how these additives interact with the cathode, and why they are so imperative in copper electrowinning.

Stellenbosch University https://scholar.sun.ac.za

2.8 Summary

It has been shown in this review that organic additives play a significant role in the copper electrodeposition process. Organic smoothing agents facilitate the formation of smoother, brighter, and denser copper cathodes. The organic smoothing agents interact with the surface of the cathode by competing with copper atoms for adsorption on high energy nucleation sites. The adsorption mechanisms of distinct types of organic additives vary, because of the unique molecular characteristics of each organic additive. Very little work has been done to describe the adsorption mechanisms of modified polysaccharides and polyacrylamides that are currently being used in electrowinning processes. Guar has been the industry standard organic additive in copper electrowinning for almost 50 years and little literature was found on its adsorption mechanisms during this process. Recent studies have shown that by utilizing various types of organic additives in the copper deposition process different current densities, cathode morphologies, and cathode purities were achieved. Therefore, by using electrochemistry, more specifically CV and EIS, the polarization behaviour and mechanisms of selected polyacrylamides and Guar can be investigated during the copper electrodeposition process. Electrowinning tests can serve to describe the type of crystal growth developed in the presence of each selected organic additive respectively. The combination of electrochemical and electrowinning tests will effectively aid in the process of describing the adsorption mechanisms of the relevant smoothing agents, and to relate their molecular characteristics to cathode morphology and potentially energy efficiency.

Stellenbosch University https://scholar.sun.ac.za

3 EXPERIMENTAL

Experimental work for this study is divided into two major phases. During the first phase, fundamental electrochemical studies were conducted on a three-electrode (RDE) setup. Cyclic voltammetry (CV) and electrochemical impedance spectroscopy (EIS) tests were conducted to obtain kinetic parameters and to characterize electrode processes. More specifically, the performance of Guar was compared to that of alternative organic additives in the form of polyacrylamides (PAMs). Electrochemical impedance spectroscopy experiments allowed the electrolytic cell to be modelled as a series of resistances. Much information about the double layer capacitance, electrode processes and process kinetics could be derived from the developed resistance model. CV tests revealed information about the polarization behaviour of the various additives that were tested in the fundamental studies. These tests allowed the researcher to classify the additives as polarizing or de-polarizing agents. The polarization behaviour of the respective additives aided in proposing mechanisms for the behaviour of organic additives in copper electrowinning.

The second major phase of the experimental work involved actual electrowinning tests utilizing both a three-electrode setup and a bench scale EW setup. The electrowinning experiments on the three-electrode (RDE) setup were conducted to classify the type of nucleation and crystal growth that was promoted by each organic additive independently. Classification was based on Winand's Diagram, shown in Figure 2.7 (Winand 1994). The fundamental studies and the RDE electrowinning experiments provided the basis for the selection of the organic additives that were tested in the bench scale electrowinning experiments. The aim of the bench scale experiments was to determine how additive type effected the eventual cathode morphology under conditions like those experienced in an operating electrowinning facility (Conditions described in Section 2.7). Furthermore, the bench scale experimental work was conducted to investigate whether the results achieved on a fundamental level are translatable to a practical/macro level. Correlations were drawn from the fundamental studies to further develop possible mechanisms in which organic additives act to influence and shape the eventual morphology of the copper deposition on the cathode surface. Table 3.1 summarizes the experimental approach and gives an indication of the specific experimental technique/procedure that was used to address the hypothesis and key questions of this study.

Stellenbosch University https://scholar.sun.ac.za

Table 3.1: Summary of the experimental approach.

Hypothesis	Key Questions	Experimental
Copper cathodes produced in presence of a polyacrylamide will be smoother than those produced by Guar. Polyacrylamides polarize the cathode surface allowing for effective dispersion of Cu^{2+} ions across the cathode surface, whereas polysaccharides do not have this dispersion effect. An increase in cathode polarization will be achieved with an increase in additive concentration.	• How is the over-potential of the electrolytic cell affected by the presence of various polymeric additives in the electrowinning cell? • What is the relationship between the polymeric structure of the organic additive and the polarization behaviour experienced at the cathode surface? • What is the relationship between the concentration of the organic additive and the polarization behaviour experienced at the cathode surface?	Fundamental studies using the techniques of cyclic voltammetry and electrochemical impedance spectroscopy on a standard three-electrode setup with a RDE.
A decrease in the PAM molecular weight will increase the surface coverage of the adsorbed PAM additive resulting in an increased polarization effect. The more evenly distributed the surface coverage the smoother the eventual deposit of the copper.	• What is the relationship between cathode morphology and the structure/ characteristics of the organic smoothing agent used in the copper electrowinning process? • Will the additive type influence the current efficiency of the copper electrowinning system?	Electrowinning experimental work utilizing a three-electrode (RDE) setup to investigate nucleation and crystal growth type. Electrowinning experiments on a bench scale pilot plant setup to investigate final cathode morphology.

Stellenbosch University https://scholar.sun.ac.za

3.1 Electrochemical experiments

3.1.1 Materials

3.1.1.1 Synthetic electrolyte

A synthetic electrolyte containing 35 g/L copper (Cu^{2+}), 160 g/L sulfuric acid (H_2SO_4), and 25 mg/L chloride (Cl^-) was prepared with analytical grade reagents. De-ionized water was used for the preparation of the electrolyte. The electrolyte concentrations values were based on the analysis of operating parameters as presented in Section 2.7, as well as considering the synthetic electrolyte concentrations of similar previous works (Fabian et al. 2009; Luyima et al. 2016). The copper, sulfuric acid, and chloride concentration were kept constant during all the electrochemical experiments. The chemicals used to prepare the synthetic electrolyte are listed in Table 3.2. Sample calculations on the exact amounts of chemicals required for electrolyte and other concentrations can be seen in Appendix C – Sample calculations, Section 8.3.1.

Table 3.2: List of chemicals used to prepare the synthetic electrolyte for all experimental work.

Reagent name	Source	Grade	Molecular weight (Da)
Copper(II) sulphate pentahydrate ($CuSO_4 \cdot 5H_2O$)	KIMIX	AR	249.68
98 wt% Sulphuric acid (H_2SO_4)	KIMIX	AR	98.08
32 wt% Hydrochloric acid (HCl)	Scienceworld	AR	36.46

3.1.1.2 Additives

The molecular weight and the ionic content of the organic additives were selected as the known/controlled molecular characteristics. These molecular characteristics were deemed to be influential on the adsorption behavior of the additives (as indicated in literature review Section 2.5). To investigate the polarization behavior and compare morphology of the copper deposit on the cathode surface, Guar and polyacrylamides ranging in MW and ionic content were selected as the organic additives in the current study. Polyacrylamides were chosen based on the work of Fabian et al. (2007) where it was reported that a high MW flocculant PAM additive acted independently from Guar to produce smoother, more desirable copper cathodes.

Guar and all PAM organic additives were obtained from an industrial reagent manufacturing company (SENMIN). Although it was established that the MW of Guar varies significantly depending on the analytical technique used to determine this, literature indicated that by using the most recent techniques for determining the MW of Guar that the average MW is between 1 000 000 and 2 000 000 Da (Mudgil et al. 2014). See Table 3.3 for summarized information on Guar.

Table 3.3: Summarized information on Guar.

Product Name	Molecular Weight (Da)	Ionic Content	Steric Structure
Guar (Sendep Opt43)	1 x 10^6 – 2 x 10^6	Non-ionic	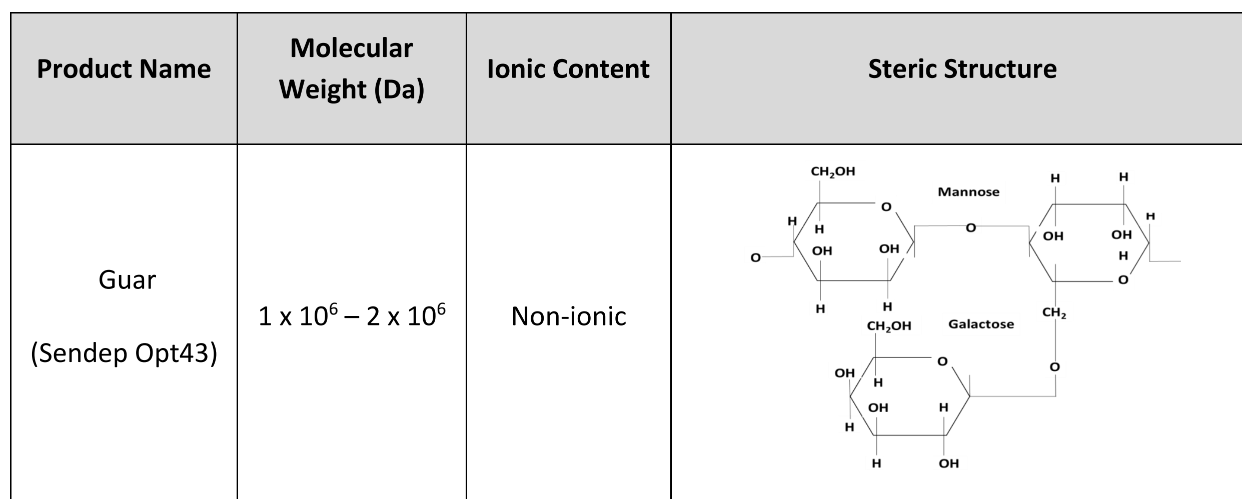

Table 3.4 illustrates the polyacrylamides that were used in this study with their respective estimated molecular weights relative to one another, and their steric structure. Although the exact MW of the additives were not revealed, the relative molecular weight range classification of the polyacrylamides was obtained from SENMIN.

Table 3.4: Polyacrylamides selected for this study with SENMIN MW classification.

Molecular Weight	Ionic Content	Steric structure
Low	Anionic	**Anionic** [CH_2 - CH - CH_2 - CH - CH_2 - CH -]$_n$ C=O, C=O, C=O NH_2, O^-, NH_2
Medium	Non-ionic	
High	Anionic	**Non-ionic** [CH_2 - CH - CH_2 - CH - CH_2 - CH -]$_n$ C=O, C=O, C=O NH_2, NH_2, NH_2
Very High	Non-ionic	

3.1.2 Equipment

All experimental work was conducted using a three-electrode setup. A 150 ml glass jacketed experimental cell was used. A schematic diagram of the utilized setup is presented in Figure 3.1. The electrodes were spaced the same distance from each other for each experimental run with the reference electrode (RE) spaced approximately 2 cm away to the left of the working electrode (WE) and the counter electrode (CE) spaced approximately 2 cm to the right. The electrolyte inside the cell was controlled at a constant temperature of 45°C by circulating hot water from a temperature-controlled water bath through the cell jacket. The cell was used in conjunction with a Gamry RDE710 rotating disk electrode. A Gamry Instruments Interface 1000 potentiostat was used to measure and control the electrochemical

Stellenbosch University https://scholar.sun.ac.za

parameters inside the cell. A platinum tip electrode with a surface area of 0.196 cm^2 was used for all CV and EIS experimental work. A graphite counter electrode and an Ag/AgCl reference electrode (0.210 V vs. standard hydrogen electrode) in 3M KCl were used.

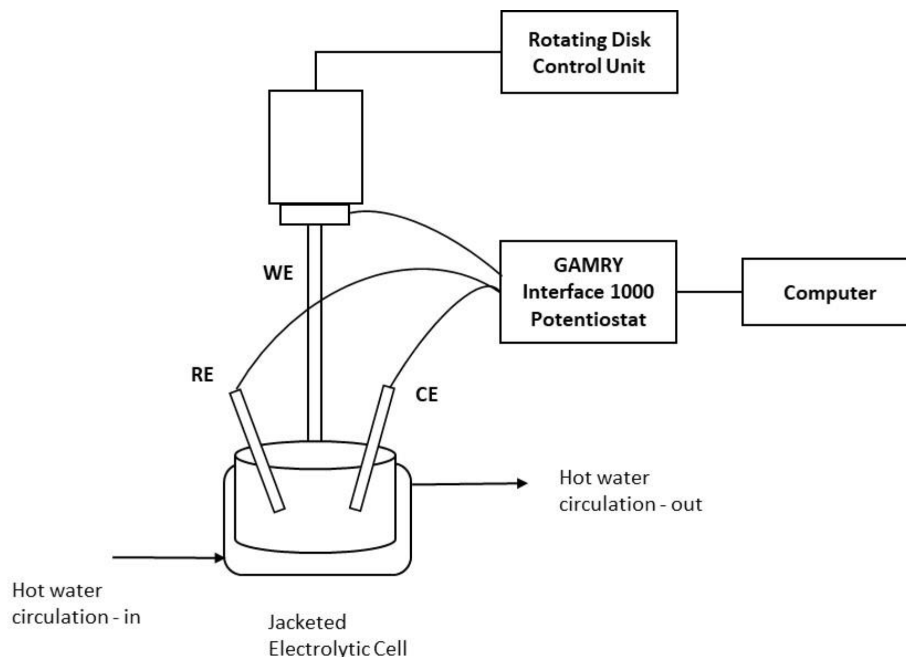

Figure 3.1:Schematic diagram of standard three electrode setup with a platinum tipped RDE.

3.1.3 Methods

The organic additives were prepared before every experiment by dissolution in de-ionized water at a temperature of 40°C for approximately 2 hours. The organic additives were added to the synthetic electrolyte 30 minutes prior to the initiation of each experiment to allow for the organic additive to hydrolyze and unfold in the acidic solution. The three electrodes were introduced to the electrolytic system 5 minutes before the initiation of each experiment. The RDE was set to rotate for 5 minutes at 500 rpm to encourage an even spread of the organic additive throughout the electrolyte and to allow reasonable time for interaction between the organic additive and the cathode surface. Two additive concentrations were investigated, namely 2 mg/L and 10 mg/L. For a stepwise methodology of fundamental work please refer to Appendix B – Stepwise methodology.

CV and EIS experiments were conducted for the following conditions: no additive labelled "Base Case", Guar (Sendep Opt43), and a Low MW (anionic), Medium MW (non-ionic), High MW (anionic), Very High MW (non-ionic) PAM additive at the two concentrations. See Table 3.5 for a full summary of the experimental design for the three-electrode experiments. The PAM additives will be referenced in this document by their MW classification only. Each unique CV and EIS run was performed at least twice, and the average values are presented in the results section. In this work high and low MW are relative terms, and each PAM additive was characterized and classified according to their MW and ionic content by their manufacturer. For a detailed stepwise methodology of the electrochemical pre-experimental methodology, refer to Appendix B – Stepwise methodology.

3.1.3.1 Additive preparation

Each organic additive was prepared anew before every experiment to eliminate the risk of additive degeneration. Exactly 200 mg of organic additive was measured and added to 100 mL of de-ionized water.

Stellenbosch University https://scholar.sun.ac.za

This solution was then placed on a heater stirrer setup at 40°C for 90-150 minutes until fully dissolved. All PAM additives were dissolved completely within the indicated time frame. Guar formed a colloidal suspension, consistent with literature (Fabian 2005a).

After the preparation of the organic additive, a specified amount (depending on the desired final additive concentration in the electrolyte) of the prepared solution was added via a pipette to 150 ml of electrolyte solution inside the jacketed vessel. The additive was then left in the electrolytic solution for another 30 minutes to allow time for the additive to unfold.

3.1.3.2 Cathode cleaning

The working electrode surface was polished using 3 µm diamond suspension and an appropriate polishing cloth. After 5 minutes of polishing, the electrode was rinsed sequentially with acetone and deionized water and left to air dry. This procedure was followed before the initiation of each experimental run. See Appendix B – Stepwise methodology, for a stepwise methodology for cleaning the cathode tip.

3.1.3.3 Cyclic voltammetry

A Gamry Instruments Interface 1000 potentiostat was used to measure and control the electrochemical parameters inside the cell. The cathodic potential, for the CV voltammograms, was cycled between 0.2 V and 0.319 V vs. standard hydrogen electrode (SHE) at a scan rate of 1 mV/s. The voltammograms were logged as current (I) vs. potential (E) and the resultant current densities were calculated by using the known cathode surface area.

3.1.3.4 Electrochemical Impedance spectroscopy

A Gamry Instruments Interface 1000 potentiostat was used to measure and control the electrochemical parameters inside the cell. EIS work was conducted after depositing copper for 6 minutes at a potential of 0.23 V vs. SHE. The frequency was swept between 100 kHz and 100 mHz and the DC voltage during the experimental runs was kept at 0.23 V while an AC voltage of 5 mV rms (root mean square) was maintained throughout. The software utilized to capture the electrochemical measurements was Gamry Framework version 7.05, while Gamry Echem Analyst version 7.05 was used for analysis and modelling purposes.

3.2 Electrowinning experiments

3.2.1 RDE Electrowinning

3.2.1.1 Materials

The same reagents and organic additives were used in the electrowinning experiments as described in Section 3.1.1. The copper, sulfuric acid, and hydrochloric acid remained at the same concentration as reported in the synthetic electrolyte for the CV and EIS experimental work.

The platinum cathode surface was exchanged for a removable stainless-steel surface during the three-electrode electrowinning experiments. The stainless-steel cathode tips were individually constructed by setting a 5- mm diameter stainless-steel disk onto a brass bolt in an epoxy resin. Electrical conductivity was ensured by sticking the cathode disk with silver loaded glue onto the bolt. Finally, the bolt was screwed into the Teflon covered RDE mount. A silicone buffer disk was inserted between the epoxy tip containing the embedded cathode surface and RDE mount to ensure that the electrolyte could not penetrate to the current conducting bolt. The cathode surface was polished with fine sand paper followed by polishing with 3 µm diamond suspension and an appropriate polishing cloth. Figure 3.2 presents the platinum and the self-made stainless- steel cathode tips used in the electrowinning experimental runs.

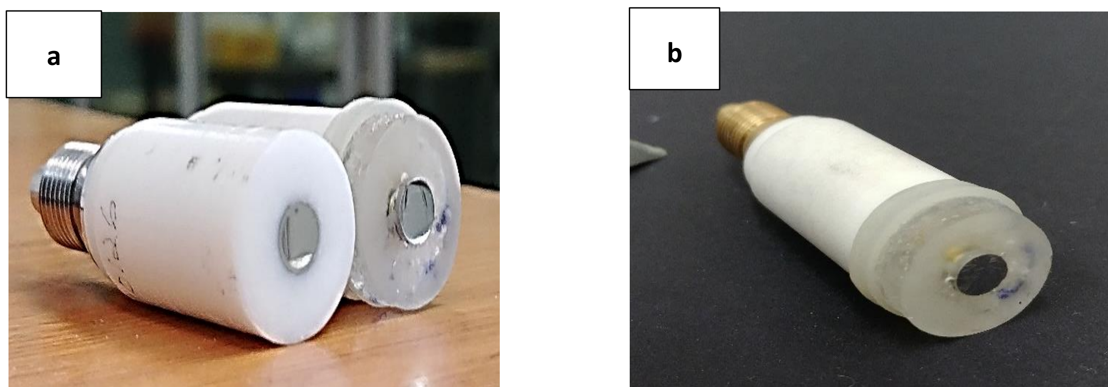

Figure 3.2: a) Polished GAMRY platinum cathode tip on left and stainless-steel cathode tip on the right. b) Self-made stainless-steel cathode tip set in epoxy resin, screwed into the Teflon RDE mount.

3.2.1.2 Equipment

The same equipment was used as for the CV and EIS experiments discussed in Section 3.1.2.

3.2.1.3 Methods

The organic additives were prepared as described in Section 3.1.3.1. for the RDE electrowinning experiments.

Additives at a concentration of 2 mg/L were added to the 150 mL electrolyte solution 30 minutes prior to every experimental run. RDE rotation was initiated 5 minutes before every experiment at 500 rpm. A chronopotentiometry experiment was then initiated on the GAMRY software for electrodeposition at a fixed current density of 300 A/m^2 for a duration 10 s. Chronopotentiometry experiments were repeated for 30 s of electrodeposition. All additives were tested at 10 s and 30 s of electrodeposition and each electrowinning experiment had its own unique cathode surface/tip. After the completion of each experimental run each cathode tip was then stored appropriately (not allowing objects to touch the cathode surface) for SEM analysis of the crystal structure.

3.2.2 Bench Scale Electrowinning

3.2.2.1 Materials

The same reagents and organic additives were used in the bench scale electrowinning experiments as described in Section 3.1.1.

3.2.2.2 Equipment

The electrowinning cell was designed and built specifically for the experimental work of the current study. Cell design was based on specifications and criteria of electrowinning cells used in operating tank houses as discussed in Section 2.7. PVC plastic was the selected material of construction for the cell because of its resistance to acid corrosion at the operational temperature. Stainless steel cathode plates of 15 x 12 cm were bolted to brass plate hangers which slotted into grooves cut into the PVC plastic cell. Similarly, cold rolled lead alloy anodes of equivalent size were bolted to brass hangers which also slotted into the grooves. The 3 mm thick lead alloy anodes were sourced from Polymer Concrete Industries. Acid resistant plastic pipes and connectors were sourced to be used as the circulation pipes. Figure 3.3 presents the actual electrowinning cell used in the experimental work. The cell was designed in such a way to allow for electrolyte overflow recirculation to the stock solution container.

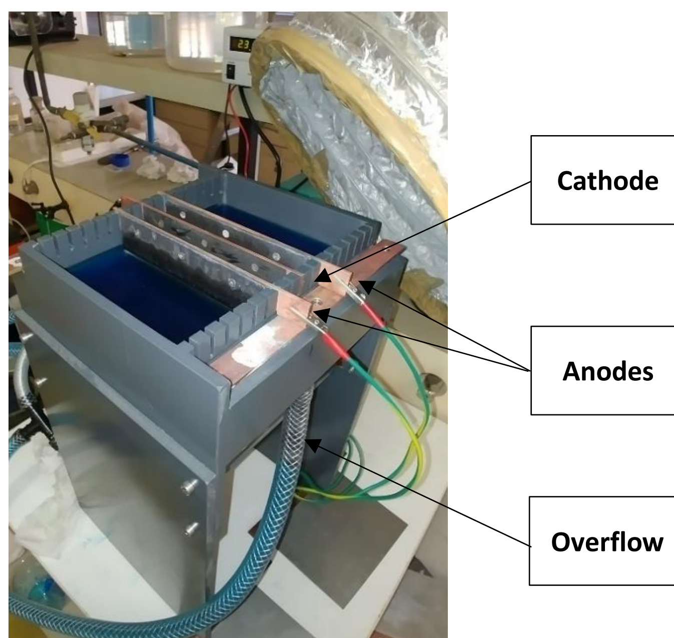

Figure 3.3: Electrowinning cell with circulating electrolyte to achieve steady state before an experimental run.

Figure 3.4 illustrates the entire setup with the water bath, circulation pump and power supply. A Manson switching mode power supply (1-16 VDC, 60 A) and a variable speed peristaltic pump were used.

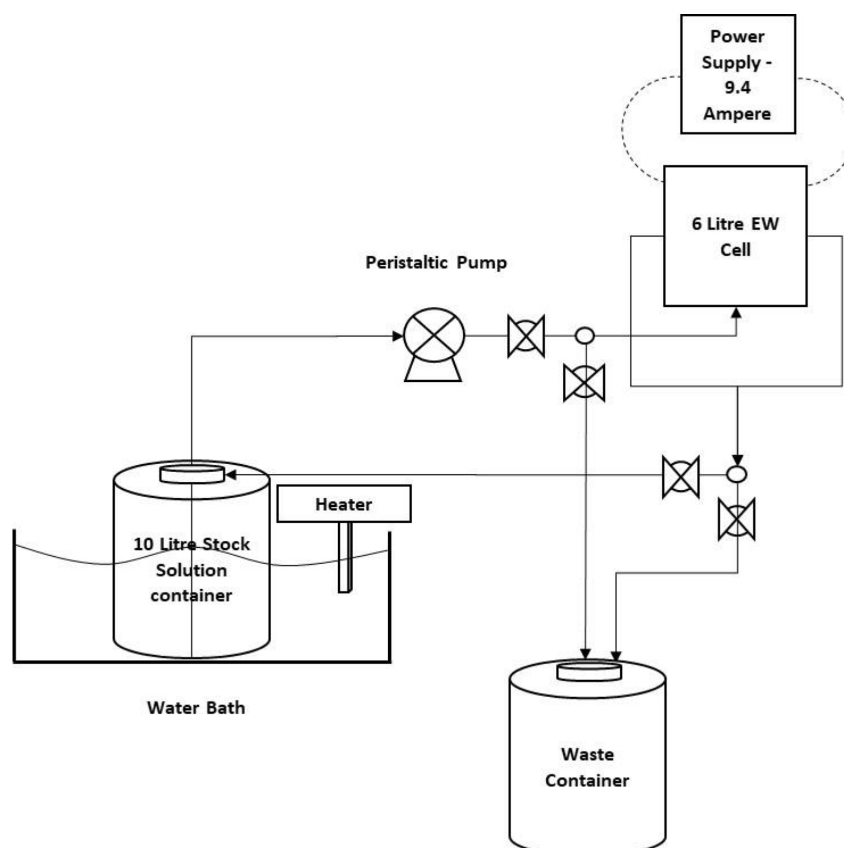

Figure 3.4: Schematic diagram of electrowinning cell and setup configuration/process.

Stellenbosch University https://scholar.sun.ac.za

3.2.2.3 Experimental Method

An electrowinning cell was designed and built to accommodate the bench scale electrowinning experimental work. The same reagents, organic additives, and preparation method were used as in all the previous experimental work of this project. The copper concentration in the electrolyte at initiation of the bench scale electrowinning experiments was increased from 35 g/L in RDE studies to 50 g/L to closer simulate the concentration of an advance electrolyte of an operating copper electrowinning facility (Beukes & Badenhorst 2009). Figure 3.4 presents a schematic process diagram of the bench scale electrowinning setup to be used as a reference during the following methodology description. A stepwise bench scale electrowinning methodology can be seen in Appendix B – Stepwise methodology.

A 15 L synthetic electrolyte was prepared of which only 10 L was heated in a warm bath to 50 °C. Thereafter, a stainless-steel cathode plate was prepared by polishing it with fine (800-1200 grit) sand paper and sequential rinsing with acetone, distilled water, and electrolytic solution. The cathode plate was then inserted in the middle of the electrowinning cell between two lead alloy anodes. The lead anodes were spaced 25 mm away on either side of the cathode centre. Every electrowinning experimental run was conducted on a new cathode plate. The 10 L electrolyte was then circulated through the bench scale electrowinning cell and back into the stock solution until steady state at a temperature of 40°C was achieved inside the electrowinning cell. The electrolyte was pumped at a volumetric flowrate of 0.0063 m^3/h, translating to an interfacial velocity of 0.2 $m^3/h.m^2$ over the total plate surface available for deposition. Once steady state was achieved (after about 20 minutes of circulation), the additives were added to the stock solution container and immediately thereafter the remaining 5 L electrolyte was added to the stock solution container to mix with the electrolyte/additive solution. The final solution had a volume of 15 L and an additive concentration of 2 mg/L. The system was then again allowed to reach steady state at constant temperature and flowrate (approximately 15 minutes) before the power supply was attached to the cathode and anode hangers and switched on to initiate the experiment. The current was controlled at a set current of 9.4 A, translating to a current density of approximately 300 A/m^2 over the entire plate.

Cathode plates were weighed before and after each experiment to be able to compare the rate of plating in each scenario. Scoping experimental tests revealed a plating rate of close to 11 g/hour for electrodeposition in a Base Case electrolyte. The electrowinning experiments were run for 24 hours each to allow sufficient time for multilayer copper deposition on the cathode plate. A vent with an extraction fan was held over the cell to safely remove acid mist from the experimental room. After each experimental run, the cathode was removed from the electrolyte bath and hung to air dry on a drying rack.

3.2.2.4 Analysis method

All cathode plates were analyzed both qualitatively and quantitatively. The analyses were performed by investigating images produced by a surface scanner. An Artec Spider surface scanner was utilized to scan the surface of each copper plate. The high-quality 3D volumetric data of each scanned plate was then imported and analyzed on Volume Graphics VGStudioMax 3.1 - a 3D data viewing and analysis software program.

Artec Spider is a hand-held 3D surface scanner that was specifically developed to be used in conjunction with computer aided design (CAD). The scanning system enables users to scan small items with complex surface structures at 1 million points per second (Kersten et al. 2016). The system works with a linear field of view between 90 x 70 mm^2 and 180 x 140 mm^2 with a measuring range of 0.17 - 0.35 m. Texture

Stellenbosch University https://scholar.sun.ac.za

mapping of objects is made possible by using structured light technology with blue LED as the light source combined with a color camera of 1.4 megapixels (Kersten et al. 2016).

A qualitative analysis of the plates was conducted by visually investigating images of the plate morphology. These images gave a good qualitative reflection of the overall surface roughness of the different plates relative to one another. In addition to the qualitative analysis, a surface roughness quantification technique was implemented as described by Du Plessis et al. (2018).

To be able to calculate a surface roughness value, six areas of interest were selected on each plate. These regions of interest were consistently selected on the same place for each plate. The six square selected regions of interest were deemed to be representative of each sample and comparable to the equivalent areas of interest of all other samples. For each square region, a geometry element (best fit plane) was then created by selecting approximately 15 points along each edge of the region; this best fit plane was subsequently fitted with a mesh of surface elements. Figure 3.5 presents the regions of interest and their corresponding best fit planes for a cathode plate produced during bench scale electrowinning experimental work.

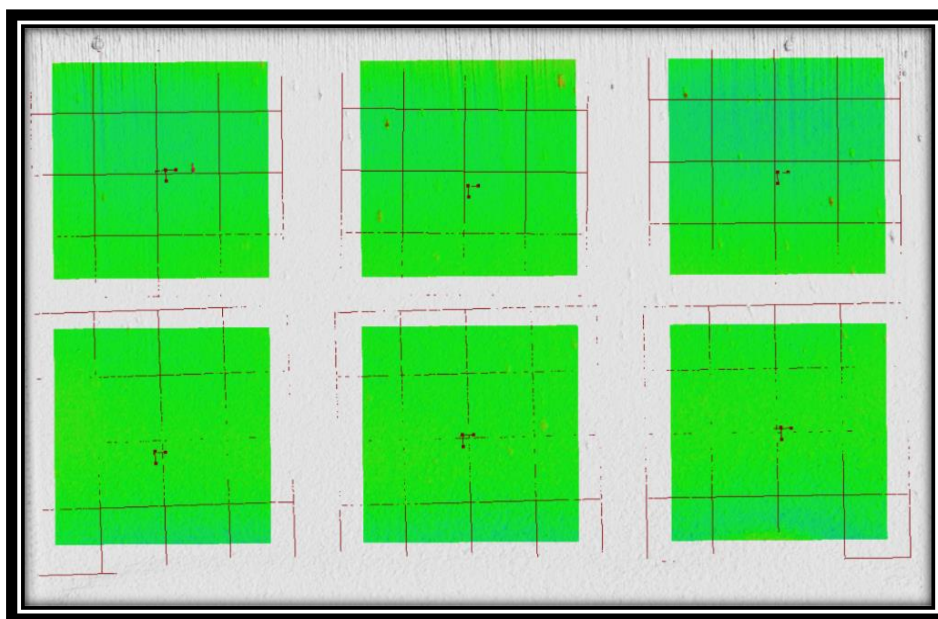

Figure 3.5: Example of surface topography analysis of a copper plate using VGStudioMax 3.1, presenting the 6 selected regions of interest with their respective geometry and mesh elements.

The deviation data could then be extracted via the software as a CSV file for quantitative analysis. The data in each CSV file contained the deviation values (distance from the best fit plane to the copper deposit surface), ranging from negative to positive deviations, in one column, and in the corresponding second the number of surface elements at which that specific deviation from the best fit plane was measured. The arithmetic mean (S_a value) of the distance from the best fit plane to the copper deposit surface measured at each of the surface elements could then be calculated (see Equation 3.1).

$$S_a = \frac{1}{A}\iint |Z(x,y)|dxdy \qquad 3.1$$

The S_a value is very similar to surface roughness of a line (R_a value). An increase in overall surface roughness will therefore result in an increase in the final S_a or R_a value. The S_a value of each plate was calculated by following the described methodology (Du Plessis et al. 2018).

Stellenbosch University https://scholar.sun.ac.za

3.3 Experimental conditions

A summary of the discussed experimental conditions is presented in Table 3.5 and Table 3.6. Both Tables are to be used in conjunction with the result analysis presented in Chapter 4 and Chapter 5 of this document for ease of reference with regards to the experimental conditions.

Table 3.5: Experimental conditions for RDE experimental work.

RDE Experiments **CV, EIS, and RDE Electrowinning**	
Copper concentration [g/L]	35
Sulfuric acid concentration [g/L]	160
Chloride ions concentration [mg/L]	25
CV & EIS additive concentration [mg/L]	2 and 10
RDE electrowinning additive concentration [mg/L]	2
Electrolyte volume [mL]	150
Additive preparation media	Water @ 40 [°C]
Cathode surface deposition area [cm^2] *CV & EIS Working electrode material [platinum] *RDE Electrowinning Working electrode material [stainless steel]	0.196
Electrolyte temperature [°C]	45
RDE rpm	500
CV Scan Rate [mV/s]	1
CV Sweep Limits [V]	0.2-0.319
EIS fixed potential [V]	0.23
Copper pre-plating time for EIS [min]	6
EIS frequency scan range [Hz]	100 000 – 0.1
RDE electrowinning time [s]	10 & 30
Additives	**Ionic content**
Guar (Sendep Opt43)	Non-Ionic

Stellenbosch University https://scholar.sun.ac.za

Low MW PAM	Anionic
Medium MW PAM	Non-Ionic
High MW PAM	Anionic
Very High MW PAM	Non-Ionic

Table 3.6: Experimental conditions for bench scale electrowinning experimental work.

Bench Scale Electrowinning	
Advanced copper concentration [g/L]	50
Sulfuric acid concentration [g/L]	160
Chloride ions concentration [mg/L]	25
Additive concentration [mg/L]	2
Current Density [A/m^2]	300
Voltage drop [V]	2.3
Deposition area [0.15 m x 0.105 m] x 2, m^2	0.0315
Net electrolyte volume [L]	15
Cell volume before plates [L]	5
Electrolyte temperature [°C]	40
Electrolyte circulation rate [m^3/hour]	0.0063
Electrowinning time [hrs.]	24
Additives	**Ionic content**
Guar (Sendep Opt43)	Non-Ionic
Low MW PAM	Anionic
Medium MW PAM	Non-Ionic
High MW PAM	Anionic
Very High MW PAM	Non-Ionic

Stellenbosch University https://scholar.sun.ac.za

4 CV AND EIS RESULTS AND DISCUSSION

4.1 Electrochemical Impedance Spectroscopy

4.1.1 EIS results

Nyquist plots represent EIS data as a function of frequency presenting the imaginary impedance on the y- axis and the real impedance on the x- axis. Figure 4.1 (a) & (b) show the Nyquist plots for each additive at 2 mg/L and 10 mg/L respectively. Each data point represents a measurement at a specific frequency, ranging from high frequencies (left side) to low frequencies (right side). The solid lines in Figure 4.1 (a) & (b) are the fitted models for each unique experimental run. The intercept on the x- axis at the high frequency region of the curves represents the solution resistance (R_S) of each experimental condition respectively. The intercept at the end of the first semicircle is the sum of the solution resistance and the charge transfer resistance (R_{CT}). The semicircle diameter in the high frequency region is therefore equal to the $R_{CT.}$ The double layer capacitance (C_{DL}) can be calculated from the frequency at the top of the semi-circle. The capacitive semi-circle or inductive loop encountered in the low frequency region is more complex and less understood in terms of numbers and parameter values. The phenomena in the low frequency region are believed to be dependent on the surface preparation of the substrate, current density, hydrodynamics, as well as the deposit growth mode and crystallographic orientation (Fabian 2005d).

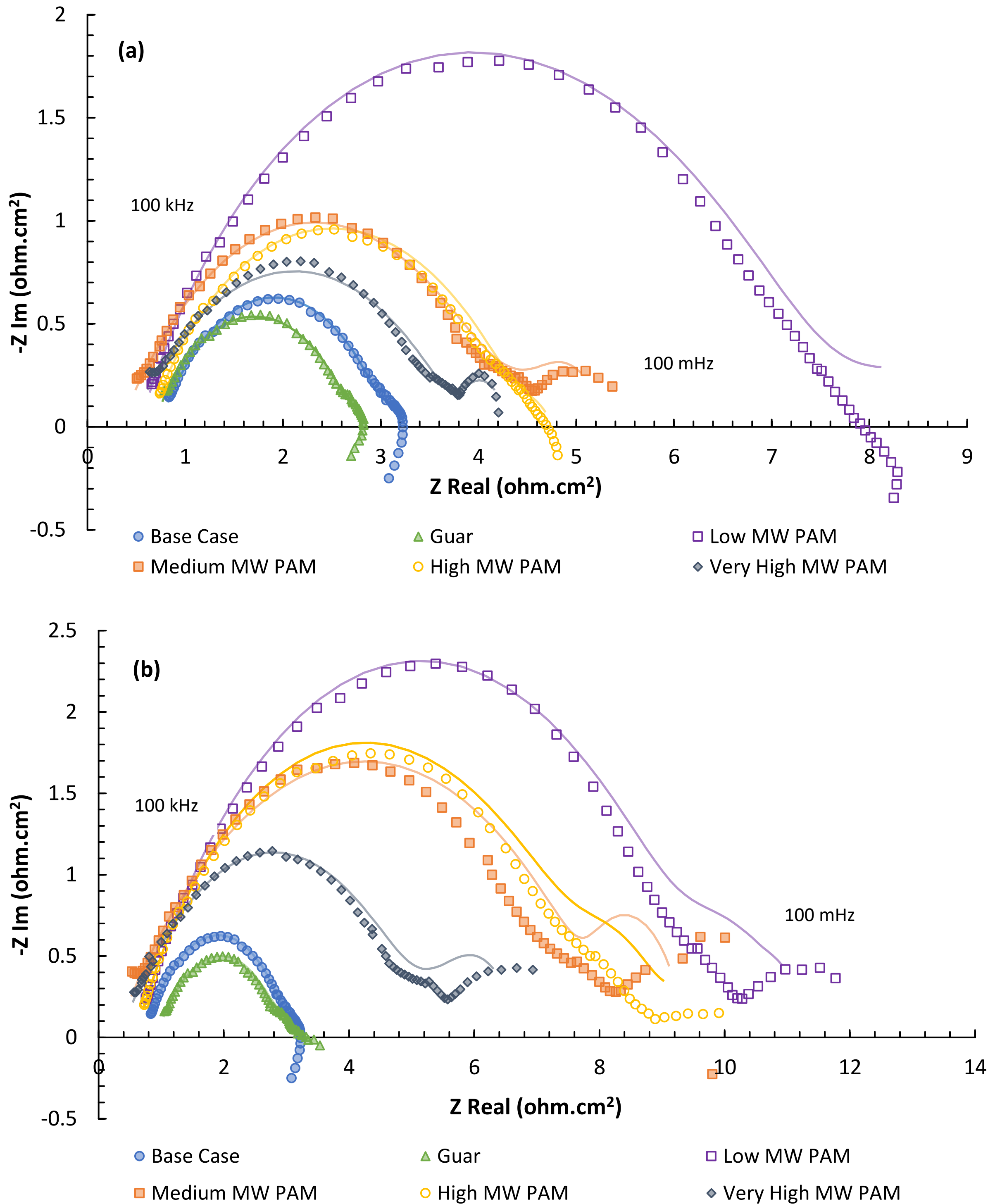

Figure 4.1: Nyquist plots showing the electrochemical impedance data for copper electrodeposition. Conditions: 35 g/L copper, 160 g/L H_2SO_4 and 25mg/L Cl at 45 °C in a RDE setup at 500 rpm, copper electrodeposited for 6 minutes prior to EIS, DC potential of 0.23V vs. SHE with AC rms potential of 5 mV. Additive concentration: a) 2 mg/L b) 10 mg/L.

4.1.2 Equivalent circuit modeling results

Copper is predominantly present as a divalent cation (Cu^{2+}) in the acidic electrolyte. During copper electroplating, the cupric ions are transported towards the negative cathodes primarily via diffusion and convection. Once at the cathode surface the cupric ion undergoes a series of known and recognized reactions before it is transformed into a solid copper deposit (Vereecken et al. 2005). These reaction

mechanisms are less understood in the presence of organic additives. EIS is an effective tool to investigate reaction mechanisms at a solution-solids interface by quantifying the real impedance. A mathematical model, presented in Figure 4.2, was implemented for further analysis of the electron transfer impedance by formulating comparable, theoretical values.

To model the current passing through the copper containing electrolyte during electrodeposition a series element solution resistance (R_S) and a constant phase element (CPE_1), are inserted into an equivalent circuit. A constant phase element is an equivalent circuit component that models the behaviour of the double layer existing between the electrolyte and an irregular surface e.g. an imperfect capacitator (Moats et al. 2014). The faradaic impedance components are considered to be non-ideal, and in the present study it includes the charge transfer resistance or polarization resistance (R_{CT}). The low frequency data is modelled to include a second constant phase element and a second resistance arranged in a parallel configuration. The low frequency components model the impedance caused by diffusion of the copper ions through the Nernst boundary layer or the interaction of copper with the organic additive. The components in the equivalent circuit, R_2 and CPE_2, were included to model the interaction of the copper with the organic additive layer; this approach was based on the model used by Fabian et al. (2009) and Moats et al. 2014 to describe the impedance behaviour caused by Guar and polyacrylamide additives.

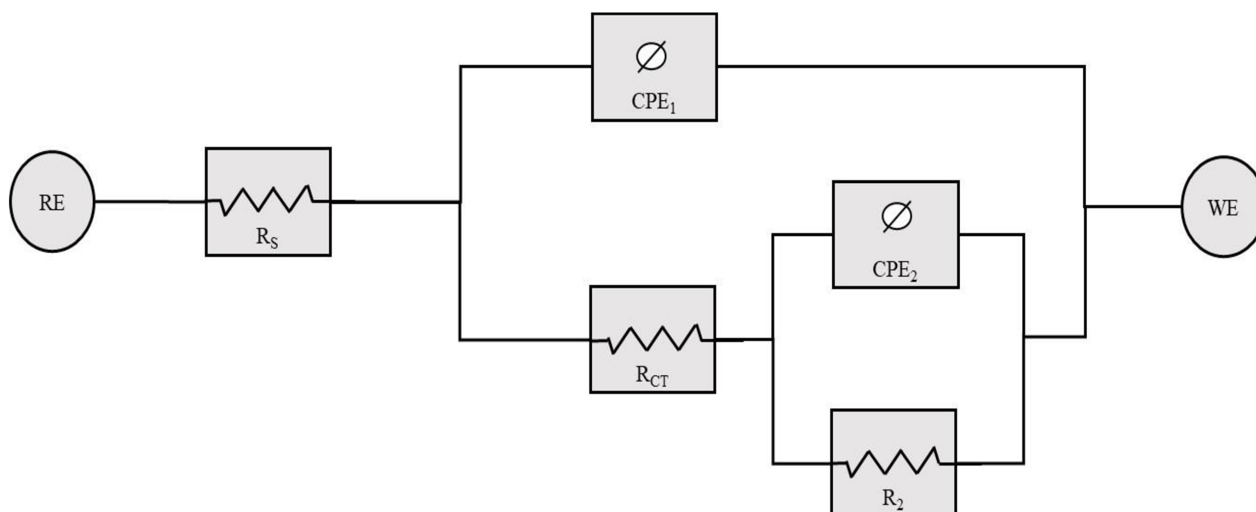

Figure 4.2:Equivalent circuit model with reference electrode (RE), solution resistance (RS), charge transfer resistance (RCT), constant phase element (CPE_1), capacitance (CPE_2), Resistance (R2), and working electrode (WE).

Table 4.1 contains the calculated impedance values modelled with the Echem Analyst Gamry software. The content of Table 4.1 is discussed along with the Nyquist plots in the subsequent discussions. The CPE elements are presented in units of siemens·second$^{\alpha}$ (S·s$^{\alpha}$). The average values of exponent α for CPE_1 and CPE_2 were 0.6 ± 0.014 and 0.81 ± 0.048 respectively. When α = 1, it indicates that the CPE acts as an ideal capacitor. The resultant arcs in impedance spectroscopy plots will be depressed in systems where behaviour in the double layer is non-ideal due to uneven current distribution, surface roughness etc. It is nearly impossible to promote homogenous crystal growth and to distribute current evenly, and therefore the α value is inserted into the model to account for this depression of the arc. The value of α did not vary significantly between concentration limits. The errors experienced with non-determinant (N.D.) values were substantially larger than the actual value.

Stellenbosch University https://scholar.sun.ac.za

Table 4.1: Summary of the parameters with their errors obtained from equivalent circuit model and model fitting.

Additive	mg/L	R_S ($\Omega.cm^2$)	R_{CT} ($\Omega.cm^2$)	CPE_1 ($mS.s^a/cm^2$)	R_2 ($\Omega.cm^2$)	CPE_2 ($S.s^a/cm^2$)	Chi-square goodness of fit
Base Case	-	0.682 ± 0.272	1.952 ± 0.069	1.47 ± 1.24	0.271 ± 0.088	0.334 ± 0.325	0.0007
Guar	2	0.664 ± 0.022	2.070 ± 0.069	2.24 ± 0.54	0.078 ± 0.064	0.323 ± 0.743	0.0004
	10	0.916 ± 0.030	1.957 ± 0.145	2.29 ± 0.62	0.457 ± 0.207	0.600 ± 0.782	0.0007
Low MW PAM	2	0.525 ± 0.017	N.D.	0.91 ± 0.21	N.D.	N.D.	0.0019
	10	0.595 ± 0.016	8.987 ± 0.163	1.32 ± 0.13	1.705 ± 0.803	1.169 ± 0.727	0.0015
Medium MW PAM	2	0.321 ± 0.017	3.841 ± 0.164	2.13 ± 0.23	1.315 ± 0.576	0.973 ±0.293	0.0013
	10	0.450 ± 0.020	5.077 ± 0.118	2.59 ± 0.27	0.641 ± 0.241	0.377 ± 0.142	0.0014
High MW PAM	2	0.614 ± 0.031	N.D.	1.69 ± 0.34	N.D.	0.270 ± 0.115	0.0005
	10	0.580 ± 0.019	6.610 ± 7.332	1.35 ± 0.24	N.D.	0.262 ± 0.595	0.0013
Very High MW PAM	2	0.426 ± 0.020	3.359 ± 0.075	2.86 ± 0.34	0.511 ± 0.217	1.255 ± 0.423	0.0015
	10	0.314 ± 0.020	4.836 ± 0.142	2.64 ± 0.26	1.673 ± 0.506	0.602 ± 0.145	0.0030

4.1.3 EIS result discussion

Figure 4.1 and Table 4.2 indicate a charge transfer resistance, R_{CT}, value of 1.95 ohm.cm^2 at 45 °C and 500 rpm in the high frequency loop for the Base Case scenario. The R_{CT} value for the high frequency loop was also determined in previous EIS studies in similar electrolytes, as shown in Table 4.2. These R_{CT} values are compared with the present study to confirm the reliability of results and experimental accuracy.

Table 4.2: Collection of charge transfer values and conditions obtained from similar previous studies.

Study Reference	***R_{CT} Value ($\Omega.cm^2$)***	***Conditions***
Kelly et al. (1999)	1.97	RDE, 400 rpm, 36 mA/cm^2
	1.47	RDE, 2500 rpm, 43 mA/cm^2
Gabrielli et al. (2006)	1.70	RDE, 100 rpm, 25 mA/cm^2
Fabian et al. (2009)	1.45	RCE, 25 rpm, 30 mA/cm^2
Current study	1.95	RDE, 500 rpm, 30 mA/cm^2

The R_{CT} value obtained in the present study correlates best with the R_{CT} value obtained in the study of Kelly et al. (1999). The slightly lower reported R_{CT} value in this work compared to that of Kelly et al. (1999) can be due to the higher disk rotation setting. A higher disk rotation setting is associated with a lower R_{CT}

Stellenbosch University https://scholar.sun.ac.za

in the system because of the higher concentration of the reductant species (Cu) being forced over the working electrode surface. Comparing the R_{CT} value of the current study with that in the work of Gabrielli et al. (2006) and Fabian et al. (2009), the higher R_{CT} value in the current study can be due to the lower chloride content in the electrolyte (25 mg/L) compared to the reported chloride content (35 mg/L) in the electrolyte used by Gabrielli et al. (2006). Fabian et al. (2009) utilized a rotating cylinder electrode (RCE) as opposed to a RDE, reporting that a more uniform current distribution may be achieved in a RCE and hence the lower reported R_{CT} value. In Figure 4.1 the system resistance decreased when Guar was added to the system, indicating that Guar de-polarized the copper deposition. The de-polarization of the copper deposition in the presence of Guar aligns with the findings of Fabian et al. (2009). It is therefore concluded that the present study produced realistic impedance values that can be corroborated with those reported in previous studies.

The Nyquist plots indicate an increasing trend of overall system resistance with a decrease in MW of the PAM organic additives at both levels of additive concentrations. Lower degrees of polarization/R_{CT} are possibly related to low surface coverage. In a previous study conducted by Grchev et al. (1991) it was concluded that the adsorption of non-ionic PAM in 0.5 M sulfuric acid solution on gold and mild steel is strongly dependent on the MW of the polymer, electrode potential, and temperature; it was found that the surface coverage of dissolved polyacrylamide at concentrations ranging between 2-3 mg/L decreased from about 0.52 to 0.02 as the MW of the polyacrylamide increased from 5×10^3 Da to 1.5×10^6 Da.

The EIS results of the present study are aligned with the findings of Grchev et al. (1991). It is concluded that at a PAM concentration of 2 mg/L the lower MW additives achieve greater surface coverage resulting in an increased polarization effect. Conversely the higher MW PAM additives achieved less surface coverage, resulting in a lower degree of polarization. Grchev et al. (1991) also determined that it is more thermodynamically favorable for low MW PAM additives to adsorb onto gold and mild steel surfaces than for high MW PAM additives based on the ΔG°_{ads} values. The calculated ΔG°_{ads} values increased with an increase in PAM MW, meaning that spontaneous surface adsorption becomes more unfavorable with an increase in the PAM MW (Grchev et al. 1991).

In the high frequency region, a significant increase in polarization/R_{CT} and CPE values was observed at an additive concentration of 10 mg/L compared to 2 mg/L, for all MWs. This dissimilar polarization behaviour at 2 mg/L and 10 mg/L of additive concentration suggests that there are interactions between the organic additive and the copper in the system, and this interaction is enhanced at higher additive concentrations due to excess additive. Such interactions may be a result of chemistry similar to that reported by Gabrielli et al. (2006) and Fabian et al. (2009), who suggested the formation of an Additive-Cl^--Cu^+ ion pair via covalent bonding. The increased R_{CT} and CPE values at 10 mg/L additive concentration are likely to be due to a passivating film of species like PAM-Cl^{-1}-Cu^+ ion pairs formed over the freshly deposited copper. It is likely that the viscosity of the solution is much increased at a PAM additive concentration of 10 mg/L, which can possibly translate to an overall increased system resistance. There is however no convincing evidence based on the values in Table 4.1 that an increased solution resistance is measured at 10 mg/L PAM additive concentration values compared to at 2 mg/L. No significant increase in polarization/R_{CT} and CPE (Table 4.1) was observed when Guar (polysaccharide) was utilized as organic additive. This agrees with the work of Luyima et al. (2016) where polysaccharide additive (HydroStar & DXG-F7) concentration was found to have had no significant effect on the R_{CT} and C_{DL} values.

The second capacitive loop can arise from diffusion of copper to the substrate surface (Warburg impedance) or because of the presence of a second electrical interface. A high degree of agitation was provided to the system to eliminate the possibility of the second capacitive loop arising because of copper

Stellenbosch University https://scholar.sun.ac.za

diffusion. It is therefore deduced that the second capacitive loop arises from the interaction of the organic additive with the copper, forming a second electrical interface. At the low frequency region in Figure 4.1 (a), a second capacitive loop (semi-circle) is observed specifically for the non-ionic additives (medium and very high MW) in contrast with the inductive loops (curling loop) observed for the Base Case, Guar and anionic additive (Low and High MW) scenarios. This suggests that the non-ionic additives interact with the copper surface in a way dissimilar to the anionic additives. Gabrielli et al. (2006) reported that the inductive loop is related to the action of an accelerator additive and a capacitive loop to a suppressor additive, and to their degree of surface coverage. Guar acted as an accelerator (de-polarizer) and therefore the presence of an inductive loop correlates with the findings of Gabrielli et al. (2006). The anionic PAM additives in this work however do not behave as accelerators but rather as suppressors, and this does not correlate well with the findings of Gabrielli (2006).

4.2 Cyclic Voltammetry

4.2.1 Result interpretation of Base Case scenario

The interpretation/analysis for CV data (voltammogram) is presented according to the explanation given by Moats et al. (2014). The voltage sweep for all experiments was initiated at a voltage of 0.319 V vs. SHE, indicated as point 1 on Figure 4.3. The curve 1-2 corresponds with the initial decreasing potential portion of the sweep, where the applied potential is greater than the copper reversible potential meaning that no copper electrodeposition occurs in this potential range. Point 2 on the curve approximates the copper reversible potential of the solution and is indicated as the point where curve 4-5 crosses the curve between points 1-3. Curve 2-3 is associated with the nucleation overpotential of the copper deposition on the platinum surface. The nucleation overpotential is equal to the difference in potential between points 2 and 3. Point 3 is determined by the change in slope of the curve where copper deposition is initiated on the cathode surface. Line 3-4 follows the trend of an increase in current density at a decrease in applied potential. The larger the difference in potential from point 1 as reference point, the larger the driving force to promote the copper deposition reaction. Therefore, as the curve progresses to point 4 nucleation and growth of copper nuclei on the cathode surface is encouraged increasingly, and hence an increase in the rate of reaction (current density) towards point 4. Point 4 marks the end of the negative cathodic sweep (forward sweep) and is reached when the applied potential is reversed to be a positive potential sweep. Curve 4-2 relays information about the polarization overpotential of the freshly deposited copper on already deposited copper. The polarization overpotential of copper onto already deposited copper is usually less that the polarization overpotential of copper deposited on stainless steel or platinum, resulting in a higher current density at the same applied potential. The curve 3-4-2 represents a non-steady state condition. The substrate will be increasingly covered in a copper deposit from 3-4-2, inferring that the shape of the curve will change for varying applied scan rates. Anodic dissolution of the copper from the substrate surface is represented by curve 2-5 (reverse sweep). Points 4 -5 include the entire positive anodic sweep where copper dissolution is systematically encouraged.

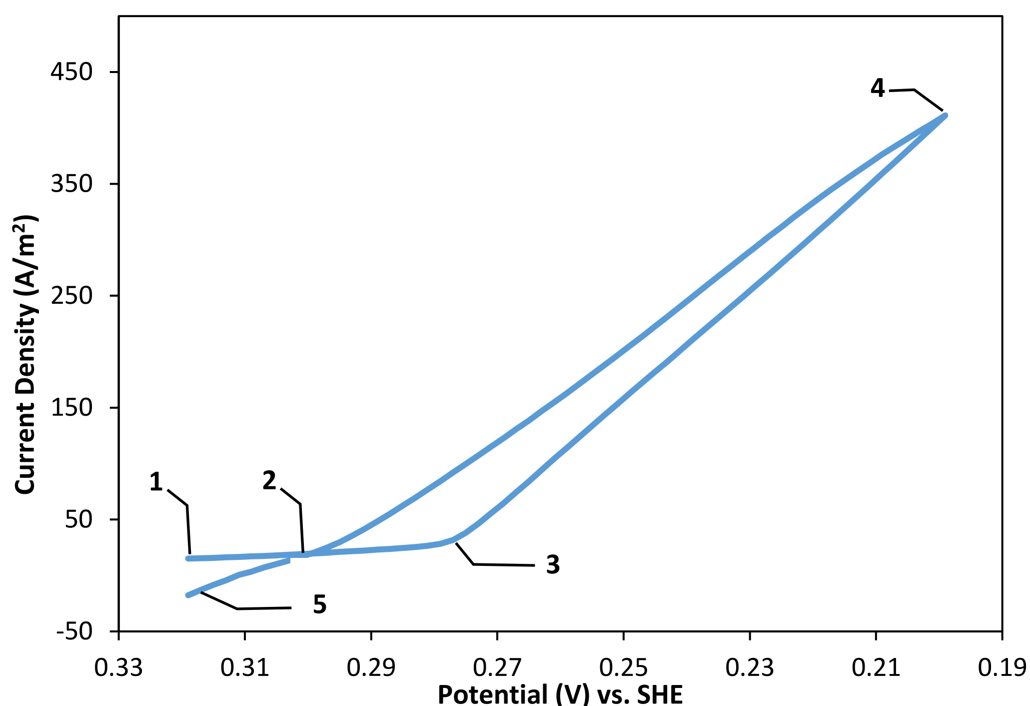

Figure 4.3: Typical voltammogram of copper deposition on a platinum surface, 35 g/L copper, 160 g/L H_2SO_4 and 25mg/L Cl^- at 45 °C in a RDE setup at 500 rpm. Voltage sweep between 0.319 and 0.2 V vs. SHE at a scan rate of 1 mV/s.

4.2.2 CV results

4.2.2.1 Voltammograms

The CV results presented in Figure 4.4 - Figure 4.8 for 2 mg/L additive concentration displayed that all PAM additives assisted to polarize the copper electrodeposition while Guar served to de-polarize the deposition. The Low MW PAM additive polarized the deposition the most with a trend towards decreasing polarization of the cathodic deposition with an increase in PAM MW. A further overall increase in system polarization was observed at an increased additive concentration of 10 mg/L. At this elevated additive concentration, the polarization behaviour of the deposition - induced by the additives- seemed to vary less between the various tested additives. A strong correlation between additive MW and polarization behaviour was observed, while no significant correlation between the ionic charge of the additive and the polarization behaviour could be observed.

The voltammograms in Figure 4.4 show that Guar slightly de-polarized the cathodic deposition at both concentrations of 2 mg/L and 10 mg/L. These findings are well aligned with those of Fabian et al. (2009) where it was found that the cathodic deposition was de-polarized in the presence of Guar. In this work, copper was plated in the presence of Guar on a stainless steel and pre-plated copper surface and in both instances, it was observed that Guar slightly de-polarized the depositions to an extent very comparable with the current results.

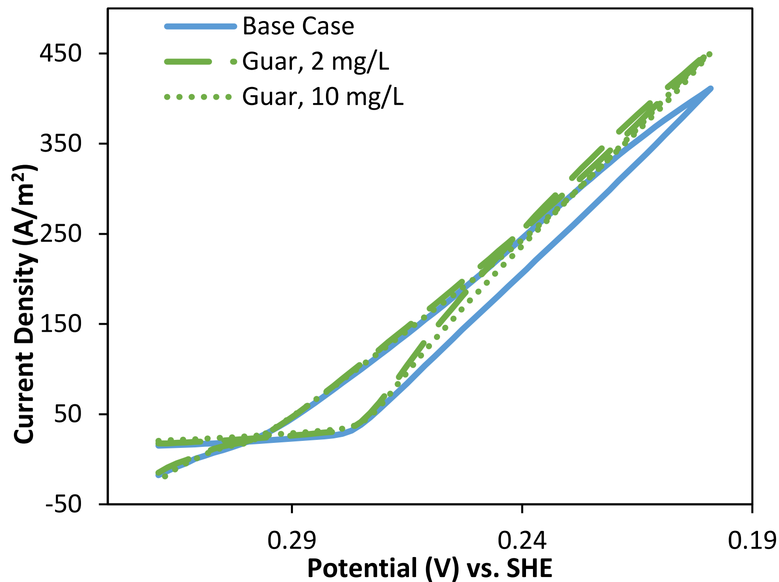

Figure 4.4: Voltammograms for Guar additive at 2 mg/L and 10 mg/L concentration compared to the base case scenario.

The resultant voltammogram in Figure 4.5 of the deposition process in the presence of 2 mg/L Low MW PAM additive shifted down significantly from the Base Case scenario. This indicates that the Low MW additives decreased the reaction kinetics of the copper deposition process. Polarization of the copper deposit is more enhanced on the forward sweep compared to the reverse sweep at 2 mg/L additive concentration. The opposite is true at an additive concentration of 10 mg/L, where the reverse sweep induced an increased polarization effect on the deposit. This trend at 10 mg/L additive concentration is observed throughout all the CV experimental results for PAM additives.

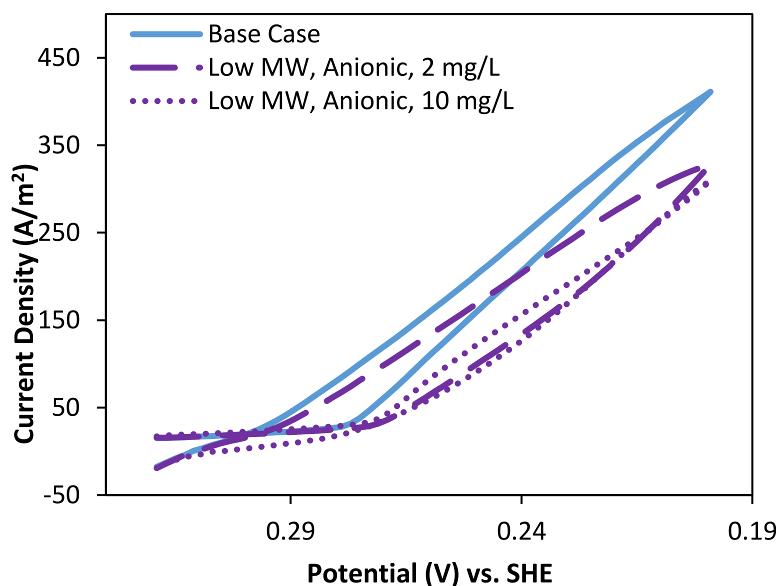

Figure 4.5: Voltammograms for the Low MW PAM additive at 2 mg/L and 10 mg/L concentration compared to the base case scenario.

The voltammograms presented in Figure 4.6-Figure 4.8 demonstrate the same polarization effect for all PAM additives with a systematic decrease in the polarization effect as MW increases. An increased

additive concentration resulted in an increased polarization effect, specifically on the return sweep. This phenomenon was observed for all the PAM additives in Figure 4.6-Figure 4.8. Small variation in polarization behaviour between the 2 mg/L and 10 mg/L concentration runs in the initial forward sweep, while a significant decrease in the rate of reaction was observed on the reverse sweep compared to the forward sweep.

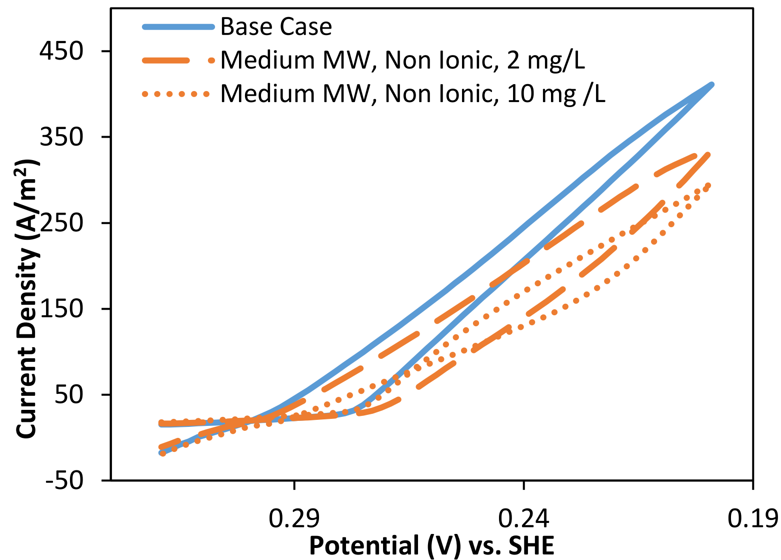

Figure 4.6: Voltammograms for the Medium MW PAM additive at 2 mg/L and 10 mg/L concentration compared to the base case scenario.

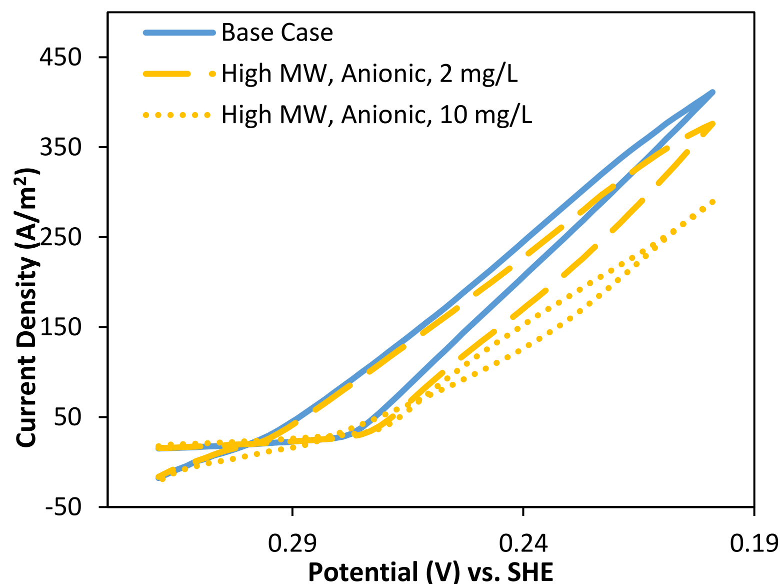

Figure 4.7: Voltammograms for the High MW PAM additive at 2 mg/L and 10 mg/L concentration compared to the base case scenario.

The Very High MW PAM additive polarized the cathodic deposition the least compared to all the other lower MW PAM additives (Figure 4.8). Fabian et al. (2009) used a very high MW PAM additive of 15 000 000 Da during CV tests and the results showed a similar polarization effect induced by the additive. Furthermore, the findings of Moats et al. (2014) and Cui (2014) support these results; it was observed in

Stellenbosch University https://scholar.sun.ac.za

these studies that a polyacrylamide “Cyquest N-900” also polarized the cathodic deposition. The exact MW of the Cyquest N-900 product was not disclosed however.

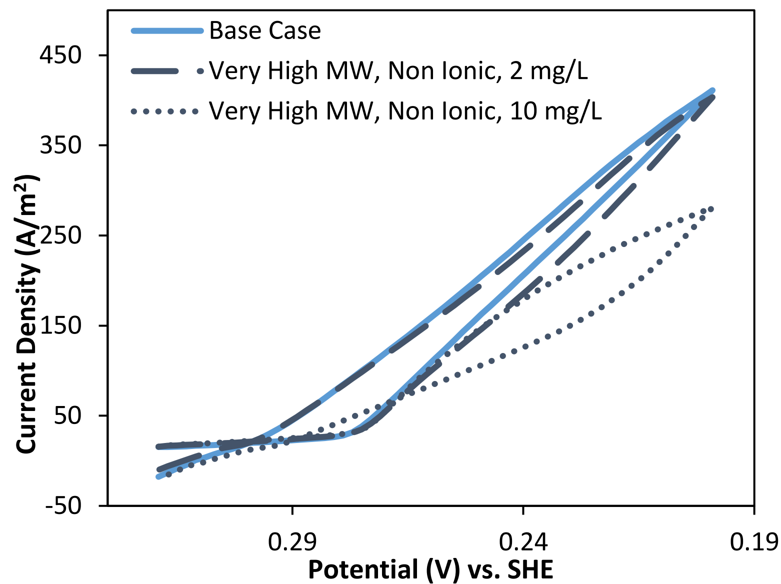

Figure 4.8: Voltammograms for the Very High MW PAM additive at 2 mg/L and 10 mg/L concentration compared to the base case scenario.

The results presented in Figure 4.4-Figure 4.8 are presented in combination with each other in Figure 4.9 and Figure 4.10 to enable the reader to compare the CV performance of the different experimental scenarios at 2 mg/L and 10 mg/L additive concentration. The previously discussed trends are clear and apparent on these graphs. An increased polarization effect for a decrease in PAM additive MW at an additive concentration of 2 mg/L. At an additive concentration of 10 mg/L the PAM additives polarized the cathodic deposition more significantly compared to at 2 mg/L, especially on the reverse sweep, associated with copper plating on copper. Guar consistently de-polarized the cathodic deposit at both lower and higher concentration values.

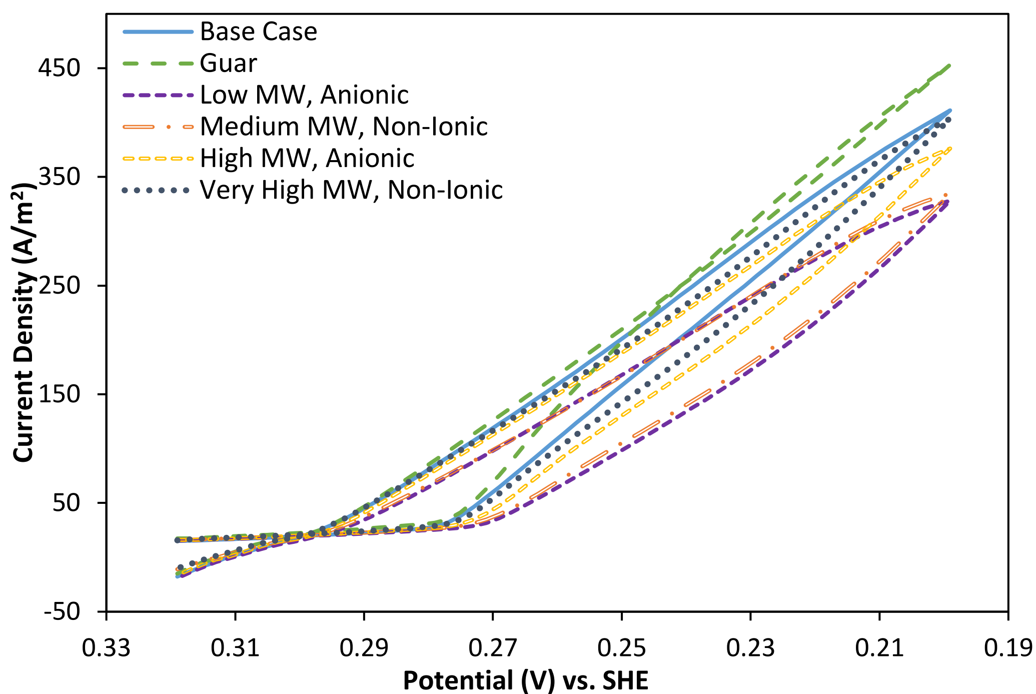

Figure 4.9: Voltammograms of all additives at 2 mg/L used during CV experimental work plotted on one graph.

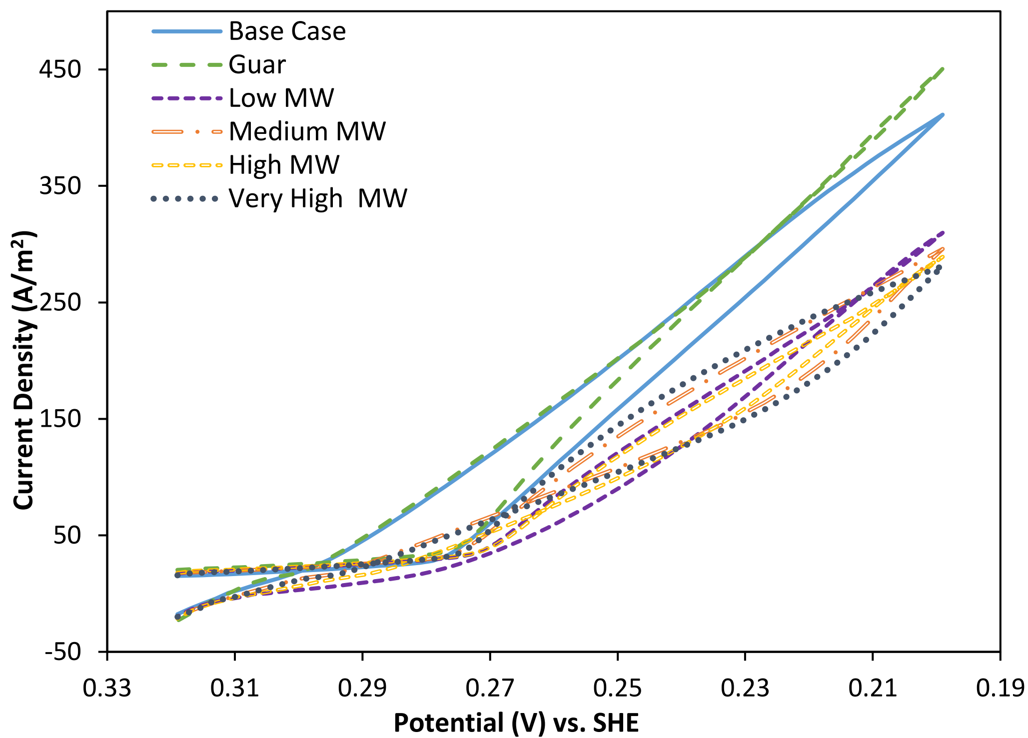

Figure 4.10: Voltammograms of all additives at 10 mg/L used during CV experimental work plotted on one graph.

Stellenbosch University https://scholar.sun.ac.za

4.2.2.2 Polarization overpotential

Polarization overpotential refers to the voltage (reaction driving power) required to induce a specific rate of reaction or current density (Faraday's Law) in the system. It was observed in Figure 4.4 - Figure 4.10 that at a fixed potential in the presence of various organic additives, dissimilar current densities were measured. Figure 4.11 gives an indication of the variation in measured current density at a fixed potential of 0.22 V vs. SHE on the reverse potential sweep. This potential point of 0.22 V vs. SHE was chosen for comparison purposes only.

At this voltage and at an additive concentration of 2 mg/L, no significant polarization behaviour is observed in the presence of Guar. It is noted that the average values presented in the overall voltammogram indicates slight de-polarization. The average current density values in the presence of 2 mg/L PAM additives indicate that at the same potential/driving power a systematic decrease in the rate of reaction was recorded for a decrease in PAM additive MW. However, taking experimental error into account this trend becomes less significant. The experimental error accounts for the magnitude of uncertainty and was calculated by dividing the sample standard deviation by the square root of the sample size.

Guar showed very little variation in polarization behaviour at 10 mg/L, while a significant increase in polarization of the copper deposition was recorded in the presence of the PAM additives. No prominent trend between polarization behaviour and additive MW is however recorded at the increased PAM concentration level at a voltage of 0.22 V vs. SHE. One of the findings from the work of Grchev et al. (1991) was that the maximum surface coverage in the temperature range of 20 to 80 °C for a concentration of 20 mg/L polyacrylamide, remained unaffected by the MW of the polymer. The trend at 10 mg/L PAM additive in Figure 4.11 seems to support this finding of Grchev et al. (1991) since the variation in the average current density values at 0.22 V vs. SHE is less between the experimental runs. It might be that at 10 mg/L the variation in surface coverage between the Low and Very High MW additives are starting to even out to the same maximum coverage value.

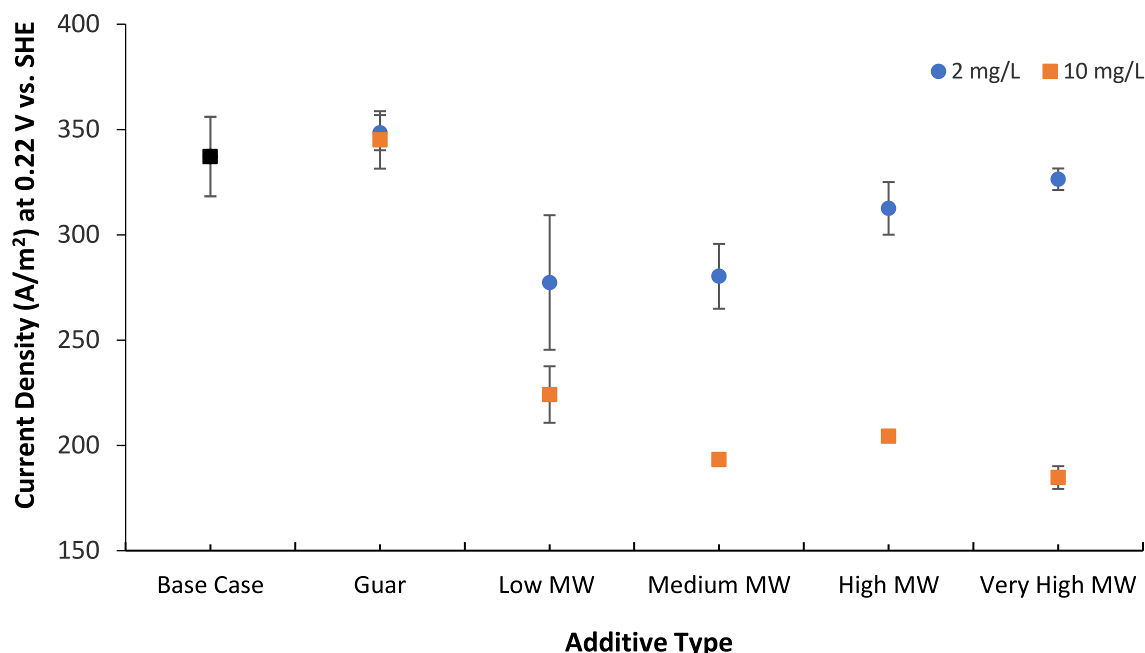

Figure 4.11: Effect of organic additives on current density measured on the return sweep at a potential of 0.22 V vs. SHE at additive concentrations of 2 mg/L and 10 mg/L.

4.2.2.3 Overpotential at nucleation

Nucleation overpotential refers to the amount of excess voltage/driving power the system requires to plate copper onto a foreign substrate surface i.e. the additional voltage required to plate copper onto the platinum surface as opposed to on a copper surface. The nucleation overpotential is equal to the difference in potential between points 2 and 3 as indicated on Figure 4.3. Figure 4.12 presents the method that was followed to calculate the nucleation overpotential values by using data from the average Base Case scenario voltammogram as an example. At point 3 in Figure 4.12 a clear change in gradient of the data is observed. Fitting linear trendlines to the data of the same gradient between points 2 and 3 and between point 3 and the following 8 data points created a point of intersection of the separate linear curves. The corresponding potential value at the intersection point of the linear curves was read of as points 3. The same methodology was used to determine point 2 on the graph. This process was repeated for every run and the average difference between points 2 and 3 (nucleation overpotential) was plotted in Figure 4.13.

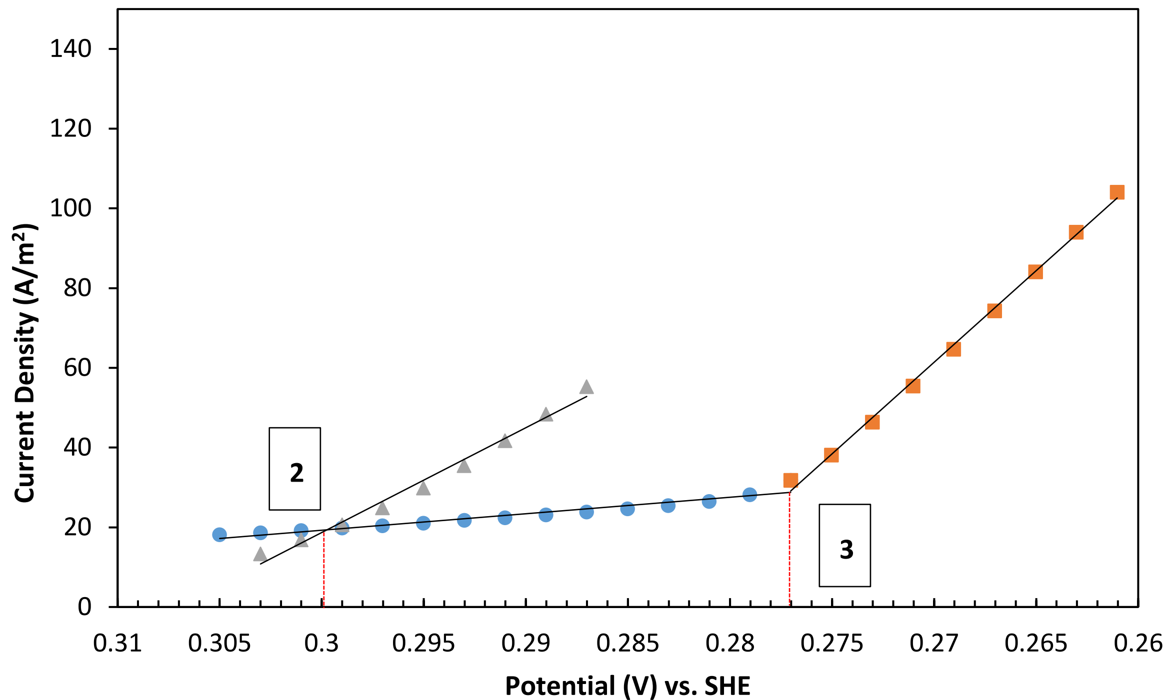

Figure 4.12: Method for calculating nucleation overpotential values.

By investigating the average values of the nucleation overpotential at an additive concentration of 2 mg/L in Figure 4.13, an increasing trend in nucleation overpotential corresponding to a systematic decrease in PAM additive MW is recorded compared to the Base Case. On average, Guar decreased the required overpotential required to initiate copper nucleation on the platinum surface.

At an additive concentration of 10 mg/L Guar performance was similar to that at 2 mg/L. The PAM additives however, decreased the polarization overpotential significantly compared to that at 2 mg/L PAM concentration. Once again, like in the polarization overpotential results, no significant trend is observed in terms of relating additive MW to the nucleation overpotential. However, it should be noted that the Low MW PAM additive significantly decreased the nucleation overpotential compared to the other PAM additives at a concentration of 10 mg/L.

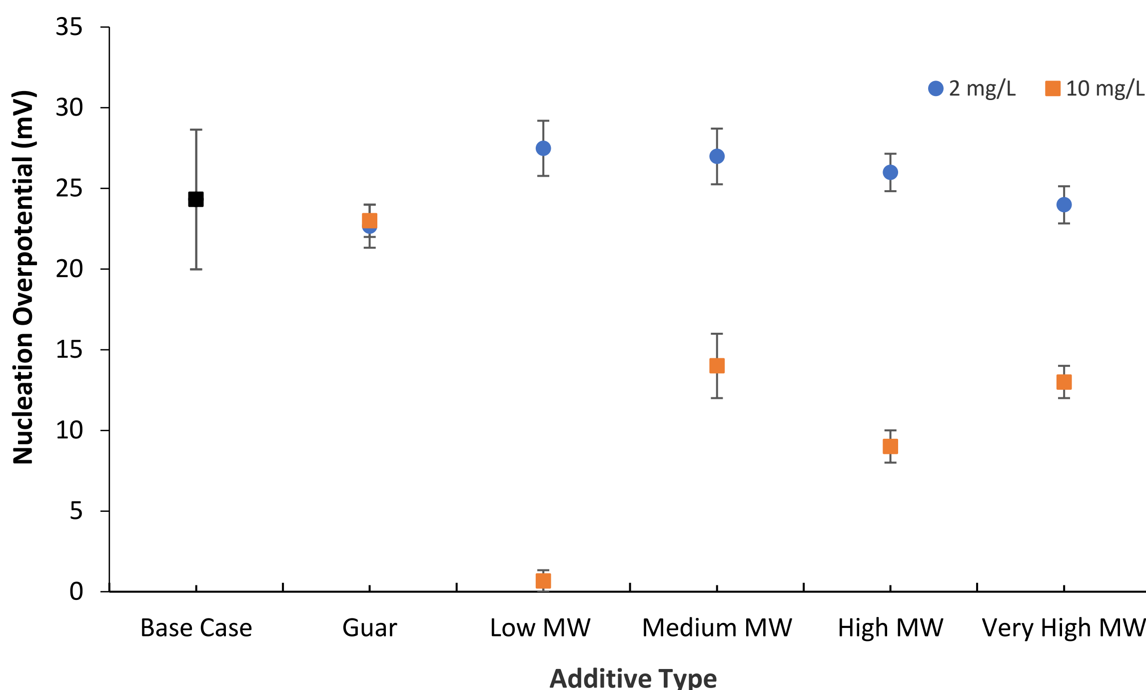

Figure 4.13: Effect of organic additives on the nucleation overpotential at additive concentrations of 2 mg/L and 10 mg/L.

4.2.3 CV results discussion

It is reported in the literature that the most effective dispersants are water soluble, low molecular weight (< 5 x 10^4) polymers (He 2009; Chamovska et al. 2006). Placing this within the context of the findings of Grchev et al. (1991) (highest surface coverage for lower MW PAM) and the findings in the EIS results of the current study, the results are found to be in line with the literature. In the EIS result analysis it was suggested that Low MW PAM additives adsorb more readily onto a copper surface compared to High MW PAM additives. It was argued that because of this increased adsorption behaviour of the Low MW additives an amplified level of system resistance was recorded for a systematic decrease in PAM additive MW. The adsorbed PAM layer on the electrode surface retarded the rate at which electrons are transmitted at the electrolyte/electrode interface.

Similarly, when considering the trends in the voltammograms in Figure 4.4-Figure 4.8, it is observed that a systematic increase of cathodic polarization behavior is recorded for a systematic decrease in the PAM additive MW at a concentration of 2 mg/L. These results are aligned with the EIS results, and therefore the same arguments for this behaviour are postulated. It is possible that more surface coverage is achieved for the adsorption of Low MW PAM additives and that a passivating film of PAM-Cl^{-1}- Cu^{+} ion pairs form on the substrate surface, inhibiting charge transfer and hence the observed polarization effect.

In accordance with the EIS results, Guar slightly de-polarized the cathodic deposit presented in the voltammograms of Figure 4.4. In Figure 4.11 the average current density measured at a potential of 0.22 V vs. SHE when Guar was used as an additive was higher, although the experimental uncertainty overlaps with the Base Case scenario. The de-polarization behaviour of Guar correlates well with the findings of Fabian et al. (2009) where Guar was observed to decrease the charge transfer resistance during EIS experiments and to de-polarize the cathodic deposit during CV experiments. The mechanism for the overall reduction in charge transfer resistance and de-polarization is not clear, however Fabian et

Stellenbosch University https://scholar.sun.ac.za

al. (2009) attempted to explain this in terms of specifically and non-specifically adsorbed molecules in the double layer structure at the electrode/electrolyte interface. The presence of adsorbed electroactive species in the double layer affects the rates of electrode processes. Referring to Figure 2.6, the Inner Helmholtz Layer contains specifically adsorbed species while the Outer Helmholtz Layer contains non-specifically adsorbed species. Anions are usually specifically adsorbed, except for fluoride, hydroxyl, and sulfate ions (Bard & Faulkner 2000; Newman & Thomas-Alyea 2004). Since each repeating unit in the Guar molecule chain contains nine OH^- (hydroxyl) groups it is accordingly concluded by Fabian et al. (2009) that Guar is non-specifically adsorbed and only interacts near the Outer Helmholtz Layer with the electrode surface via long range electrostatic forces.

Other investigations on Guar adsorption behaviour have proposed that Guar interacts with metal surfaces via hydrogen bonding (Wang et al. 2005; Vidal 2013; Mudgil et al. 2014). Wang et al. (2005) investigated the adsorption mechanism of Guar at solid (talc) to liquid (water) interfaces. The results indicated that the adsorption behaviour of Guar was not dependent on solution conditions like ionic strength and pH which is associated with longer range electrostatic forces. However, in the presence of urea which is a recognized hydrogen bond breaker, a significant decrease in Guar adsorption on the solid surface was observed. This coupled with no recorded evidence of Guar desorption, provided convincing evidence that Guar adsorption is not governed by the mechanism of electrostatic forces but rather with the mechanism of hydrogen bonding. The adsorption mechanisms of polymers remain a complex topic and there is no clear consensus amongst researchers on this.

In the present study PAM additives significantly polarized the cathodic deposition, while Guar slightly de-polarized the deposit. It is possible that the PAM additive specifically adsorbed into the Inner Helmholtz Layer while Guar was non-specifically adsorbed as described by Fabian et al. (2009). The steric structure of polysaccharides like Guar with carbon rings and large carbon branches might also play a role in its ability to migrate towards the inner Helmholtz layer. PAM's on the other hand possess linear chains with less branching, perhaps allowing for less complex interactions and a smoother preferential migration towards the Inner Helmholtz Layer to interact "more selectively" with the electrode surface. The more complex polysaccharide steric structure might experience repulsive and/or attractive forces simultaneously- depending on its immediate orientation or degree of hydrolyzation. It is well known that Guar will hydrolyze in acid solutions to break down into smaller branches containing both carbonyl and carboxyl groups (Moats et al. 2016). It is possible that the PAM additives achieve a more consistent steric orientation, structure, and degree of hydrolyzation under the described experimental conditions resulting in a high degree of adsorption on the electrode surface. The adsorbed PAM molecules could therefore perform their role as a suppressor much better.

At 10 mg/L PAM additive concentration an interesting polarization trend is observed. Firstly, it was observed that all PAM additives polarized the deposit to roughly the same extent. Secondly, it was observed that the initial extent of polarization (at point 3-Figure 4.2) on the voltammograms did not vary significantly between experimental runs at 2 mg/L and 10 mg/L. However, as copper nucleation and growth proceeded (from point 3-4 - Figure 4.2) the extent of polarization increased significantly between experimental runs at 2 mg/L and 10 mg/L additive concentration. This phenomenon can possibly be explained by the findings of Broseta et al. (1995), where the effects of substrate hydrophobicity on PAM adsorption were investigated. The study investigated the adsorption of non-ionic and anionic polyacrylamides as a function of the substrate hydrophobicity. It was concluded in the study of Broseta et al. (1995) that both the non-ionic and anionic PAM additives adsorbed readily onto hydrophobic surfaces, but the adsorption almost vanished on hydrophilic surfaces. These effects were interpreted in terms of competition between substrate/PAM interactions and substrate/water short-range interactions.

Stellenbosch University https://scholar.sun.ac.za

Broseta et al. (1995) explains this adsorption behavior by reasoning that with an increase in the substrate hydrophobicity the affinity of water molecules and hydrophilic monomers towards the surface decreases leading to the selective adsorption of the PAM additives on the substrate surface.

It has long since been established that stainless steel, platinum, and gold possess hydrophilic surfaces while copper possess a hydrophobic surface (Valette 1982). Therefore, based on the arguments of Broseta et al. (1995) it is proposed that the PAM additives increasingly interacted with the electrode surface as nucleation and crystal growth of the hydrophobic copper advanced. This would explain why in Figure 4.4-Figure 4.8 the voltammograms at 10 mg/L PAM additive concentration show increasing polarization behaviour of the cathodic deposition as copper nucleation is encouraged with the forward sweep and decreasing polarization behaviour is recorded on the reverse sweep.

It is suggested that the non-ionic PAM's adsorb on the hydrophobic substrate surface via hydrogen bonding (short-range interactions) with its apolar backbone (Broseta & Medjahed 1995). This contrasts with the description of the adsorption mechanism of non-ionic PAM's as given by Fabian et al. (2006) where it is proposed that the PAMs bond via hydrogen bonding between the amide functional group and the substrate surface. It should be noted in the study of Broseta et al. (1995) that the anionic PAMs adsorbed much more readily onto hydrophobic surfaces when the pH was decreased from pH 7 to pH 4.2 and the salinity was increased from 20 g/L to 100 g/L. The non-ionic PAM adsorbed equally well at both tested pH and salinity limits. In neutral conditions, the anionic PAM additives are less likely to adsorb via hydrogen bonding (as is the case for non-ionic PAM adsorption) due to repulsive electrostatic interactions between the negative carboxylic group and the negative electrode surface. As the pH decreases the concentration of H^+ ions in the electrolyte increase, enabling interaction between the anionic PAM and the negative substrate surface via the bridging H^+ ions in the electrolyte. Divalent cations present in the electrolyte will also allow adsorption of anionic additives in a similar fashion. Both EIS and CV results show no clear evidence of a relation between ionic content and additive adsorption/polarization. This might be because the experimental runs were conducted at very low pH values which completely negated the repulsive electrostatic forces between the anionic PAMs and the substrate surface, resulting in similar PAM adsorption behavior between the anionic and non-ionic additives.

5 ELECTROWINNING STUDIES

5.1 Fundamental electrowinning studies

SEM micrographs of the electrodeposits, at 300 A/m^2, on stainless steel are presented in this section. Stainless steel was selected as the cathode surface to approximate industrial conditions. The current density and cathode material of construction was selected based on the review on copper electrowinning operating parameters presented in Section 2.7. All Figures labelled (a) & (b) represent micrographs taken after 10 s of electrodeposition while Figures labelled (c) & (d) represent corresponding micrographs taken after 30 s of electrodeposition. The micrographs are presented to provide a qualitative supportive analysis to the quantitative fundamental CV and EIS work.

For ease of reference to the micrographs, the results and discussion are presented together in this section. It should be noted that according to Winand (1992) it is extremely difficult to attribute a specific crystal structure/classification to a deposit without cross-section crystallographic examination, except for FI type growth which can normally be identified easily by external examination. Nevertheless, the technique of external examination was used in a comparative manner to be able to suggest possible crystal growth types when different additives were used based on the external differences in the deposits.

5.1.1 Base Case

The copper deposits after 10 s and 30 s of deposition without the addition of any additives are presented in Figure 5.1.

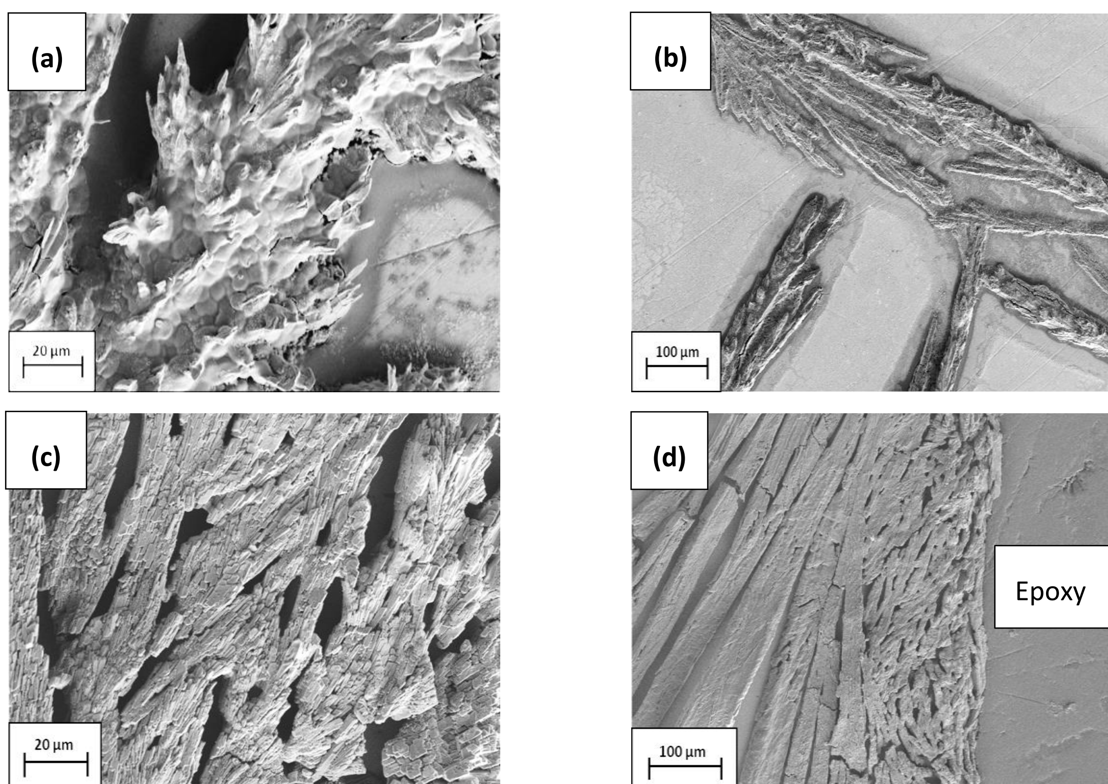

Figure 5.1:SEM micrographs of copper crystal deposit on stainless steel surface in a Base Case electrolyte at 300 A/m2. a-b) After 10 s deposition. c-d) After 30 s deposition.

After 10 s of deposition a rough, spiky, dendrite-like growth structure has developed transforming into a cubic-rectangular crystal structure after 30 s of deposition. At the base of the peaks in the 10 s deposit micrographs a spherical/nodular (3D) crystal structure is observed, indicating that the nodules develop

Stellenbosch University https://scholar.sun.ac.za

into the rough dendrite peaks. Based on the classification of Fisher (1969) in Figure 2.7, which Winand also utilized in 1992 to describe crystal structure, this crystal structure in Figure 5.1 (a)-(b) can be classified to be FI growth type. FI growth type can be expected at low inhibition levels with whiskers, then dendrites, and finally powder forming when the current density is increased (Winand 1992). Since low inhibition levels are expected with no addition of additives, this classification is justified.

After 30 s of deposition it seems as if enough time has passed for lateral crystal growth to occur, with large crystal structure formation. The crystal structure has converted to large 2D cubic crystals with gaps between the crystals, increasing the probability of electrolyte entrapment. The discrepancies between the structure after 10 s and 30 s deposition could be due to the absence of an additive which serves to control the crystal growth type more consistently. This is observed on a fundamental level where the error bars in Figure 4.11 and Figure 4.13 generally seem to be smaller when additives are introduced to the system, implying tighter experimental control and consistency when additives are used. The crystal type and structure that forms after 10 s and 30 s of deposition are more consistent when additives are used. Therefore, it is possible that when no additives are used several types of crystals or mixtures of crystal structure types can develop due to the lack of control over the system. Based on the presented evidence it is concluded that the Base Case electrodeposition scenario produced instantaneous nucleation, and 2D, FI type crystal growth transforming into a FI/BR type crystal growth after 30 s of electrodeposition.

Stellenbosch University https://scholar.sun.ac.za

5.1.2 Guar

The copper deposits after 10 s and 30 s of electrodeposition in the presence of Guar are presented in Figure 5.2.

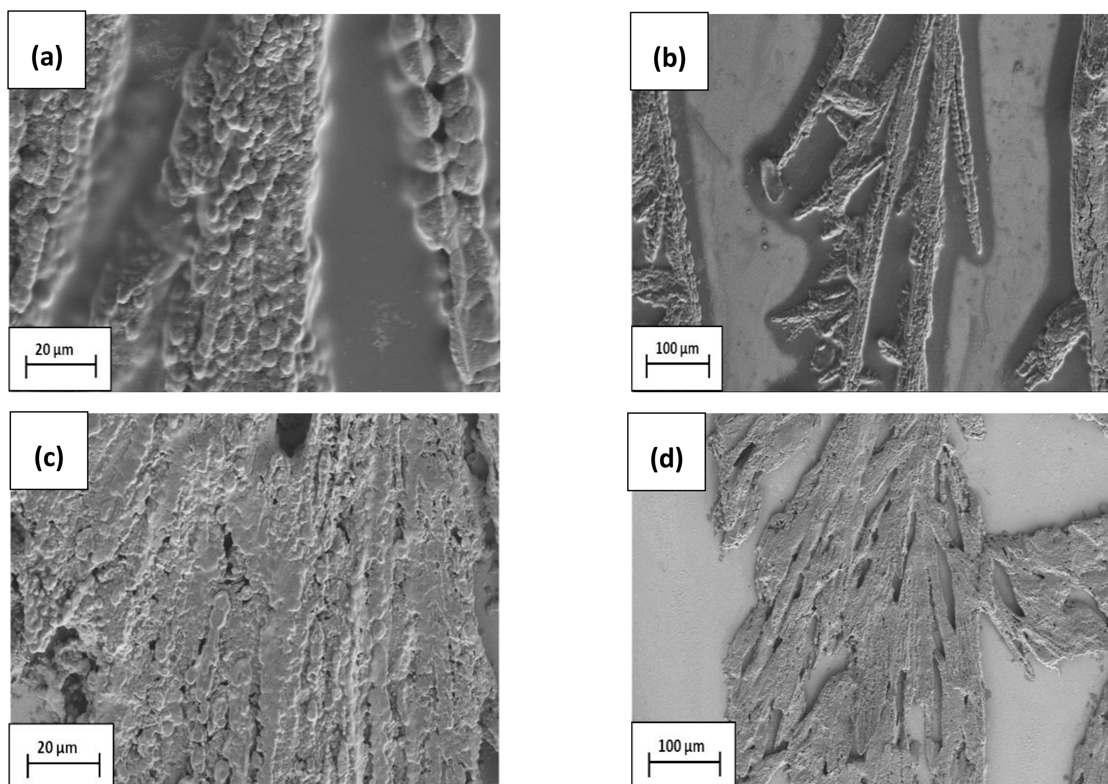

Figure 5.2: SEM micrographs of copper crystal deposit on stainless steel surface in the presence of guar at 300 A/m2. a-b) After 10 s deposition. c-d) After 30 s deposition.

After 10 s of electrodeposition spherical, nodular-like growth structures have developed. The crystal structure remained consistent after 30 s of electrodeposition. Based on the classification of Fisher (1969) which Winand also utilized in 1992 to describe crystal structure type, this crystal structure in Figure 5.2 is classified to be UD growth type. UD crystal growth is attained at very high inhibition intensity and low current density or at low inhibition intensity and high current density and is characterized by a dispersion type, uniform, small grain structure deposit. Usually, promoting this type of crystal growth is most expensive due to the cost of the excessive amount of additive and energy related to drive the reaction. When running at these extreme levels of current density and inhibition level, one also runs the risk of producing a powder like deposit which is not desirable (Winand 1992). Since the average current density is increased (as observed in CV) and the overall system resistance is decreased (as observed in EIS) in the presence of Guar, this classification is justified. Based on the presented evidence it is concluded that the electrodeposition in the presence of Guar produced progressive nucleation, and 3D, UD type crystal growth. It should be noted that the UD type crystal growth achieved in these runs are very close to the border of 2D, FI type growth since the average current density only increased slightly from the Base Case scenario and the system resistance decreased marginally from the Base Case scenario.

Stellenbosch University https://scholar.sun.ac.za

5.1.3 Low MW PAM

The copper deposits after 10 s and 30 s of electrodeposition in the presence of a Low MW, anionic PAM additive is presented in Figure 5.3.

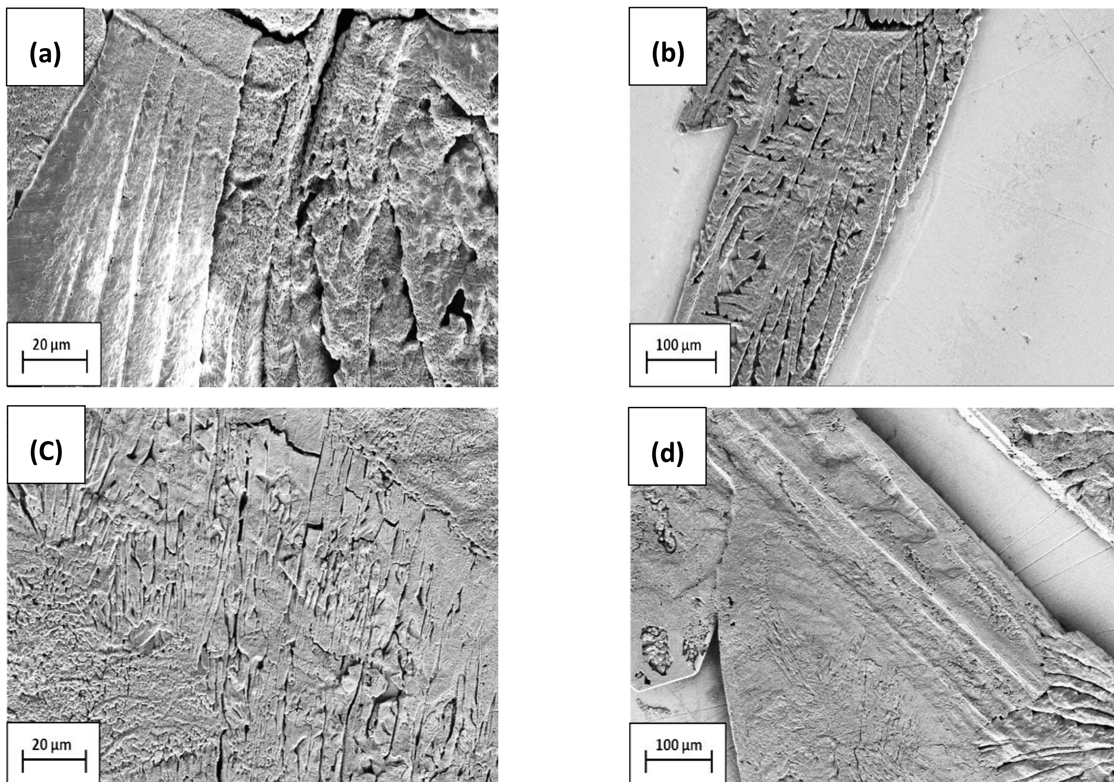

Figure 5.3: SEM micrographs of copper crystal deposit on stainless steel surface in the presence of a Low MW PAM at 300 A/m2. a-b) After 10 s deposition. c-d) After 30 s deposition.

After 10 s of deposition smooth, compact, flat growth structures developed, transforming into an even more compact deposit with the same crystal structure observed after 30 s of electrodeposition. This crystal structure in Figure 5.3 is classified to be FT growth type. FT crystal growth is characterized by elongated crystals that grow perpendicular to the cathode surface and is observed at relatively high inhibition and current density levels. This type of growth is usually desired in copper electrowinning processes due to the coherent deposit morphology achieved which also reduced the risk of electrolyte entrapment (Winand 1992). Since the average current density decreased (CV) and the overall system resistance has increased (EIS) significantly in the presence of the Low MW PAM, this classification is justified. Compared to the Base Case and Guar conditions the growth is much more suppressed and there are a lot less nuclei present on the cathode surface. This suggests that the rate of nucleation is much slower compared to the Base Case and Guar scenarios. For the Low MW additive, it is apparent that the voids between the already deposited copper fills over time to produce a smooth compact crystal structure rather than a more porous nodular/dendrite structure typically characterized by high nucleation rates. Based on the presented evidence it is concluded that the electrodeposition produced in the presence of the Low MW, anionic PAM followed progressive nucleation, and delivered 2D, FT type crystal growth.

5.1.4 Medium MW PAM

The copper deposits after 10 s and 30 s of electrodeposition in the presence of a Medium MW, non-ionic PAM additive is presented in Figure 5.4.

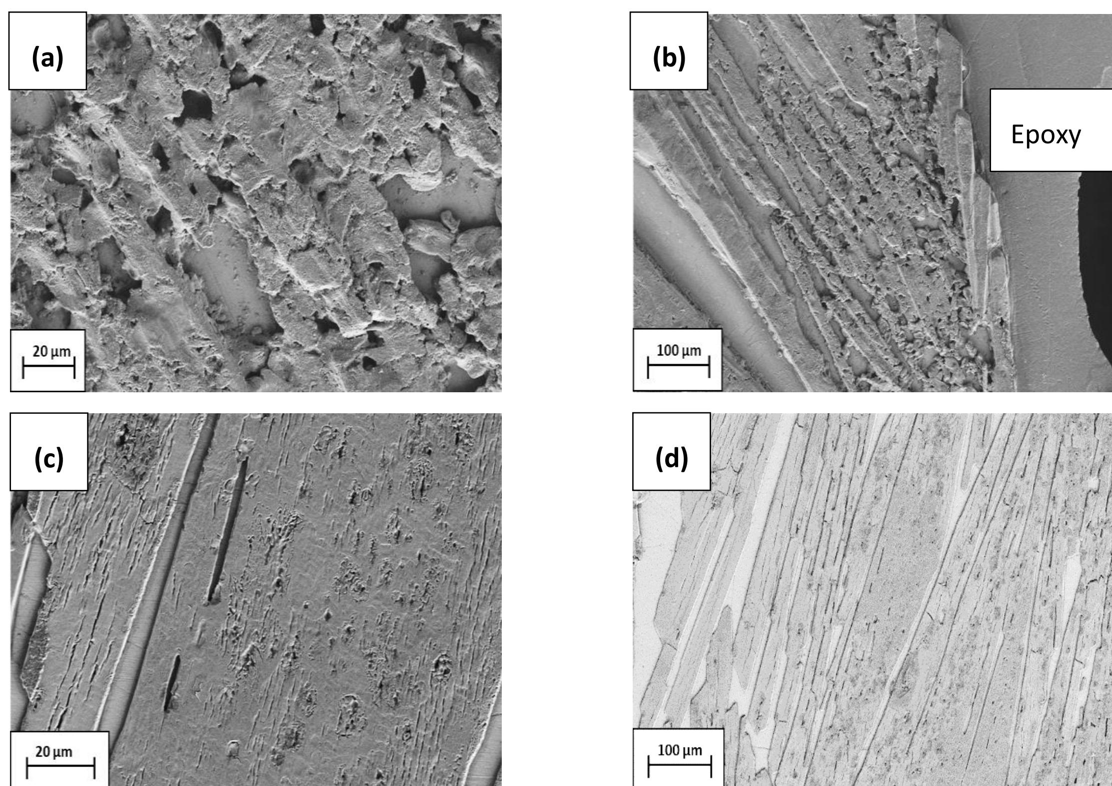

Figure 5.4: SEM micrographs of copper crystal deposit on stainless steel surface in the presence of a Medium MW PAM at 300 A/m2. a-b) After 10 s deposition. c-d) After 30 s deposition.

After 10 s of deposition slightly rough, porous, growth structures have developed, transforming into a flat and smooth crystal structure with small voids and cracks after 30 s of electrodeposition. In Figure 5.4, it is evident that more lateral (1D) growth transpired compared to the growth observed for when the Low MW additive was used. In Figure 5.3 less lateral growth and more vertical growth is observed. The Medium non-ionic PAM additive can be classified as BR or FT growth type. According to Winand (1992), BR crystal type is observed at moderate inhibition and current density levels with the deposit usually characterized with good lateral growth with the possibility of electrolyte entrapment due to the development of large crystal formations. The CV results revealed that when a Medium MW PAM additive was used the electrodeposit was polarized but not to the same extent as when the Low MW additive was used. The EIS data indicated that the system resistance increased with the Medium MW additive, but not nearly to the same extent as when the Low MW additive was used. The moderate increase in system polarization and resistance supports the finding on a fundamental level that BR or FT growth type can develop in the presence of this additive. The rate of nucleation is slower compared to the Base Case and Guar deposition scenarios. For the Medium MW additive, it is apparent that the porous voids present after 10 s of deposition develops into a more compact, smooth structure over time. It should be noted that most of the areas on the deposit after 10 s were comparable to the compact and smooth deposit obtained after 30 s of deposition (the most porous section of the deposit is presented in the micrographs). Based on the presented evidence it is concluded that the electrodeposition produced in the presence of the Medium MW, non-ionic PAM, followed progressive nucleation, and delivered 2D, BR type or FT type crystal growth. Fischer (1969) further describes a growth type Z which is a mixture or overlapping zone

between BR and FT type crystal growth. Considering the combined results for the Medium MW PAM additive it might be prudent to classify the type of crystal growth promoted by this additive to be type Z crystal growth.

5.1.5 High MW PAM

The copper deposits after 10 s and 30 s of electrodeposition in the presence of a High MW, anionic PAM additive is presented in Figure 5.5.

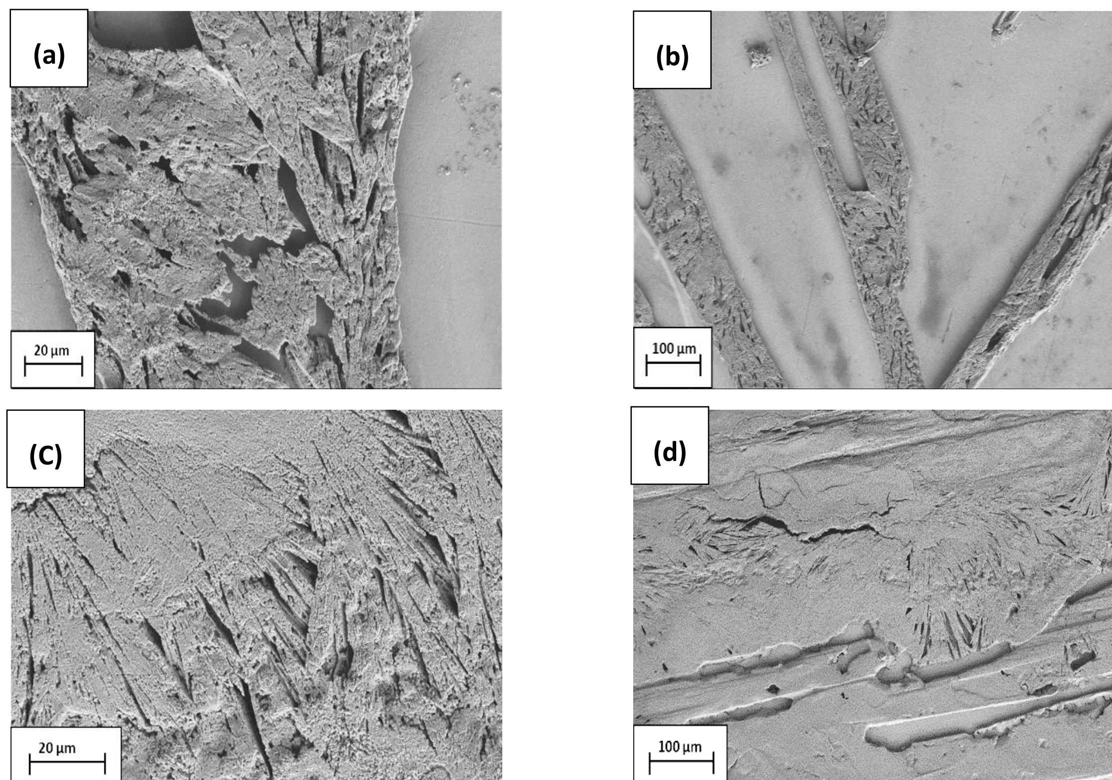

Figure 5.5: SEM micrographs of copper crystal deposit on stainless steel surface in the presence of a High MW PAM at 300 A/m2. a-b) After 10 s deposition. c-d) After 30 s deposition.

After 10 s of deposition flat but porous, vertical growth structures have developed, transforming into a flat smooth, less porous crystal structure after 30s of electrodeposition. In Figure 5.5, it is evident that protruding vertical growth occurred comparing very well with the Low MW scenario copper deposit in Figure 5.3. Both additives, in this case, and in the case of the Low MW additive were anionic. The anionic content of the additives appears to promote enhanced vertical growth compared to the non-ionic additives. The crystal growth type for the High MW, anionic additive can be classified to be FT growth type. The CV results revealed that when a High MW additive was used the electrodeposit was polarized but not to the same extent as when the Low MW, or Medium MW additives were used. The EIS data indicated that the system resistance increased for the High MW additive, close to the same resistance as for the Medium MW additive, but not nearly to the same extent as when the Low MW additive was used. The increase in system polarization and resistance support the fundamental finding that FT growth type can develop when using this additive. The crystal structure in Figure 5.5 is most comparable to the crystal structure in Figure 5.3 achieved in the presence of a Low MW PAM additive, but more porous like the deposition achieved in the presence of a Medium MW PAM additive. This can indicate that more of the Low MW additive adsorbed onto the substrate surface compared to the High MW additive. Based on the

presented evidence it is concluded that the electrodeposition produced in the presence of the High MW, anionic PAM, followed progressive nucleation, and delivered 2D, FT type crystal growth.

5.1.6 Very High MW PAM

The copper deposits after 10 s and 30 s of electrodeposition in the presence of a Very High MW, non-ionic PAM additive is presented in Figure 5.6.

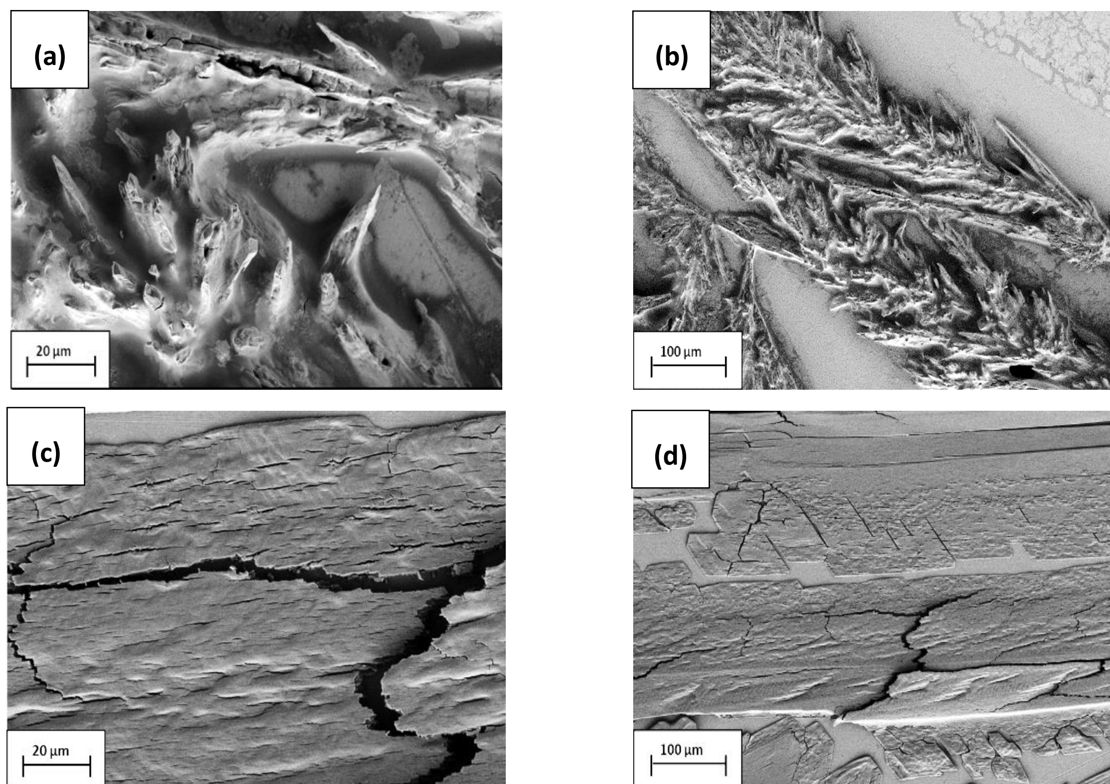

Figure 5.6: SEM micrographs of copper crystal deposit on stainless steel surface in the presence of a Very High MW PAM at 300 A/m2. a-b) After 10 s deposition. c-d) After 30 s deposition.

After 10 s of deposition spiky, rough, dendrite-like growth structures have developed, transforming into flat smoother structures, with cracks present after 30 s of electrodeposition. Cracks in electrodeposits are usually associated with internal stresses in the deposits. According to Stein (1996), there are numerous factors that can cause internal stresses in electrodeposits, including pH, electrolyte concentrations, temperature and current density. Since the High MW additive polarized the system the least of the additives investigated, it is possible that the increased current at which copper plated in the presence of this additive caused a heightened degree of internal deposit stress compared to the other Lower MW additives. Internal stresses were however not measured in this study. The structure of the deposit in Figure 5.6 after 10 s of electrodeposition is very comparable to the crystal structure achieved in the Base Case scenario in Figure 5.1. The Very High MW additive micrographs reveal a slightly smoother and less porous structure without the presence of pronounced nodules at the base of the peaks. It is concluded that the Very High MW additive controlled the crystal growth more, delivering a smoother but still undesirable cathode morphology. In Figure 5.6, it is evident that the crystal type varied between a dendrite-like and a smooth surface, implying that the Very High MW additive was ineffective in controlling the copper deposit growth in the system. In the 30 s deposit micrographs the structure is analogous to the deposit structure achieved when using the Medium MW additive. In both these cases the additives were non-ionic, implying a possible relationship between the ionic content and the morphology, also seen

Stellenbosch University https://scholar.sun.ac.za

in both anionic additive cases. Although inconclusive, a relationship between both non-ionic additives and both anionic additives were also observed and discussed in the EIS Nyquist plot results. The crystal growth type for the Very High MW, non-ionic additive can be classified to be FI growth type. The CV results revealed that when a Very High MW additive was also used the electrodeposit was marginally polarized but not to the same extent as when the Low MW, Medium MW, or High MW additives were used. The EIS data indicated that the system resistance increased with the Very High MW additive, with a lower system resistance than when the Low, Medium, and High MW additives were used. The slight (compared to other PAM additives) deviation in system polarization and resistance from the Base Case scenario supports the finding on a fundamental level that FI growth type, as with the Base Case scenario, can develop when using the Very High MW additive. Based on the presented evidence it is concluded that the electrodeposition produced in the presence of the Very High MW, non-ionic PAM, is difficult to predict and in this case to describe. It can follow instantaneous nucleation or progressive nucleation, and delivered 2D, FI and/or FT type crystal growth.

5.2 RDE results conclusions presented on Winand's Diagram

The finding from Grchev et. al. (1991), that increasingly higher MW PAM additives adsorb less onto the metallic substrate surface in an acidic solution, are consistent with the results obtained in both the fundamental and the electrowinning experiments. The SEM micrographs supports the fundamental CV and EIS findings and provides additional qualitative evidence to the quantitative results obtained in EIS and CV experimental work. Fabian et al. (2009) argued that Guar is non-specifically adsorbed into the Outer Helmholtz Plane due to the abundant presence of non-specifically adsorbed hydroxyl groups on Guar molecules. Therefore, Guar interacted with the electrode surface only via long-range electrostatic forces, having almost a benign effect on polarization with slight depolarization recorded. It was further argued that PAMs are specifically adsorbed and bond via hydrogen bonding to the electrode surface which could explain why the electrode is polarized in the presence of the PAMs. These interpretations from previous findings seem to be well aligned with the results achieved in the RDE electrowinning SEM micrographs.

Based on these results and interpretations a map is presented in Figure 5.7, plotting the interpretation of the combined results (CV, EIS, and three-electrode electrowinning) of each additive on Winand's diagram. Adcock et. al. (2002) also used this classification developed by Fisher (1969), and the diagram of Winand (1992) to classify and describe the crystal growth type and structure in a study which presented a newly extended theory on measuring polarization parameters that impact on the electrodeposit morphology (Adcock et al. 2002). The goal of utilizing this map is to predict cathode morphology for the application of various distinct organic additive types with different molecular characteristics, and therefore ultimately to predict product quality based on operating conditions.

Figure 5.7 is based on the current density measurements in the CV data and the inhibition/polarization/charge transfer resistance results gathered from both EIS and CV data. The SEM micrographs provided the necessary qualitative information to correlate the crystal structure with those obtained in the present study. The x- axis represents the fraction/percentage of the recorded current density over the diffusion limiting current density. The y-axis represents the inhibition intensity which in the context of the experiments of this investigation relate to the degree of polarization or charge transfer resistance achieved in the presence of each additive. Since electrowinning facilities usually operate at around 50% of the DLC, and plant conditions were simulated as closely as possible in this study, it can be expected that the Base Case scenario will be mapped at around 50% of the total length of the x-axis (given that the total length of the x-axis represents 100% of the DLC) (Shukla 2013). Furthermore, since little

Stellenbosch University https://scholar.sun.ac.za

inhibition is expected at the Base Case (absence of additives) it should be mapped close to the x-axis at a low inhibition level. Figure 5.7 contains the first attempt at mapping the predictions of the crystallographic structures obtained in the presence of the various organic additives with two assumptions:

i. A FT crystal structure developed in the presence of a Medium MW PAM organic additive.
ii. The relative boundaries on the map proposed by Winand were not altered or changed purposely from the original map, as given by Winand (1992), to fit the experimental data.

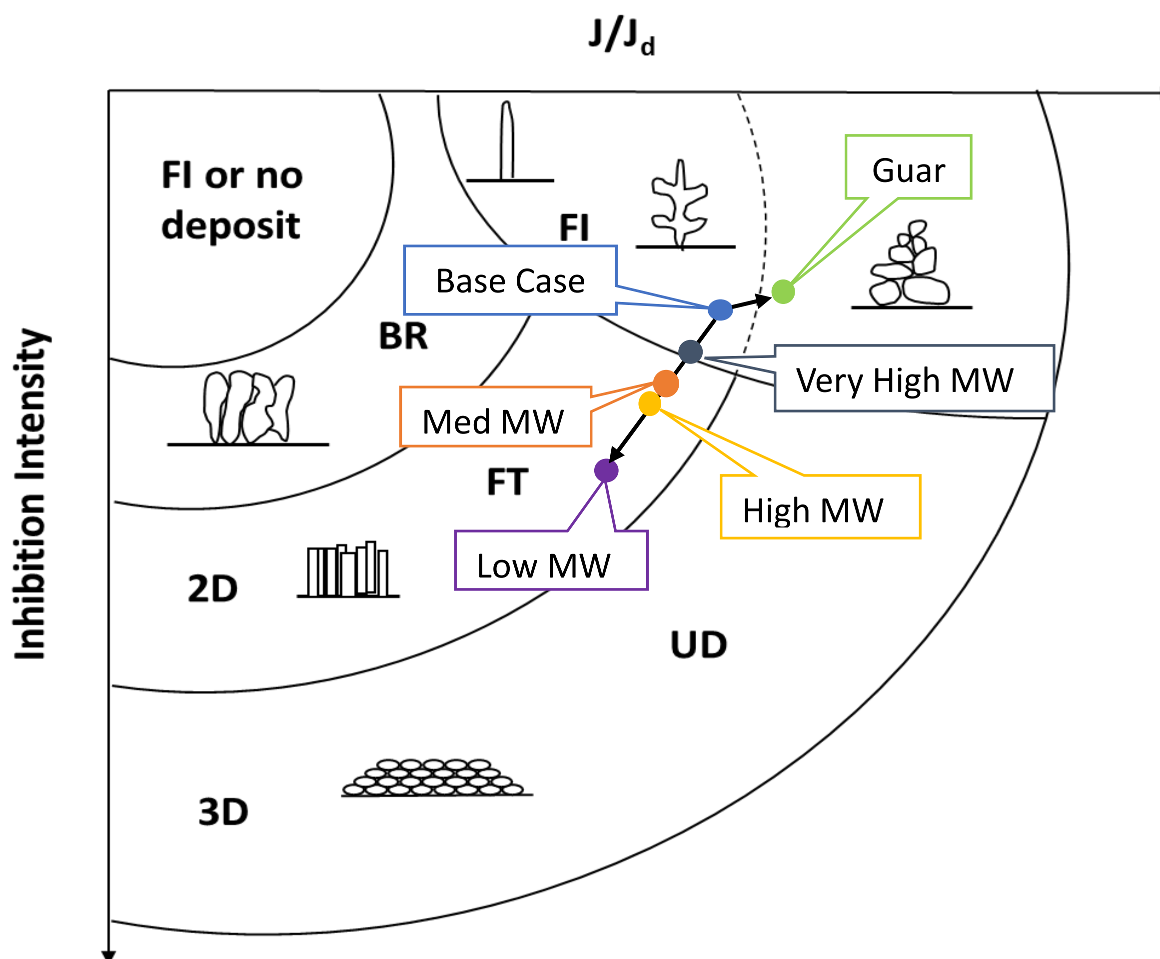

Figure 5.7:First interpretation of simplified diagram for predicting the crystallographic structure based on CV, EIS, and RDE electrowinning results for copper deposited for 10s in the presence of various additives, ranging in MW and ionic content by utilizing the diagram adapted from Winand, 1992.

From the Base Case as reference point the rest of the scenarios for the varying organic additives were mapped. Guar slightly depolarized the cathodic deposition meaning that on average an increase in current density was observed. Therefore, the shift on the map to the right on the x-axis away from the Base Case scenario. Guar also acted to decrease system inhibition by decreasing the charge transfer resistance and hence the shift towards the x-axis for a lower inhibition intensity. Lastly, the crystallographic structure of Guar showed that a 3D, UD type crystal structure developed after 10 s and 30 s of electrodeposition. Based on this combined result interpretation of the crystallographic structure predicted by Guar, it is placed as indicated on Figure 5.7 .

The Very High MW PAM additive performed the closest to the Base Case scenario on a fundamental level with increased charge transfer resistance recorded in EIS experimental works as well as increased polarization behavior recorded during CV. RDE electrowinning experiments revealed that the Very High,

Stellenbosch University https://scholar.sun.ac.za

non-ionic, PAM delivered both FI and FT type crystal structures with spiky and rough formations after 10 s of deposition and smoother, cracked formations after 30 s of electrodeposition. Based on the presented evidence, the crystallographic structure as predicted in the presence of a Very High MW PAM additive is mapped close to the Base Case scenario, with slight adjustment for an increased charge transfer and lower current density measurement. This places the prediction on the border of FI and FT type crystal growth indicating that the findings from EIS, CV, and RDE electrowinning studies fit logically onto Winand's Diagram.

Similar performance was recorded for the Medium and High MW PAM additives on a fundamental level. Both showed an increase in charge transfer resistance compared to the Very High MW PAM additive as well as an increased polarization effect. For these reasons the crystallographic predictions of these two additives are shifted further down (inhibition) and, to the left (current density), as indicated on Figure 5.7. Examination of the RDE electrowinning experimental results indicated that a stronger crystallographic relationship existed between the Medium MW PAM and the Very High MW PAM additive (after 30 s of electrodeposition). This was attributed to the fact that both additives are non-ionic in nature. The High MW PAM additive showed a crystallographic structure much closer to the Low MW additive and this might similarly be because both these additives are anionic in nature. For these reasons, the crystallographic prediction in the presence of a Medium MW PAM was mapped closer to the Very High MW additive crystallographic prediction compared to the corresponding prediction of the High MW PAM in the 2D, FT type area on Figure 5.7.

Lastly, the Low MW PAM additive showed the highest degree of polarization in CV experimental work and the highest resistance to charge transfer in EIS studies. The resulting SEM micrographs from the RDE electrowinning studies showed that 2D, FT type crystal growth served to describe the crystal structure the best. Therefore, the crystallographic prediction in the presence of a Low MW PAM additive were mapped furthest from the Base Case in the 2D, FT crystal type sector on Figure 5.7, accounting for the increased inhibition and decreased measure current density.

It should be noted that boundaries between the various deposit classifications are not fixed but merely gives a representation or interpretation of where the possible crystallographic borders could be. A more in-depth study at various current density levels will have to be conducted to plot the boundary locations more accurately. An alternative crystallographic structure boundary placement of Winand's Diagram is proposed in Figure 5.8 to fit the current results and data of the present study more effectively. It should however be emphasized that more detailed work should follow to be able to confidently determine the boundaries of this map.

Stellenbosch University https://scholar.sun.ac.za

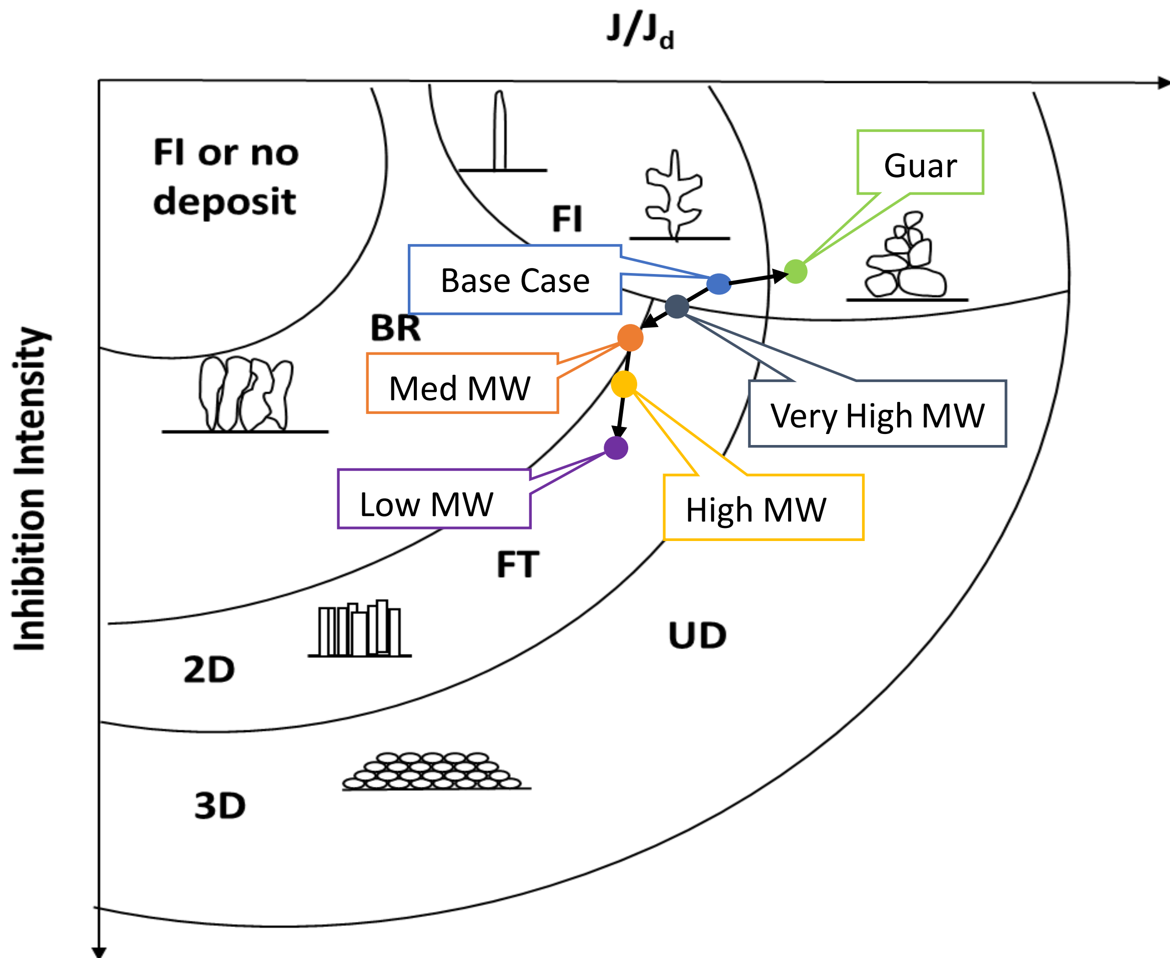

Figure 5.8: Second interpretation of simplified diagram for predicting the crystal growth type based on CV, EIS, and RDE electrowinning results for copper deposited for 10s in the presence of various additives, ranging in MW and ionic content by utilizing the diagram adapted from Winand, 1992.

In Figure 5.8 the BR crystallographic structure boundary was shifted closer to the FT crystallographic structure upper boundary to allow for the crystallographic prediction in the presence of the Medium MW PAM additive to be on the border of BR and FT, and therefore type Z crystal structure. This allows for a closer interpretation of the combined evidence from EIS, CV, and RDE electrowinning experimental work. Most importantly, it can be concluded that Winand's Diagram can be used effectively as a tool to interpret and predict the crystallographic structures of copper deposits in the presence of various organic additives.

Stellenbosch University https://scholar.sun.ac.za

5.3 Bench scale electrowinning results

Bench scale electrowinning experiments were conducted to validate the effectiveness of using the PAM additives to control localised growth (dendrites) in a continuous electrowinning system using parallel plates. The morphology of each plate was quantified for a more accurate comparison of the additive performance on a larger scale. The methodology for producing the 3D cathode images and the arithmetic mean surface deviation (S_a values) is discussed in Section 3.2.2.4 of this report. Section 5.3 of the report is divided into a qualitative and a quantitative analysis of the cathode plates achieved when using various organic additives.

The following data were utilized and discussed in the results and discussion of the bench scale electrowinning results.

- Colour images of the copper plates.
- Images of the plates indicating the changes in surface deviation (from a reference plane) to ± 0.3 mm with a colour scale.
- Minimum to maximum surface deviation values which were converted into S_a values.
- Mass of the copper deposit that was weighed.

Images of the plates indicating the changes in surface deviation to ± 1 mm with a colour scale from a reference plane are included in Appendix D -Bench scale electrowinning supportive results.

5.3.1 Qualitative analysis

In this section of results presentation and discussion a clear distinction is drawn between uneven copper growth and rough dendrite-like localized growth. Uneven growth refers to an uneven plate surface topography, whilst maintaining a smooth appearance. This type of plate morphology can be visualized as a smooth plate with gradually altering surface gradients. In other words, the transition from a lower reference surface point to a higher reference surface point is smooth and gradual. This type of smooth, uneven growth can occur due to prominent and preferential polarization on large parts of the plate surface.

Localized growth, or dendrite-like nodular growth, refers to a rough surface topography with a jagged like surface deposit. In other words, the transition from a low surface reference point to a high surface reference point is sudden and inconsistent in nature. This type of growth originates from copper depositing preferentially on “high – energy” active sites (Fabian 2005). It is believed that organic additives achieve a levelling/smoothing effect by preferentially adsorbing onto the active sites, thereby inhibiting further development and growth of the dendrite structure. Localized growth translates into the most unwanted surface morphology since this type of growth is unpredictable in nature and poses a high risk of cell short-circuiting. Severe dendrite growth tends to trap suspended solids and electrolytic solution which impacts the deposit’s ductility and conductivity negatively. Is has been reported that extreme cases of nodular growth lead to shattering of the copper plates during the stripping procedure (Cifuentes et al. 2014).

Stellenbosch University https://scholar.sun.ac.za

5.3.1.1 Colour image analysis

Colour images of the resultant cathode plates for all experimental conditions are presented in Figure 5.9. These images were used to draw out qualitative information on the additive performance during the bench scale copper electrowinning experiments. The plate images are orientated with the bottom of the plate pointing upwards.

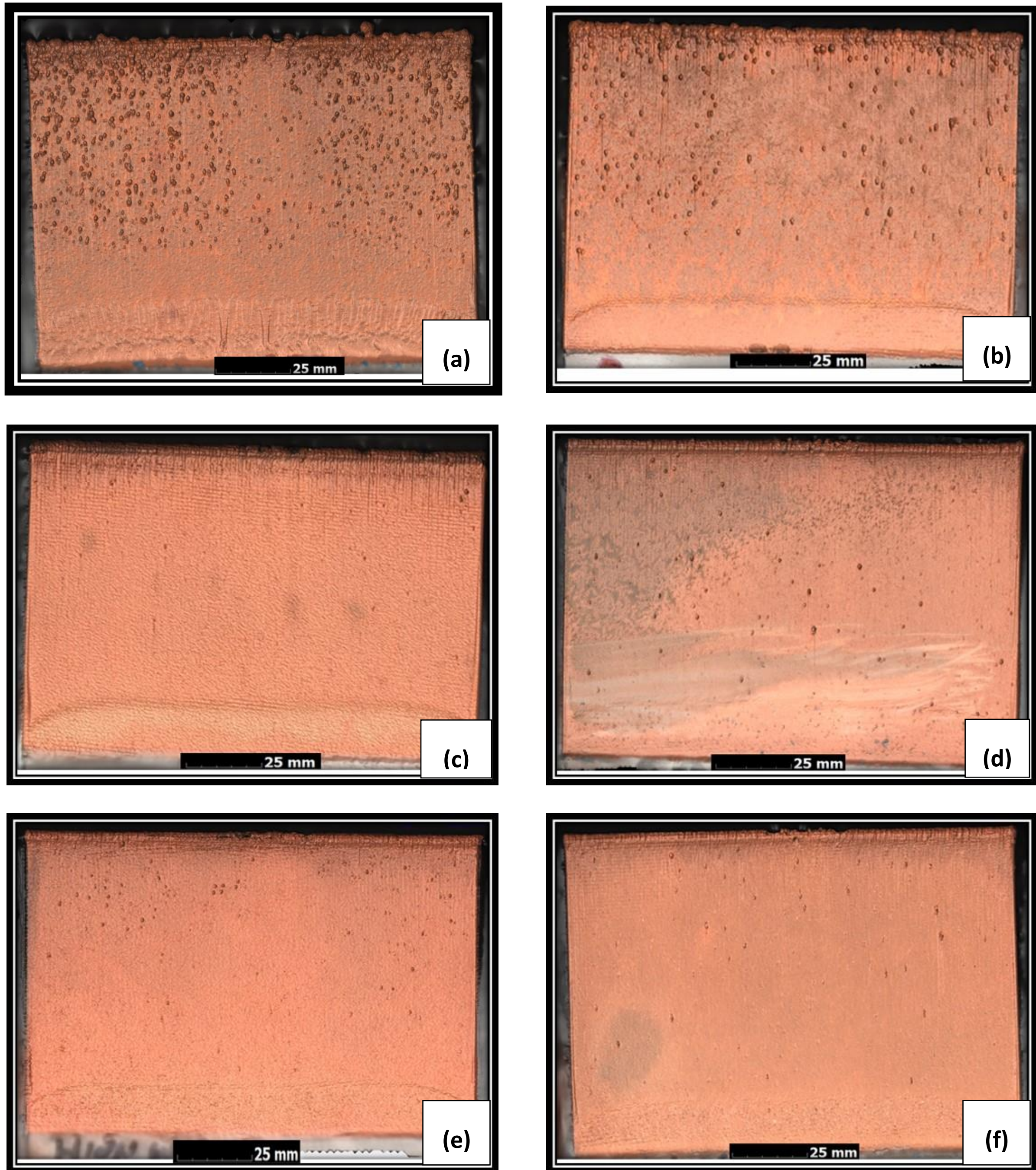

Figure 5.9: Colour image of resultant copper plate achieved in a) Base Case scenario; b) 2 mg/L Guar; c) 2 mg/L Low MW PAM; d) 2 mg/L Medium MW PAM; e) 2 mg/L High MW PAM; f) 2 mg/L Very High MW PAM.

The copper deposited in a Base Case electrolyte is presented in Figure 5.9 (a). A very rough surface topography is observed. The surface of the cathode is evidently covered in nodules and dendrites, increasing in concentration moving towards the bottom part of the plate. The resultant copper deposit is

Stellenbosch University https://scholar.sun.ac.za

comparable to the SEM micrographs of copper nucleation structures in a Base Case electrolyte in Figure 5.1. Both the SEM micrographs and the bench scale electrowinning images provide evidence of localized growth, nodules and dendrites, and an overall rough surface area. This is unmistakable evidence that an undesirable cathode morphology develops in the absence of an organic smoothing agent in the electrolyte.

In the presence of 2 mg/L Guar, the ensuing copper deposit was much smoother compared to the Base Case scenario. As indicated in Figure 5.9 (b), less dendrite formation and localized growth prevailed in the presence of Guar even though the surface can still be classified as rough and irregular. Fabian et al. (2007) investigated the plate morphologies of copper electrowinning in an electrolytic solution in the presence of Guar and an activated Very High MW non-ionic PAM. In this study the resultant plate morphology in the presence of Guar as an additive was described as "dendritic and discontinuous" and a rough needle-like copper deposit developed. Further examination of plate cross sections under a scanning electron microscope revealed that the crystal structure that developed in the presence of Guar was porous (Fabian et al. 2007). A similar description was given by Sun and O'Keefe (1992) for a copper deposit in the absence of any additives. Based on the results of the current study, it is concluded that Guar delivered an overall smoother cathode morphology compared to the copper deposit in a Base Case electrolyte. However, many similarities exist between the plate structure and characteristics of the Base Case deposit and the deposit that developed in the presence of Guar.

A bright copper deposit was produced in the presence of a Low MW PAM additive. Figure 5.9 (c) reveals a shiny copper plate with little to no localized growth, which is desired in operating copper electrowinning facilities. EIS and CV studies revealed that the Low MW PAM additive caused the highest degree of charge transfer resistance and polarization of all additives. Three-electrode and bench scale electrowinning experimental work revealed that smooth compact 2D, FT type crystal growth developed on the cathode surface. It is possible that the short-range hydrogen bonding between additive and substrate, coupled with the increased adsorption behaviour of the Low MW PAM additive, acted to almost entirely neutralise the active sites on the cathode surface. The much-improved deposit structure achieved in the presence of the Low MW PAM additive is not consistent with the findings of Vereecken and Winand (1976). However, numerous studies thereafter delivered comparable results to the current study (Fabian et al. 2007; Helsten & Moats 2013; Tshimwanga et al. 2011). In conclusion, a Low MW, anionic polyacrylamide additive has shown its ability to be an effective smoothing agent under the current experimental conditions.

A smooth overall morphology is attained for copper electrowinning in the presence of the non-ionic Medium MW PAM additive (Figure 5.9 (d)) and the anionic High MW PAM additive (Figure 5.9 (e)). However, in both cases more localized growth is observed on these cathode plates compared to the plate achieved in the presence of the Low MW PAM additive. Electrochemical experiments revealed that the Medium MW and the High MW PAM additives performed very similar in terms of increasing charge transfer resistance and polarization at the electrolyte/electrode interface. These conclusions suggest that there is a relationship between the degree of polarization caused by the additive and the eventual cathode plate morphology, since the two plates are very comparable in terms of the occurrence of nodular growth.

Visually, the Very High MW PAM additive delivered a smooth and bright copper deposit (Figure 5.9 (f)). The deposit morphology is not as smooth as the deposit achieved in the presence of the Low MW PAM additive, but it is smoother, or at least as smooth as the copper deposits achieved in the presence of the Medium and High MW PAM additives. Fundamentally, the Very High MW PAM additive polarized the

Stellenbosch University https://scholar.sun.ac.za

cathodic deposit the least compared to the other PAM additives. The charge transfer resistance at the electrolyte/electrode increased in the presence of the Very High MW additive, but not to the same extent as the rest of the lower MW PAM additives. Following the trend of increased surface smoothness for an increased polarization effect, it was expected that the deposit in the presence of the Very High MW PAM additive would be significantly rougher, or at least close to the roughest of all the resultant deposits in the presence of the PAM additives. Three-electrode electrowinning experiments revealed that after 10 s of deposition a rough surface with evidence of localized growth developed correlating well with the nucleation growth deposit of the Base Case scenario. After 30 s of electrodeposition a smoother flatter surface developed corresponding more with a 2D/ FT type crystal growth type. These conflicting deposit structures achieved under the same experimental conditions demonstrates that the Very High MW additive might be less capable of controlling eventual smoothness of the copper surface. However, a smooth and bright copper deposit was achieved during the bench scale electrowinning experiments.

The copper deposit that developed in the presence of the Low MW PAM additive appears to be the brightest of all the deposits while the Base Case scenario cathode plate appears to be the dullest. It is hypothesized that in the absence of a smoothing agent a porous copper deposit structure developed (as discussed in Section 5.1.1), enabling electrolyte entrapment and crystallization in the pores. It is possible that the entrapped crystalized electrolyte caused this discolouration. The blue-grey tinge on the plate surface is noticeable on all copper plates, but less so on the plates where PAM additives were utilized. Investigation of the RDE electrowinning SEM micrographs revealed that the suppressive nature of the Low MW PAM additive delivered the densest deposit structure, and this seems to be corroborated in the bench scale electrowinning results. The significant discoloration on the top left-hand side of Figure 5.9 (d) (Medium MW PAM) was due to horizontal placement of the cathode during the drying process which allowed electrolytic solution to pool and crystalize on the plate surface.

5.3.1.2 Colour scale surface topography analysis

The colour scale shows the relative height of each copper nodule in each region of interest. Figure 5.10 provides valuable insight regarding the relative distance of surface deviations (negative and positive) from the best fit planes.

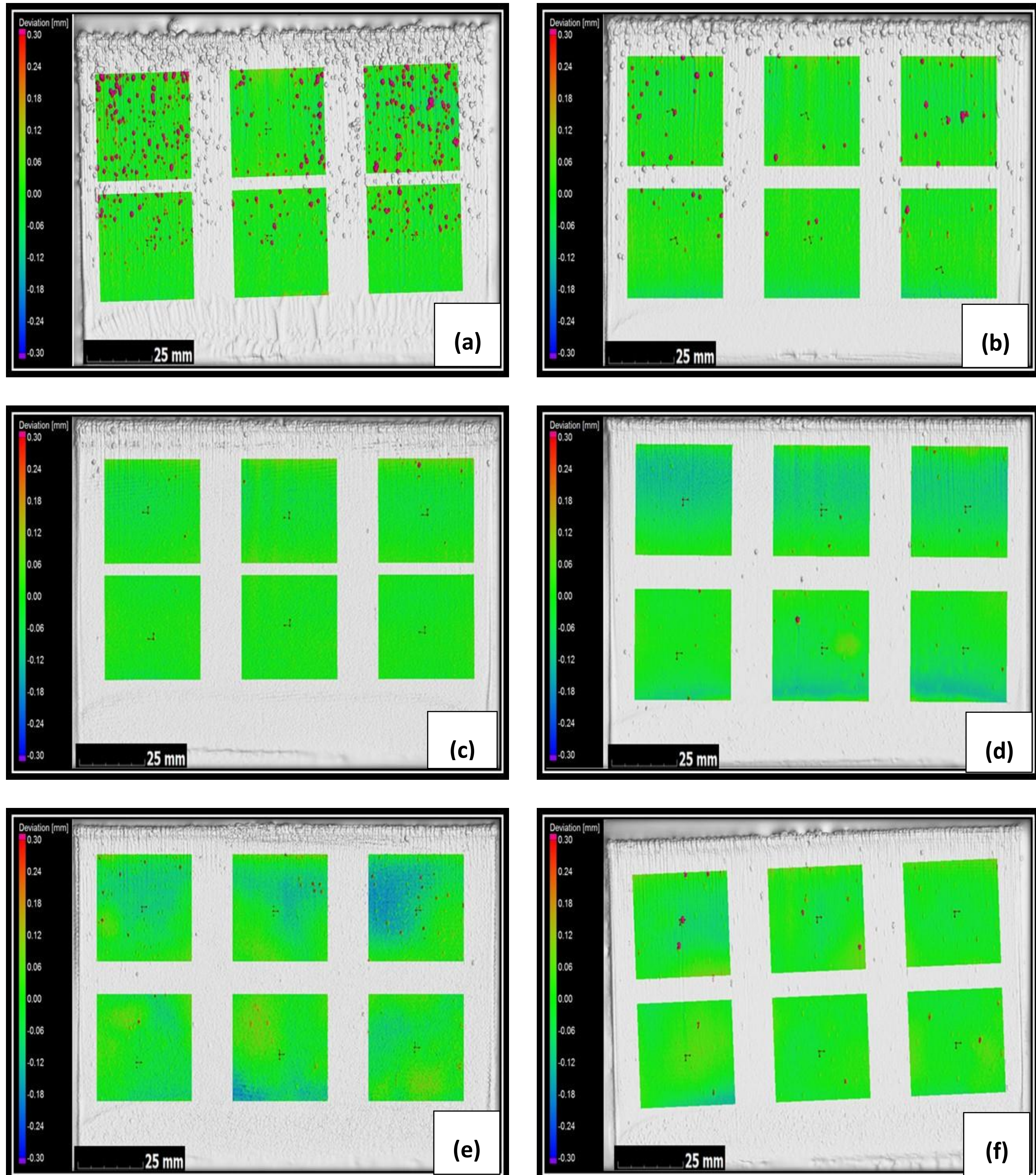

Figure 5.10: Cathode surface topography delivered in a; a) Base Case; b) 2mg/L Guar; c) 2 mg/L Low MW PAM ; d) 2 mg/L Medium MW PAM; e) 2 mg/L High MW PAM; f) 2 mg/L Very High MW PAM; electrolyte, with a surface height colour scale indicating ± 0.3 mm deviation on the six selected regions of interest.

It is apparent from Figure 5.10 (a) and (b), that in the absence of any additives, and with Guar as an additive, a flat surface with sporadic deviations most of which exceeds 0.3 mm in height developed. This

Stellenbosch University https://scholar.sun.ac.za

gives compelling evidence of localized growth, meaning selective growth of copper on a certain spot or area on the plate surface. The plate morphology did however improve in the presence of Guar. Yet Guar seemed unable to effectively adsorb on all the high - active energy sites. The lack of consistent additive interaction/adsorption substantiates the theory of weaker longer-range bonding of guar molecules with the cathode surface from the Outer Helmholtz Plane as described in Section 4.2.3 of this report.

The deviation scale in Figure 5.10 (c) shows virtually no negative or positive deviation from the best fit plane. This provides further evidence that the Low MW PAM adsorbed evenly and effectively onto the cathode surface. There seems to be a direct correlation between an increased polarizing effect and a smoother cathode surface.

By investigating both Figure 5.10 (d) and (e), it is concluded that the polarization behaviour induced by the Medium and High MW PAM additive resulted in less localized growth. It is possible that these additives adsorbed unevenly/preferentially on the plate surface as indicated by the increased negative deviations from the best fit plane. This evidence provides further support for the theory of more complete surface adsorption and coverage of Lower MW PAM additive as proposed by Grchev et al. (1991).

Figure 5.10 (f) depicts a more monotone colour scale for the deposit achieved in the presence of the Very High MW PAM additive. Very little negative surface deviation is observed which is in contrast with the deposits achieved in the presence of the Medium and High MW additive respectively (Figure 5.10 (d) and (e)). Limited negative and positive surface deviations possibly implies more consistent surface coverage, although this contrasts with the previous findings from Grchev et al. (1991) (at low PAM concentrations). Consistent with the theory of low surface coverage for Higher MW PAM additives, it is conceivable that the Very High MW additive although achieving a low surface coverage, can selectively migrate and adsorb on active sites. This would enable and even/smooth crystal growth pattern. Ultimately, by visual inspection only, it is difficult to explain the occurrence of such a smooth plate achieved in the presence of a Very High MW PAM additive considering the evidence and arguments presented thus far.

5.3.2 Quantitative analysis

The quantitative analysis method was described in Section 3.2.2.4 of this report. The high-quality 3D volumetric data of each scanned plate were imported and analyzed on Volume Graphics VGStudioMax 3.1. This software allowed for the evaluation of surface roughness in a quantitative manner by exporting the surface deviation data in CSV format. The average deviation of the copper deposit surface from the reference plane measured at each of the surface elements (S_a value) was calculated for each copper plate and is presented in this section. The S_a values is therefore a measure of the average surface roughness, which is the average deviation from the normalized flattest surface plane.

5.3.2.1 Normalization of reference planes

As discussed in Section 3.2.2.4, the distance from the best fit plane (reference plane) to the copper deposit surface was measured at each of the surface elements; the density distribution of these deviations from the reference plane for the respective additives tested are shown in Figure 5.11. The flattest part of the cathode surface is where the highest deviation density is observed (i.e. the peak of the density distribution curve). The position of the reference plane in each of the selected regions on each of the plates was effectively normalized by making the flattest part of the plate the “new” reference plane. This enabled relative comparison of the distribution of copper surface deviations away from the normalized flattest surface between the plates on the same axis as seen in Figure 5.11.

Essentially, Figure 5.11 can be explained in the following way: a narrower distribution of deviations implies that less surface deviation developed from the flattest plane during the electrodeposition process, and hence a lower total surface roughness value can be expected.

It therefore appears as if the High or Medium MW PAM additive resulted in the largest spread of surface area away from the reference plane, and consequently had the roughest surface area. It was explained that localized growth is much more unwanted and damaging compared to smooth uneven growth. Cathode indentations (negative deviations) are much less harmful in an electrowinning facility than erratic large protrusions (positive deviations). Deviation distributions with long tails, especially in the positive direction, are therefore undesirable.

Figure 5.11 gives useful insight: a smaller proportion of the plate produced in the presence of a Medium and High MW can be considered smooth compared to the Base Case which seem to have a narrower distribution around the reference plane. However, large dendrites were more prominent on the plate achieved in the Base Case experimental condition (Figure 5.9 (a)), which is indicated in Figure 5.11 by the long distribution tail in the positive direction.

Appendix D -Bench scale electrowinning supportive results, Section 8.4.2 provides an interpretation of Figure 5.11 by eliminating negative deviations from the data to demonstrate the distribution tail for the Base Case scenario more clearly.

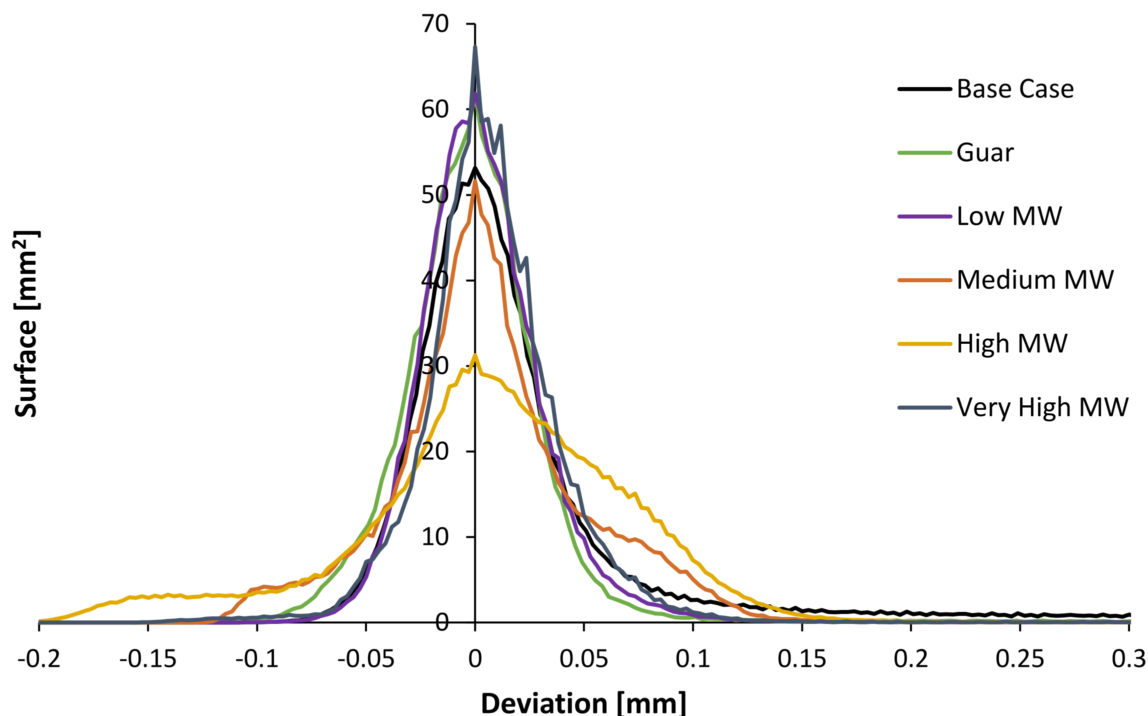

Figure 5.11: Average total surface elements (area) deviation from the flattest surface plane (normalized) for each plate achieved in the presence of its unique additive.

5.3.2.2 Average deviation from the normalized reference plane (S_a value)

The S_a values calculated for the copper plates produced when adding the different additives are shown in Figure 5.12. It is important to note that for Figure 5.12 the S_a value is calculated by factoring in both negative (indentations) and positive (protrusions) surface deviations. In other words, negative deviations are converted to absolute values and then combined with the positive deviations to calculate an overall mean surface deviation for each deposit. Figure 5.12 reveals that the copper plate produced in the

absence of any additive had the highest S_a value of 63.43 µm, followed sequentially by the deposits in the presence of the High MW PAM, Medium MW PAM, Guar, Very High MW, and finally the Low MW PAM with a S_a value of 23.45 µm.

Considering both negative and positive deviations from the flattest part of the surface it is clear the High and Medium MW additives performed the worst of all additives. It was previously suggested, based on the qualitative evidence, that these additives possibly adsorbed unevenly onto the cathode surface and caused localized polarization on the cathode plate. It looks as if the localized polarization resulted in uneven crystal growth, although relatively smooth compared to the Base Case and Guar experimental plates. This is also evident from the data presented in Figure 5.11 where a wide deviation distribution but a short tail on distribution was observed for the Medium and High MW scenarios (i.e. a relatively substantial proportion of intermediate deviations and few dendrites).

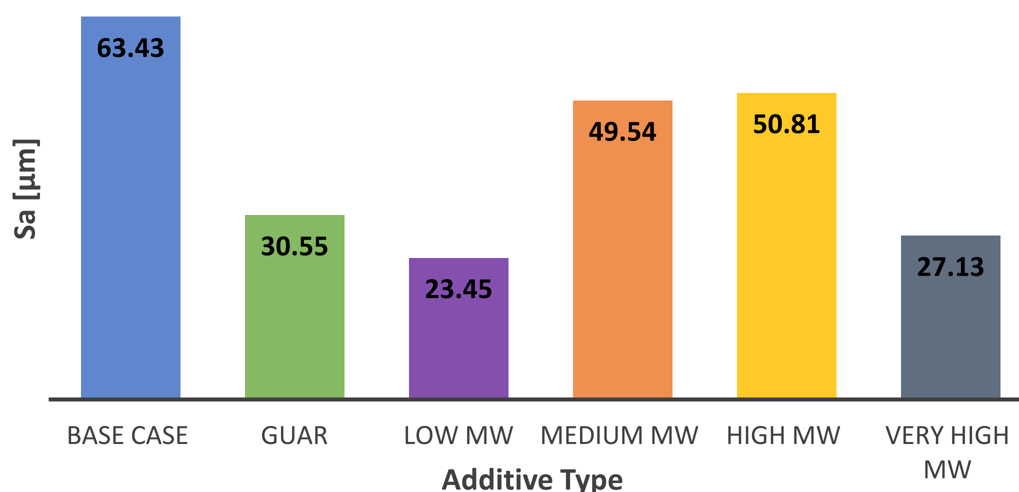

Figure 5.12: Calculated arithmetic meant surface deviation (Sa value) of copper deposit during electrowinning experiments at 300 A/m^2 & 40 ^{o}C in the presence of various organic additives – considering both negative and positive deviations.

By accounting for negative deviations when calculating the mean surface deviation from the normalized flattest part of the plane, equal weight is given to uneven growth and localized growth. In the context of the qualitative evidence presented in Section 5.3.1, negative deviations on the plate topography will not cause short-circuiting, nor will it necessarily lead to a lower quality cathode plate in terms of ductility, purity, porosity, and entrapment, whereas localized growth will. The S_a values were therefore recalculated to describe cathode quality by giving much more weight to localized growth. This was done by considering only positive deviations from the reference plane, since positive deviations are directly related to nodules and localized growth. The calculated S_a values without considering negative deviations are presented in Figure 5.13.

Stellenbosch University https://scholar.sun.ac.za

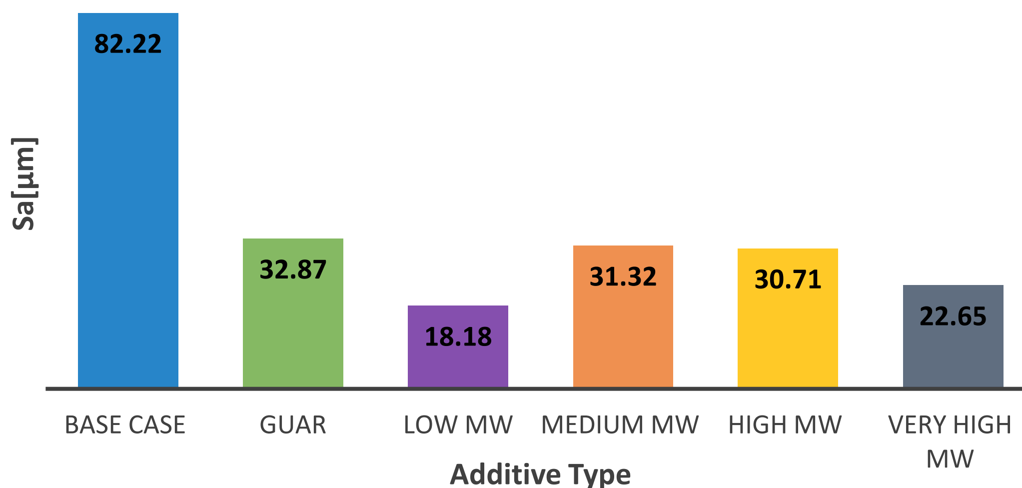

Figure 5.13: Calculated arithmetic meant surface deviation (Sa value) of copper deposit during electrowinning experiments at 300 A/m^2 & 40 ^oC in the presence of various organic additives – considering only positive deviations.

Compared to the results in Figure 5.12, it is noted that all the S_a values decreased except for the S_a values of the copper plates produced without any additives and in the presence of Guar. This suggests that more positive deviations (protrusions) were captured further away from the flat copper surface for the Base Case and Guar plates compared to the plates achieved in the presence of the other PAM additives. For all the PAM experimental cases the positive deviations (protrusions) were spread closer to the flat surface, and therefore their S_a values decreased. This is an indication of improved cathode quality for when all PAM additives were used, as is consistent with the qualitative analysis.

It is also noted that the resulting trend in Figure 5.13 is very consistent with the conclusions made on the qualitative analysis: the Base Case scenario delivered the roughest plate morphology, followed by the plate produced in the presence of Guar. The Low MW PAM additive delivered the smoothest most desirable cathode deposit. This additive almost eliminated localized growth and produced an even cathode surface. This is shown by its very low S_a value of 18.18 µm. The Medium and High MW PAM followed Guar to deliver a much-improved plate morphology without complete elimination of localized growth. These additives also delivered an uneven surface morphology with regular deviation, although smooth in nature, from the flat surface. The Very High PAM delivered a much-improved plate morphology compared to the Base, Guar, Medium MW, and High MW scenarios which is consistent in the S_a value presented in Figure 5.13.

5.3.2.3 Rate of copper deposition

The total mass of copper deposited and the average rate of copper deposition for each plate is presented in Table 5.1. Table 5.1 also includes the calculated current efficiency (CE) values. The CE was calculated as described in Section 2.4.1 of this report. In practical terms, the current efficiency is the ratio between the charge spent on plating the actual amount of copper, and the total charge spent for a theoretical amount of copper that was expected to plate at a 100% efficiency (see Section 2.4.1.2). It was calculated that a theoretical amount of 267.44 grams of copper was expected to plate on each cathode at a current of 9.4 A and over a time of 24 hours. Comparing this with the actual amount of copper deposited on each plate, it is determined that a very high CE was accomplished in the EW cell. The reason for this might be that there were no contaminant metals added in the electrolyte which would compete with the copper to

Stellenbosch University https://scholar.sun.ac.za

plate in the system. Secondly, much care was given with the EW cell, to reduce resistance. This study was aimed at isolating the performance of the organic additives, and this was achieved by reducing interferences within the system. See Current efficiency calculations, Section 8.3.2 for sample calculations.

Table 5.1: The amount and average rate of copper deposited during 24 hours of electrowinning at 300 A/m² & 40 °C in the presence of various organic additives with the corresponding calculated CE values.

Additive Type	Amount of copper deposited (g)	Rate of deposition (g/hour)	CE (%)
Base Case	265.37	11.06	99.22
Guar	266.41	11.10	99.61
Low MW	266.58	11.11	99.68
Medium MW	267.91	11.16	100.17
High MW	266.95	11.12	99.82
Very high MW	266.98	11.12	99.83

The differences in the amount of copper that was deposited on the plates varied slightly and is directly related to the difference in the CE. The total mass of all copper plates was within 2.54 grams of each other. The current efficiencies of each electrowinning scenario did not vary by more than 1 %. The CE in the presence of no-additive was the lowest at 99.22%. The CE in the presence of Guar and the Base Case scenario were lower than the current efficiencies in the presence of PAM additives.

The fact that the highest CE values were calculated for the PAM additives might indicate that the CE of copper electrowinning is improved in the presence of the PAM additives. The variance between the CE values are however so small that this theory cannot be substantiated. Since the CE was measured by the total mass of the copper deposited, and the variance in total mass deposited between the scenarios was so low, it might be that variance of mass of dried electrolyte on the cathode surface contributed to the small variance in total mass of the copper deposits. Little evidence exists to prove that CE is improved in the presence of PAM additives. Sufficient evidence exists however, to prove that at the very least no significant difference in CE was measured between using the various organic additives in the present experimental conditions. This enables the selection of an additive that shows qualitative and quantitative evidence of being the highest performing organic additive in this copper electrowinning facility, without having to compromise on CE. It is recommended that future studies investigate the CE of copper electrowinning in the presence of these organic additives in an electrolyte that contains metal impurities as is expected in a real life operating facility. This investigation will serve to confirm or reject the hypothesis that the organic additives affect the CE of a copper electrowinning facility.

Stellenbosch University https://scholar.sun.ac.za

6 CONCLUSIONS & RECOMMENDATIONS

6.1 Conclusions

The fundamental studies investigated polyacrylamide (PAM) additives which are structurally different from one another, and their effects on copper electrodeposition were characterized and compared to that of a Base Case scenario and Guar. A three-electrode cell was utilized to conduct EIS and CV experimental work to characterize the effects of molecular weight (MW) and ionic charge of the organic additives on electrodeposition within the metal solid interface boundary. These techniques were implemented to draw out impedance information, specifically relating to the system polarization behaviour (R_{CT}).

The EIS data (Nyquist plots) and subsequent equivalent circuit modelling results were found to be reliable, since the base case R_{CT} value compared well with previous studies and all minor divergences could be accounted for. Polarization resistance and double layer capacitance increased for a decrease in PAM additive MW. The R_{CT} values at 2 mg/L additive concentration gradually increased from 3.36 Ω to approximately 7 Ω as the PAM additive MW decreased from very high to low. Increased polarization behaviour for lower PAM MW additives was attributed to a higher degree of surface adsorption/coverage achieved compared to high MW additives. It was determined that the formation of secondary loops in the low frequency region is because of a secondary electrical interface layer caused by the additives. Capacitive semi-circles were found for non-ionic PAM additives. These were absent for the anionic PAM additives where evidence of inductive loops was observed. This phenomenon should be investigated further. No clear correlation between polarization behaviour and additive ionic content was observed.

EIS and CV results indicated that an increased additive concentration of 10 mg/L enhanced the polarization resistance and double layer capacitance, and these occurrences were explained by the formation of PAM- Cl^--Cu^+ ion pairs, adsorbing onto the hydrophobic copper cathode surface. It was proposed that Guar is non-specifically adsorbed and only interacts near the Outer Helmholtz Layer with the electrode surface via long range electrostatic forces, explaining its non-existent polarizing affect. It was suggested that the non-ionic PAM's adsorb on the hydrophobic copper substrate surface via hydrogen bonding (short-range interactions) with their apolar backbone. At low pH conditions it is proposed that the anionic PAMs bond in a similar fashion due to the abundance of H^+ ions in the electrolyte. The short-range interactions between the PAMs and the electrode surface and the increasing surface coverage for lower MW PAM explained the polarization behavior observed in both EIS and CV results.

Electrowinning experiments were conducted in a three-electrode setup and in a bench scale facility. Three-electrode copper electrowinning experiments were conducted to investigate the nucleation and crystal growth structures of copper in the presence of varying types of polymeric additives. To achieve this, copper was deposited in an acid electrolyte for 10 s and 30 s in the presence of the selected polymers. The resultant deposits were qualitatively analysed via SEM micrographs and mapped on Winand's Diagram which predicts crystal structure as a function of current density and inhibition intensity. Bench scale electrowinning experiments were aimed at validating the effectiveness of using various smoothing agents to control localised growth (dendrites) in a continuous electrowinning system using parallel plates. The CE's of each electrowinning experiment in the presence of the various additives were also calculated based on the mass of copper that was plated in each run respectively. Furthermore, it was desired in both three-electrode and bench scale electrowinning experiments to establish a correlation between

Stellenbosch University https://scholar.sun.ac.za

fundamental EIS and CV work and the resulting cathode morphologies in the presence of each additive respectively.

RDE electrowinning experimental work indicated that the deposit that was formed in the absence of an additive was rough, spiky, and had dendrites. The deposit structure that developed in the presence of Guar was sphere-shaped, 3D crystals and overall smoother than the deposit in the absence of additives. The copper deposits after 10 s and 30 s of electrodeposition in the presence of PAM additives followed a general trend of increasing crystallographic smoothness (flatness) with increasing inhibition/polarization levels. The Very High MW PAM additive polarized the deposition the least based on EIS and CV results and delivered a morphology most comparable with the morphology of the deposit achieved in the absence of using an organic additive. The Low MW PAM additive polarized the cathodic deposit the most as was shown in EIS and CV results and delivered the most desirable crystallographic morphology. In the presence of the Low MW PAM additive a smooth, compact, 2D, FT type crystallographic structure was achieved. The crystallographic structures of each deposit could be mapped on Winand's Diagram and it was shown to be consistent with literature, and EIS and CV experimental work.

Bench scale electrowinning results revealed that both a qualitative and quantitate analysis of the results was necessary to make accurate conclusions on which polymeric additive performed the best in terms of eliminating localized growth. The following major conclusions were drawn after conducting a qualitative and quantitate analysis of the copper plates in the presence of the selected organic additives:

- The Low MW PAM had the lowest calculated S_a (mean surface height) value of 18.18 µm, and this additive delivered the smoothest and arguably the brightest deposit with an almost complete absence of localized growth.
- PAM additives generally delivered much improved cathode deposits in terms of eliminating localised growth compared to the deposits achieved in the presence of Guar and a Base Case electrolyte.
- The Medium and High MW PAM additives delivered a smooth but uneven deposit. Image analysis of the surface topography revealed a lot of negative surface deviation on both these deposits.
- All additives delivered cathode deposits consistent with evidence from fundamental and RDE electrowinning experimental work except for the Very High MW PAM additive which delivered mixed results in all electrowinning experimental work.
- The CE values calculated for each experiment in the presence of varying organic additives did not change with more than 0.95%, indicating that the various organic additives had little to no effect on the system CE.

6.2 Recommendations

The exact MW of the organic additives could not be determined in this study. Only the relative MWs of the organic additives compared to each other were determined. The exact MW of the organic additives would enable the researcher to directly correlate the actual MW values and polarization performance of additives during copper electrowinning. Furthermore, a MW range could then be proposed to design PAM additives for the electrowinning industry which would deliver the optimal performance in terms of plate morphology and CE.

The electrolyte used in the electrowinning studies did not contain impurities as electrowinning facilities do contain in actual operations. The reason for this was to be able to isolate the performance of the organic additives in the electrowinning cell and to compare their performance with each other. Various metallic ions are present in the electrolyte of an actual electrowinning operation, iron ions being the most

Stellenbosch University https://scholar.sun.ac.za

common metallic impurity. It is proposed in future investigations to determine the impact of metallic impurity type, and their concentration on the CE and cathode morphology in the presence of the organic additives utilized in this study.

Operating conditions remained constant in the current study. It might be prudent to vary the most important operating conditions in copper electrowinning experiments, like current density and temperature to determine if changes in these parameters affect the performance of the organic additives. Operating limits can then be proposed for the tested parameters to achieve optimal performance in conjunction with the additive.

In EIS experimental work inductive loops were observed on the secondary interface that formed in the presence of the anionic PAM additives. Non-ionic PAM additives formed a capacitive secondary loop. Further investigation is warranted to determine the relationship between ionic content and the type of crystal growth, by means of inspecting cross sectional cuts of the cathode plates via SEM.

The performance of the additives proposed in this study can be compared, especially the best performing Low MW PAM additive with current PAM market products like Cyquest N900 under the same experimental conditions.

The effects of PAM additive present in low concentrations on downstream processes like the SX stage following electrowinning are little understood. Future studies should investigate how PAM additives might cause crud formation or change the surface properties of the organic phase used in SX circuits leading to a reduced selective transfer of the copper ions from the organic phase to the advanced electrolyte.

Stellenbosch University https://scholar.sun.ac.za

7 REFERENCES

Adcock, Peter & Adeloju, Samuel & Newman, O.M.G. (2002). Measurement of polarization parameters impacting on electrodeposit morphology I: Theory and development of technique. *Journal of Applied Electrochemistry*. 32. 1101-1107. 10.1023/A:1021251603240.).

Bard, A.J. & Faulkner, 2000. *Electrochemical Methods*, John Wiley & Sons, Inc.

Berlic, C. et al., 2014. Study of the instantaneous nucleation phenomena in soft matter systems by means of Monte Carlo simulation. *Digest Journal of Nanomaterials and Biostructures*, 9(1), pp.197–204.

Bernu, C.J., Sandoval, S.P. & Morales, C.R., 2010. Development and commercialization of modified polysaccharide smoothing agent for copper electrowinning. *SME Annual Meeting and Exhibit 2010*.

Beukes, N.T. & Badenhorst, J., 2009. Copper electrowinning: Theoretical and practical design. *Journal of the Southern African Institute of Mining and Metallurgy*, 109(6), pp.343–356.

Bott, A.W., 2000. Controlled Current Techniques. *Current Separations*, 18(4), pp.125–127.

Broseta, D. & Medjahed, F., 1995. Effects of Substrate Hydrophobicity on Polyacrylamide Adsorption. *Journal of Colloid And Interface Science*, 170(2), pp.457–465.

Budevski, E., Staikov, G. & Lorenz, W.J., 2000. Electrocrystallization Nucleation and growth phenomena. *Electrochimica Acta*, 45(15–16), pp.2559–2574.

Chamovska, D. B., Grchev, T.P. & Cvetkovska, M. V., 2006. The Impact of Polyacrylamide Molecular Weight on Its Adsorption Behavior at the Gold / Acidic Solution. *Turk J Chem*, 30, pp.653–661.

Cifuentes, R., Bravo, R. & Schwarz, N., 2014. Effective Grain Modification in Copper Electrowinning with DXG-F7. *Journal of the Southern African Institute of Mining and Metallurgy*. pp 389-397

Cooper, W.C. & Mishra, K.K., 1987. The nature of copper electrowon in the presence of iron using sulfur dioxide sparging. *Hydrometallurgy*, 17(3), pp.305–313.

Cui, W., 2014. Effect and Interactions of Commercial Additives and Chloride Ion in Copper Electrowinning. *Masters disertation.* Missouri University of Science and Technology. Columbia.

Dini, J.W. & Snyder, D.D., 2011. Electrodeposition of Copper. *Modern Electroplating: Fifth Edition*, pp.33–78.

Dresher, W.H., 2001. How Hydrometallurgy and the SX/EW Process Made Copper the "Green" Metal. *JMM.,* 45 (1)., pp. 45 - 57.

Du Plessis, A., Sperling, P., Beerlink, A., Kruger, O., Tshabalala, L., Hoosain, S. & Le Roux, S., 2018. *Standard method for microCT-based additive manufacturing quality control 3: surface roughness*, Stellenbosch.

Durai, L., Dhanasekaran, R. & Ramasamy, P., 1987. Nucleation and Growth Kinetics of Electrocrystallization. *Colloid Interface Sci*.,115(2) pp. 372-77.

Ehsani, A., Yazıcı, E.Y. & Deveci, H., 2016. The Effect of Temperature on the Electrowinning of Copper., *Conference proceedings 18th International Metallurgy & Materials Congress* pp.654–658.

Fabian, C., Ridd, M.J. & Sheehan, M., 2006. Rotating cylinder electrode study of the effect of activated polyacrylamide on surface roughness of electrodeposited copper. *Hydrometallurgy*, 84, pp.256–263.

Fabian, C.P. et al., 2009. Modeling the Charge-Transfer Resistance to Determine the Role of Guar and Activated Polyacrylamide in Copper Electrodeposition. *Journal of elcetrochemical society*, 10, pp.400–407.

Fabian, C.P. (James C.U., 2005b. Copper Electrodeposition in the Presence of Guar or Activated Polyacrylamide.Chapter 1-3. *PhD Thesis*. James Cook University.

Fabian, C.P. (James C.U., 2005c. Copper Electrodeposition in the Presence of Guar or Activated

Stellenbosch University https://scholar.sun.ac.za

Polyacrylamide. Chapter 5-7. *PhD Thesis*. James Cook Unoiversity.

Fabian, C.P. (James C.U., 2005d. Copper Electrodeposition in the Presence of Guar or Activated Polyacrylamide - Chapter 4. *PhD Thesis*. James Cook University.

Fabian, C.P., Ridd, M.J. & Sheehan, M.E., 2007. Assessment of activated polyacrylamide and guar as organic additives in copper electrodeposition. *Hydrometallurgy*, 86(1–2), pp.44–55.

Fischer, H., 1969. Electrocrystallization of Metals under Ideal and Real Conditions. *Angewandte Chemie International Edition*, 8(2) pp. 108.

Gabe, D.R. & Walsh, F.C., 1983. The rotating cylinder electrode: a review of development. *Journal of Applied Electrochemistry*, 13(1), pp.3–21.

Gabrielli, C., Moçotéguy, P., Perrot, H., Nieto-Sanz, D & Zdunek, A., 2006. A model for copper deposition in the damascene process. *Electrochimica Acta*, 51(8–9), pp.1462–1472.

Gebbie, J., 2013. A theoretical study of crystal growth in nanoporous materials using the monte carlo method. *Doctor of Philosophy*. University of Manchester.

Grchev, T., Cvetkovska, M., Stafilov, T. & Schultze, J.W., 1991. Adsorption of polyacrylamide on gold and iron from acidic aqueous solutions. *Electrochimica Acta*, 36(8), pp.1315–1323

He M., 2009, The influence of adsorbed polymer on clay and copper mineral particles' interactions., *Doctoral Dissertation Applied Science.* University of South Australia, Brisbane, 2-3.

Helsten, T. & Moats, M.S., 2013. An investigation of modified polysaccharide and polyacrylamide on plating polarization and surface roughness in copper electrowinning. In *Copper 2013 International Conference*. Santiago, Chile.

Hinatsu, J. & Foulkes, F., 1991. Electrochemical kinetic parameters for the cathodic deposition of copper from dilute aqueous acid sulfate solutions. *Canadian journal of chemical engineering*, 69 pp. 571.

Kelly, J., Tian, C. & West, A., 1999. Leveling and Microstructural Effects of Additives for Copper Electrodeposition. *Journal of The Electrochemical Society*, 146(7), pp.2540–2545.

Kersten, T.P., Pryzybilla, H.J., Lindstaedt, M., Tschirschwitz, F & Misgaiski-Hass, H., 2016. Comparative geometrical investigations of hand-held scanning systems. *International Archives of the Photogrammetry, Remote Sensing and Spatial Information Sciences - ISPRS Archives*, 41, pp.507–514.

Lee, H.-G., 2012. Materials Thermodynamics With Emphasis on Chemical Approach, Postech, Korea: World Scientific.

Lu, F., 2011. Rotating Disk Electrode - a hydrodynamic method. Power Point presentation.

Luyima, A., Moats, M.S., Cui, W., and Heckman, C., 2016, "Examination of copper-electrowinning smoothing agents. Part II: Fundamental electrochemical examination of DXG-F7," *Minerals & Metallurgical Processing*, Vol. 33, No. 1.

Mirza, A., Burr, M., Ellis, T., Evans, D., Kakengela, D., Webb, L., Gagnon, J., Leclercq, F & Johnston, A., 2016. Corrosion of lead anodes in base metals electrowinning. *Journal of the Southern African Institute of Mining and Metallurgy*, 116(6), pp.533–538.

Moats, M.S. & Free, M.L., 2007. A Bright Future for Copper Electrowinning. *Journal of The Minerals, Metals & Materials Society*, 96(8), pp.1562–1564.

Moats, M.S., Luyima, A., and Cui, W., 2016, "Examination of copper electrowinning smoothing agents. Part I: A review," *Mineral & Metallurgical Processing*, Vol. 33, No. 1.

Moats, M.S., Luyima, A., and Oliveira, T., 2014, "Examination of selected copper electrowinning additives," *Proceedings of Hydrometallurgy*, Victoria, BC, Canada, CIM.

Mudgil, D., Barak, S. & Khatkar, B.S., 2014. Guar gum: Processing, properties and food applications - A

Stellenbosch University https://scholar.sun.ac.za

Review. *Journal of Food Science and Technology*, 51(3), pp.409–418.

Najminoori, M., Mohebbi, A., Arabi, BG & Daneshpajouh, S., 2015. CFD simulation of an industrial copper electrowinning cell. *Hydrometallurgy*, 153, pp.88–97.

Newman John, Thomas-Alyea Karen E., 2012. *Electrochemical systems*, John Wiley & Sons (2012).

Ngandu, F., 2016. Investugating the effects of selenium and thiourea concentration on copper. Master of Engineering (Extractive Metallurgical Engineering).

Owais, A., 2007. Effects of material and shape of starting cathodes on electrowinning of copper powder. *JPME.,* 10 (2).pp.12–21.

Pasa, A.A. & Munford, M.L., 2006. Electrodeposition. *Encyclopedia of Chemical Processing*, pp.821–832.

T. Robinson, J. Jenkins, S. Rasmussen, M. King, and W. Davenport, “Copper electrowinning—2003 world tankhouse operating data,” *in Proc. Copper* - Cobre, J. E. Dutrizac and C. G. Clement, Eds., Santiago, Chile, Dec. 2003, vol. V, pp. 421–472.

M. Schlesinger, M. King, K. Sole, W. Davenport., 2011, Extractive Metallurgy of Copper (5), *Elsevier*, Amsterdam.

Shao, W., Pattanaik, G. & Zangari, G., 2007. Influence of Chloride Anions on the Mechanism of Copper Electrodeposition from Acidic Sulfate Electrolytes. *Journal of The Electrochemical Society*, 154(4).

Shukla, A., 2013. Modeling and measuring electrodeposition parameters neat electrode surfaces to faciliatate cell performance optimization. *Masters thesis.* University of Utah.

Stein, B., 1996. A practical guide to understanding, measuring and controlling stress in electroformed metals. *Electroforming Symposium.*

Tshimwanga, N., Maweja, K. & Tshula, K., 2011. Hydrometallurgy Efficacy of polyacrylamide and protein flocculants in preventing anode depassivation induced Pb-contamination of copper electrowinning cathodes. *Hydrometallurgy*, 105(3–4), pp.240–245.

Valette, G., 1982. Hydrophilicity of metal surfaces. Silver gold and copper electrodes. *Journal of Electroanalytical Chemistry and Interfacial Electrochemistry.*, 139, pp.285–301.

Vereecken, J. & Winand, R., 1976. Influence of polyacrylamides on the quality of copper deposits from acidic copper sulfate solutions. *Surface Technology*, 4(3), pp.227–235.

Vereecken, P.M. Binstead, RA., Deligianni & H., Andricacos., PC., 2005. The chemistry of additives in damascene copper plating. *IBM Journal of Research and Development*, 49(1), pp.3–18.

Vidal, C.A.G., 2013. *Molecular weight effects in guar gum adsorption and depression of talc*. Masters thesis. University of British Columbia.

Wang, J., Somasundaran, P. & Nagaraj, D.R., 2005. Adsorption mechanism of guar gum at solid-liquid interfaces. *Minerals Engineering*, 18(1), pp.77–81.

Winand, R., 1992. Electrocrystallization - theory and applications. *Hydrometallurgy*, 29(1–3), pp.567–598.

Winand, R., 1994. Electrodeposition of metals and alloys-new results and perspectives. *Electrochimica Acta*, 39(8–9), pp.1091–1105.

Stellenbosch University https://scholar.sun.ac.za

8 APPENDICES

8.1 Appendix A – Derivations and supporting equations

8.1.1 Mass transfer

The transient mass balance is given by Equation 8.1.

$$\frac{\partial c_i}{\partial t} = -\nabla \cdot N_i + R_i \tag{8.1}$$

Where

$\frac{\partial c_i}{\partial t}$	Accumulation rate
$\nabla \cdot N_i$	Input differential volume
R_i	Production of species *i* in mol/cm^3·s

The differential volume element is the rate at which the concentration changes. When considering electrochemical systems, the value of R_i can often be assumed to be zero. This assumption arises from the fact that the reaction in the system is usually restricted to the electrode surface. Furthermore, the system can be considered as electrically neutral except for a thin electrical double layer present at all surface interfaces in the system. It is therefore reasonable to accept Equation 8.2 as true for the described system.

$$\sum_i z_i c_i = 0 \tag{8.2}$$

Equation 2.5 can be inserted into Equation 8.1 to formulate Equation 8.3, which can be used to determine the concentration distribution in a system if velocity and potential differences are known.

$$\frac{\partial c_i}{\partial t} = -\nabla \cdot [-D_i \nabla c_i - z_i u_i \mathrm{F} c_i \nabla \Phi + c_i v_i] + R_i \tag{8.3}$$

8.1.2 Nucleation and growth in electrocrystallization

According to Durai et al. (1987) a 2-D nucleus (center of crystallization) must first come into existence before a new layer of depositing material can continue to grow. The size of the critical 2-D nucleus can be calculated by using Equation 8.4.

$$n_{crit} = \left(\frac{A\sigma}{2z\eta e}\right)^2 \tag{8.4}$$

The critical Gibbs free energy required to form a nucleus with a size consisting of n_{crit} atoms can then be calculated with Equation 8.5.

$$\Delta G_{crit} = \frac{A^2\sigma^2}{4z\eta e} \tag{8.5}$$

8.1.3 Electrode potential

The electrode potential determines the energy of the electron transfer and hence the current in the electrochemical circuit. Electrode potential and current are therefore dependent variables of one another

Stellenbosch University https://scholar.sun.ac.za

and their relationship with the Gibbs Free energy need to be defined. Electrical work is a product of the charge (q) in coulombs/mole and the voltage (V). See Equation 8.6.

$$w_{elec} = -qV \tag{8.6}$$

The negative sign indicates that work is done to the surroundings. From Faraday's law (equation 2.11) it is known that the electrical charge is equal to the number of Coulombs (per equivalent Faraday) and the valency n. If the system is assumed to be reversible then w_{elec} is equal to $w_{elec\ max}$. By substituting Equation 2.11 into Equation 8.6, Equation 8.7 is established.

$$w_{elec\,max} = -nFE \tag{8.7}$$

When a system undergoes a reversible process at constant T and P, ΔG is equal to $w_{elec\ max}$ (Lee 2012). Subsequently Equation 8.7 can be manipulated into Equation 8.8.

$$G = -nFE \tag{8.8}$$

Finally, by inserting Equation 8.8 into Equation 2.20 the Nernst Equation 2.21 is given for an electrode or half-cell.

8.2 Appendix B – Stepwise methodology

Additive preparation methodology:

Guar:

1. Fill a glass beaker with 100-mL of de-ionized water.
2. Place glass beaker containing water on heater stirrer at 40 °C and wait for water to reach this temperature.
3. Measure and confirm temperature with thermometer.
4. Weigh 200 mg of guar and add to glass beaker containing de-ionized water at 40 °C. (Concentration in the beaker is 2mg/mL)
5. Allow for guar to unfold in solution on heater/stirrer for 2 hours.

Polyacrylamide:

1. Fill a glass beaker with 100-mL of de-ionized water.
2. Place glass beaker containing water on heater stirrer at 40 °C and wait for water to reach this temperature.
3. Measure and confirm temperature with thermometer.
4. Weigh 200 mg of polyacrylamide and add to glass beaker containing de-ionized water at 40 °C. (Concentration in the beaker is 2mg/mL)
5. Allow for the polyacrylamide to unfold in the solution on heater/stirrer for 2 hours.

Polysaccharide:

1. Fill a glass beaker with 100-mL of de-ionized water.
2. Place glass beaker containing water on heater stirrer at 40 °C and wait for water to reach this temperature.
3. Measure and confirm temperature with thermometer.

Stellenbosch University https://scholar.sun.ac.za

4. Weigh 200 mg of polysaccharide and add to glass beaker containing de-ionized water at 40 °C. (Concentration in the beaker is 2mg/mL)
5. Allow for the polysaccharide to unfold in the solution on heater/stirrer for 2 hours.

Electrolyte preparation methodology:

Preparation of 4 L solution:

1. Clean 5L sealable glass container.
2. Add 2L of deionized water to the container.
3. Add 348 mL of sulfuric acid to the container.
4. Weigh 550.1 g of copper sulfate pentahydrate and add to the sulfuric acid/water mixture.
5. Add 0.067 ml of HCl with pipette
6. Fill container up with de-ionized water to 4 L mark.
7. Stir the synthetic electrolyte solution until the copper sulfate pentahydrate crystals are completely dissolved.

Preparation of 1 L solution:

1. Clean 5L sealable glass container.
2. Add 250 ml of deionized water to the container.
3. Add 88.73 mL of sulfuric acid to the container.
4. Weigh 137.52 g of copper sulfate pentahydrate and add to the sulfuric acid/water mixture.
5. Add 0.017 ml of HCl with pipette
6. Fill container up with de-ionized water to 1 L mark.
7. Stir the synthetic electrolyte solution until the copper sulfate pentahydrate crystals are completely dissolved.

Electrochemical pre-experimental methodology:

1. Rinse the reactor vessel with de-ionized water and leave to drip dry for 2 minutes.
2. Initiate heated water circulation by switching on the water bath motor.
3. Set the required experimental temperature on the heater-circulation motor.
4. Measure out 150 mL electrolyte stock solution and add to the reactor vessel.
5. Wait until the electrolyte inside the reactor vessel has reached the set point temperature.
6. Take 0.15 mL sample from organic additive prepared solution with pipette.
7. Add the 0.15 mL content in pipette to the 150mL electrolyte at the set temperature.
8. Initiate rotation of the electrode at 500 rpm to ensure complete even mixing and spread of organic additive throughout the electrolyte sample.
9. Allow for 30 minutes of electrode rotation before initiation of the experiment.
10. While the electrode is rotating, allowing for the additive to unfold, the experimental conditions are set on the GAMRY software.
11. Initiate the experimental run on GAMRY software.

Cathode cleaning methodology:

1. Unscrew cathode from RDE setup.
2. Rinse cathode surface with de-ionized water
3. Polish cathode surface with fine grit (800-1200) sandpaper to remove most of the copper.
4. Rinse with de-ionized water.

Stellenbosch University https://scholar.sun.ac.za

5. Polish cathode surface with supplied cathode cleaning polishing surface and a 3-micron diamond suspension for 5 minutes.
6. Ensure that the cathode surface is visually bright and clean.
7. Rinse surface in Acetone
8. Rinse in de-ionized water.
9. Leave to air dry.

Bench scale electrowinning pre-experimental methodology:

1. Set warm bath to a setpoint temperature of 50 °C.
2. Prepare 15 L electrolyte solution.
3. Polish cathode surface with fine sand paper and sequential rinsing with acetone, distilled water, and electrolytic solution.
4. Weigh the blank cathode.
5. Insert cleaned cathode in the middle of the electrowinning cell.
6. Insert 2 anode plates, one on each side of the cathode plate, 25 mm away from the cathode.
7. Pour 10L of electrolyte solution into stock solution container.
8. Switch on pump and allow electrolyte circulation though the electrowinning cell until steady state is achieved at 40°C.
9. Add the desired amount of dissolved organic additive to the 10L stock solution.
10. Add the remaining 5 L of electrolyte to the stock container and allow at least 15 minutes for system to reach steady state at 40°C.
11. Switch on Power Supply and set the current at 9.4 A, translating to 300 A/m^2.
12. Allow electrowinning to take place for a total duration of 24 hours.
13. Switch off Power Supply and remove cathode from electrolyte.
14. Hang cathode to air dry.
15. Weigh cathode plate and store for further analysis.

8.3 Appendix C – Sample calculations

8.3.1 Concentration calculations

8.3.1.1 Electrolyte

The calculations of the amount of chemicals needed in the electrolyte is based on a synthetic electrolyte concentration of 160g/L sulfuric acid, 35 g/L copper and 25 mg/L chloride. De-ionized water was used to make up the rest of the 1L volume in the electrolyte sample. The densities at 25 °C, and molecular weights of the relevant chemicals was sourced from open literature and are presented in Table 8.1.

Stellenbosch University https://scholar.sun.ac.za

Table 8.1: Presentation of relevant chemicals densities at 25 °C, and their respective molecular weights.

Element/Molecule	MW	Unit
Cu	63.546	g/mol
$CuSO_4.5H_2O$	249.685	g/mol
H_2SO_4	98.079	g/mol
H_2O	18.01528	g/mol
HCl	36.46094	g/mol
	Density	
Cu	8960	kg/m^3
$CuSO_4.5H_2O$	2286	kg/m^3
H_2SO_4	1840	kg/m^3
H_2O	1000	kg/m^3
HCl	1490	kg/m^3

To have a final concentration of 35 g/L of copper in a 1-liter solution, 35 grams of copper need to be present. It was calculated that a total of 137.52 of copper sulfate pentahydrate is required to add 35 g of copper to the solution.

$$n_{Cu} = \frac{m_{Cu}}{M_{Cu}}$$

$$n_{Cu} = \frac{35}{63.546}$$

$$n_{Cu} = 0.55078\ moles$$

$$Because\ of\ stoichiometric\ proportions\ in\ \mathrm{CuSO_4.5}H_2\mathrm{O}\ \therefore$$

$$1\ \mathrm{mole\ Cu} = 1\ \mathrm{mole}\ SO_4 = 5\ \mathrm{moles}H_2\mathrm{O}\ in\ 1\ mole\ of\ \mathrm{Cu}SO_4.5H_2\mathrm{O}$$

$$0.55078\ \mathrm{mole\ Cu} = 0.55078\ \mathrm{mole}\ SO_4 = 2.7539\ \mathrm{moles}H_2\mathrm{O}\ in\ 0.55078\ mole\ of\ \mathrm{Cu}SO_4.5H_2\mathrm{O}$$

Translated to mass:

$$35\ \mathrm{g\ Cu} + 52.91\ \mathrm{g}\ SO_4 + 49.61\ \mathrm{g}\ H_2\mathrm{O} = 137.52\ g\ of\ \mathrm{Cu}SO_4.5H_2\mathrm{O}\ \mathrm{required}$$

For sulfuric acid requirements in a I L electrolyte solution:

$$Volume\ H_2SO_4\ required = \frac{Mass}{Density}$$

$$Volume\ H_2SO_4\ required = \frac{160g}{1840\ kg/m^3}$$

$$Volume\ H_2SO_4\ required = \frac{0.160\ kg}{1840\ kg/m^3}$$

$$Volume\ H_2SO_4\ required = 0.08696\ L$$

Stellenbosch University https://scholar.sun.ac.za

The chloride requirement was calculated similarly.

8.3.1.2 Organic additive

The sample calculations of the organic additive concentration added to the electrolyte is based on a 2 mg/L final concentration.

Organic additive is prepared with de-ionized water at 2g/L. A total of 0.2 g organic additive is weighed and then added to 100 ml of de-ionized water:

$$Organic\ additve\ concetration\ in\ preparation\ stage = \frac{0.2\ grams\ organic\ additive}{0.1\ L\ de-ionized\ water}$$

$$Organic\ additve\ concetration\ in\ preparation\ stage = 2\ \frac{g}{L}$$

After preparation, the organic additive solution is added to the electrolyte to form a final concentration of 2 mg/L. A total of 0.15 mL of organic additive preparation solution is extracted with a pipette. This sample contains 0.3 mg of organic additive assuming a perfect distribution of organic additive in the preparation solution:

$$Amount\ of\ organic\ additive\ in\ 0.15\ pipette\ sample = \frac{\frac{0.2\ g}{100\ ml}}{0.15\ ml}$$

$$Amount\ of\ organic\ additive\ in\ 0.15\ pipette\ sample = 0.3\ mg$$

The concentration of organic additive in the electrolyte sample therefore translates to:

$$Organic\ additve\ concetration\ in\ electrolyte = \frac{0.0003\ grams\ organic\ additive}{0.150\ L\ electrolye}$$

$$Organic\ additve\ concetration\ in\ electrolyte = 2\ mg/L$$

The volume addition to the electrolyte due to the water present in the pipette sample is so insignificant compared to the total volume inside the vessel reactor of 150 mL, that it is assumed to be negligible.

8.3.2 Current efficiency calculations

The Base Case electrowinning plate is used in the sample calculation to calculate the CE of the specific Base Case electrowinning run.

$$Total\ actual\ copper\ mass\ plated = 265.37$$

According to Faraday's Law:

$$Q = n.F.M$$

$$Q = n.F.\frac{m_{theoretical}}{M}$$

$$I \times t = n.F.\frac{m_{theoretical}}{M}$$

$$9.4 \times (24 \times 3600) = 2 \times 96487 \times \frac{m_{theoretical}}{63.546}$$

$$Theoretical\ copper\ mass\ plated = 267.44\ g$$

Current Efficiency:

Stellenbosch University https://scholar.sun.ac.za

$$\varepsilon = \frac{\frac{dM_{Cu}}{dt}}{I \cdot \frac{t}{nF}} = \frac{Q_r}{Q_{total}}$$

$$\varepsilon = \frac{n.F.M_{actual}}{n.F.M_{theoretical}}$$

$$\varepsilon = \frac{265.37\ g}{267.44\ g}$$

$$\varepsilon = 99.22\%$$

Stellenbosch University https://scholar.sun.ac.za

8.4 Appendix D -Bench scale electrowinning supportive results

8.4.1 Qualitative

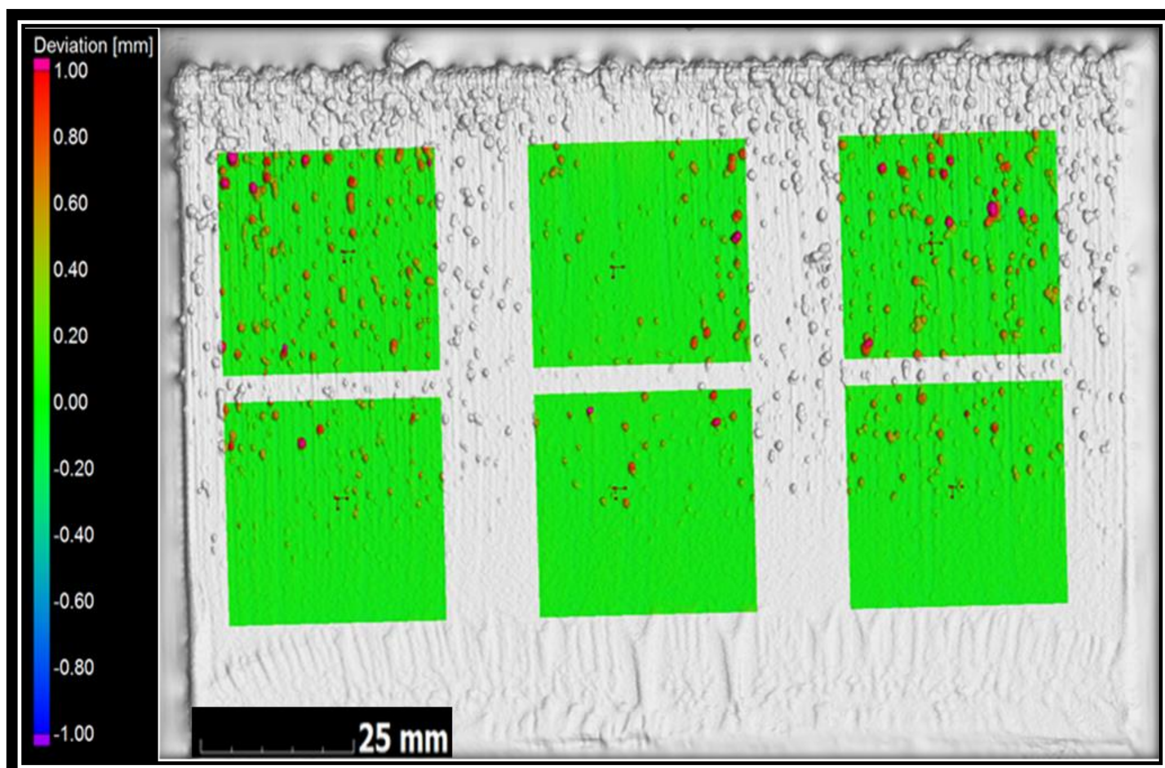

Figure 8.1: Cathode surface topography delivered in an electrolyte containing no additive with a surface height colour scale indicating ± 1 mm deviation on the six selected regions of interest.

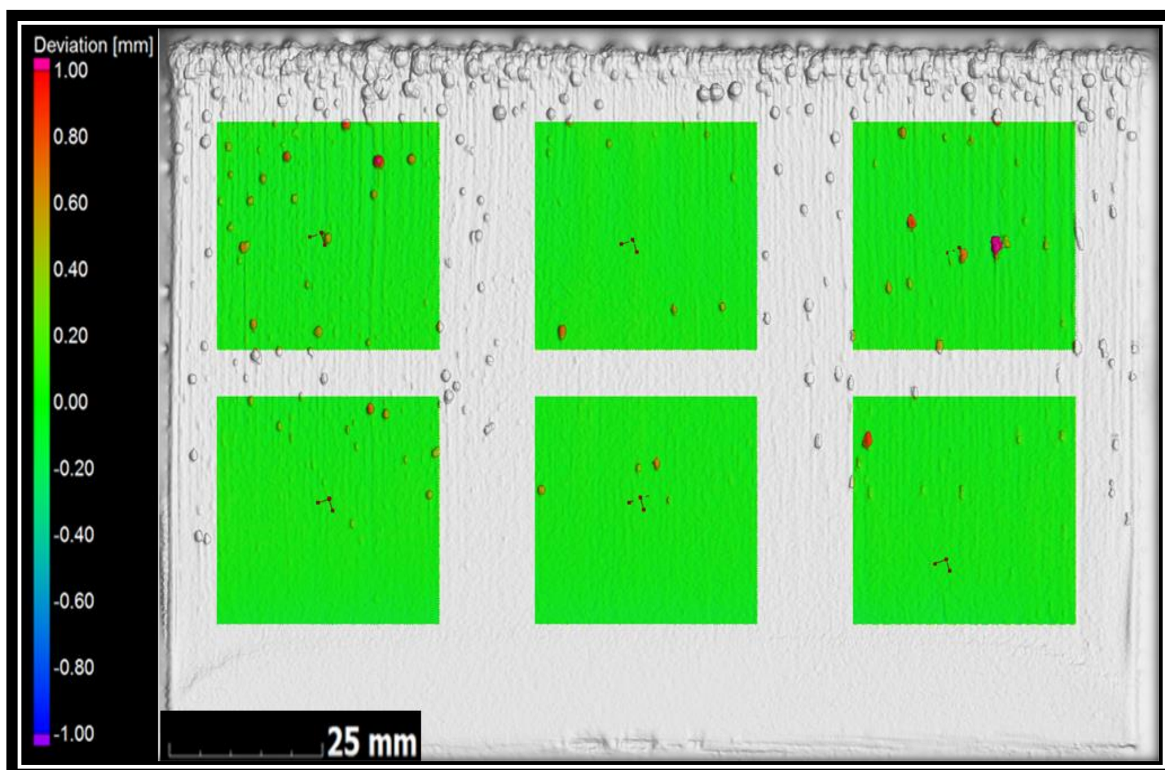

Figure 8.2: Cathode surface topography delivered in an electrolyte containing 2mg/L Guar additive with a surface height colour scale indicating ± 1 mm deviation on the six selected regions of interest.

Stellenbosch University https://scholar.sun.ac.za

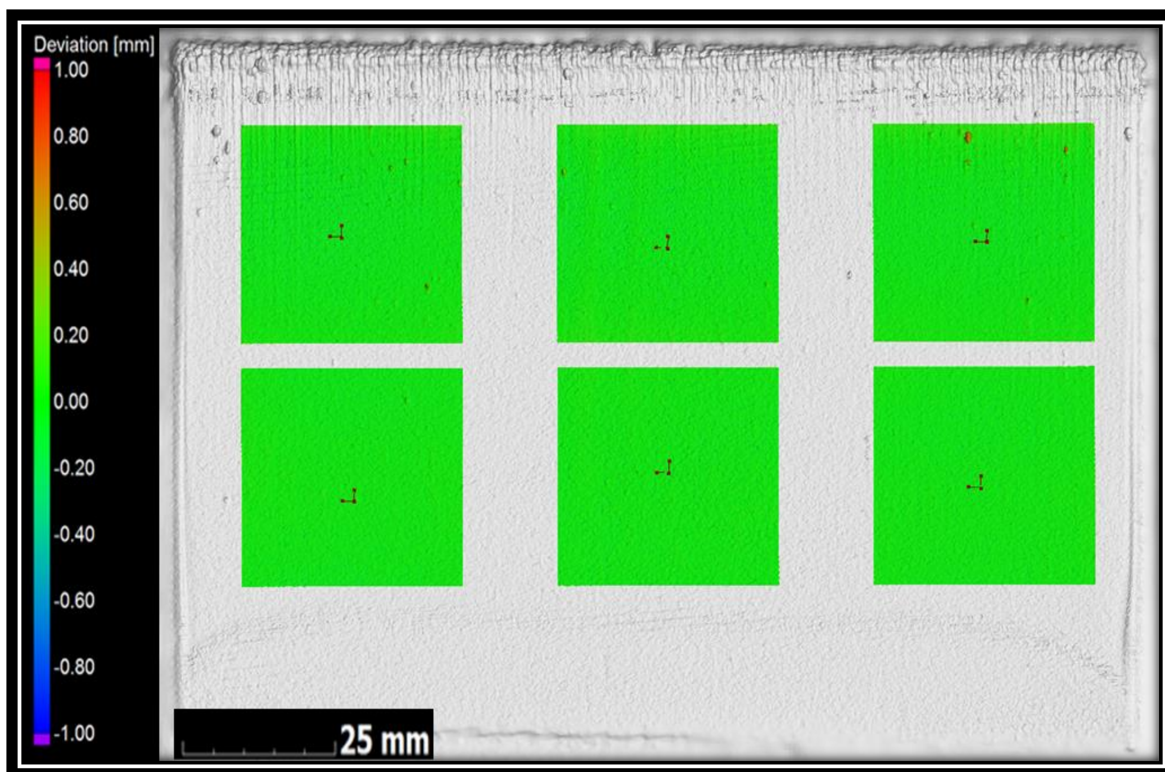

Figure 8.3: Cathode surface topography delivered in an electrolyte containing 2mg/L Low MW PAM additive with a surface height colour scale indicating ± 1 mm deviation on the six selected regions of interest.

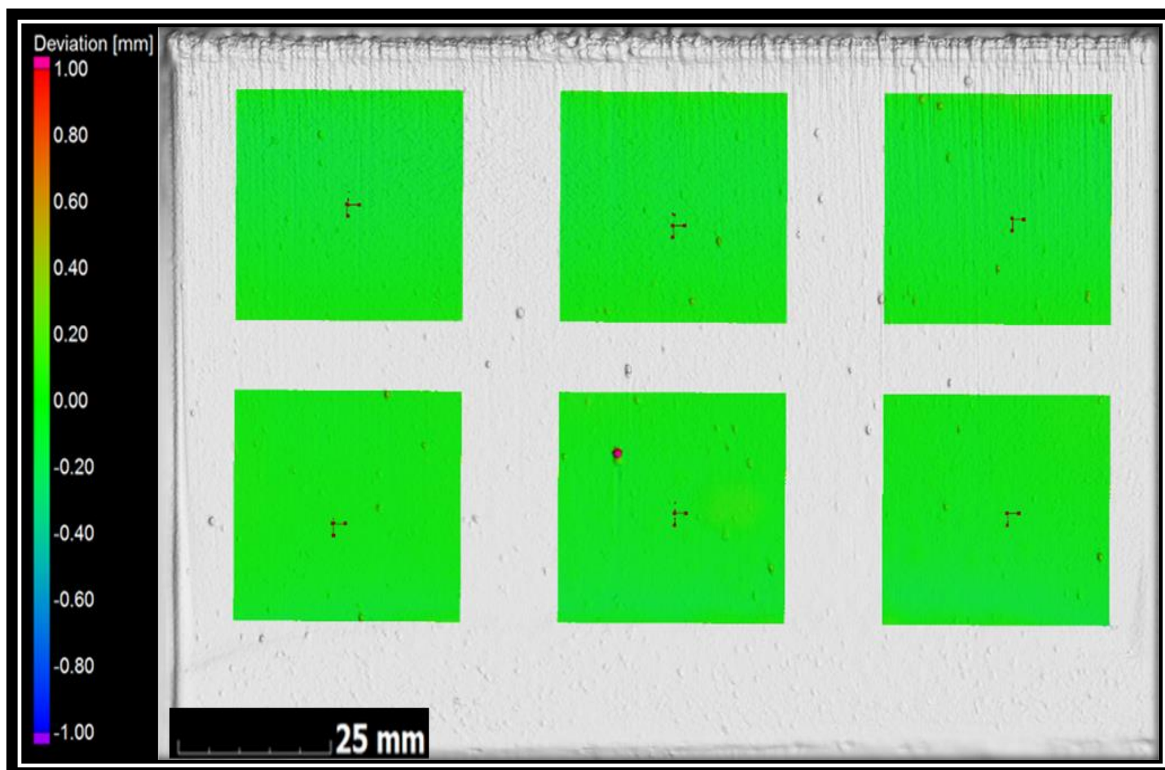

Figure 8.4: Cathode surface topography delivered in an electrolyte containing 2mg/L Medium MW PAM additive with a surface height colour scale indicating ± 1 mm deviation on the six selected regions of interest.

Stellenbosch University https://scholar.sun.ac.za

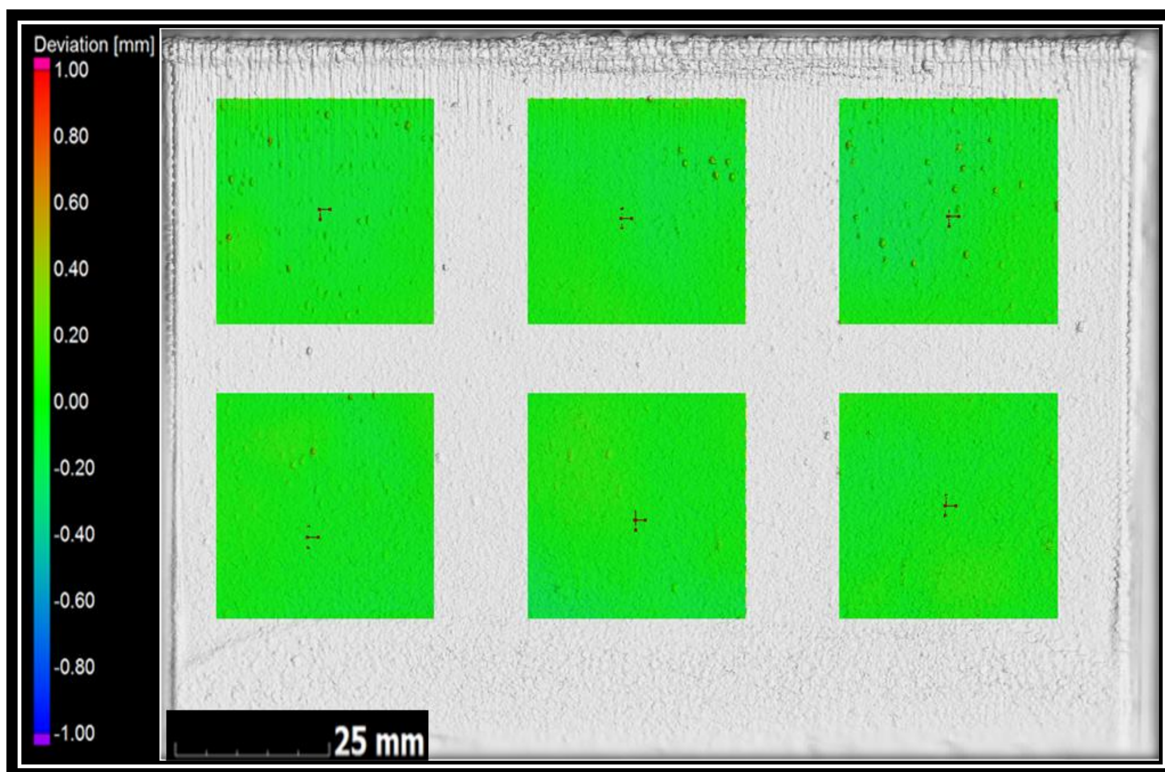

Figure 8.5: Cathode surface topography delivered in an electrolyte containing 2mg/L High MW PAM additive with a surface height colour scale indicating ± 1 mm deviation on the six selected regions of interest.

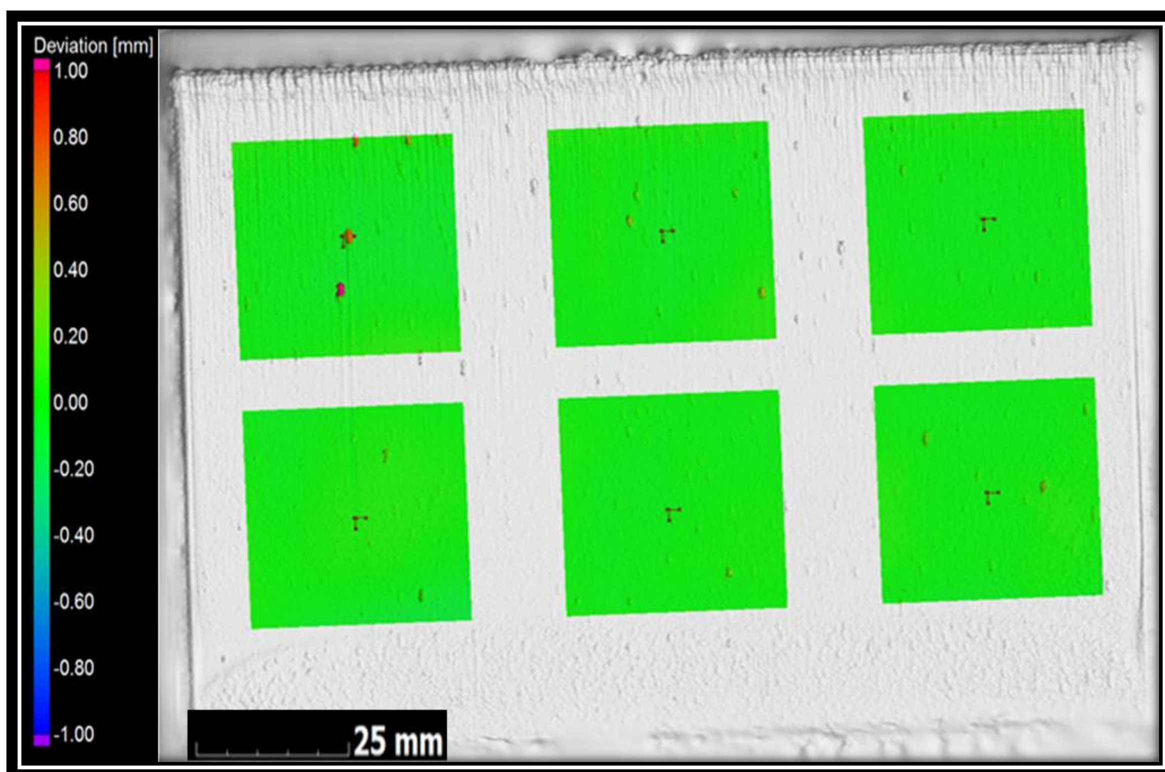

Figure 8.6: Cathode surface topography delivered in an electrolyte containing 2mg/L Very High MW PAM additive with a surface height colour scale indicating ± 1 mm deviation on the six selected regions of interest.

8.4.2 Quantitative

Considering only positive deviation from the normalized flattest part of the surface Figure 5.11 translates into Figure 8.7.

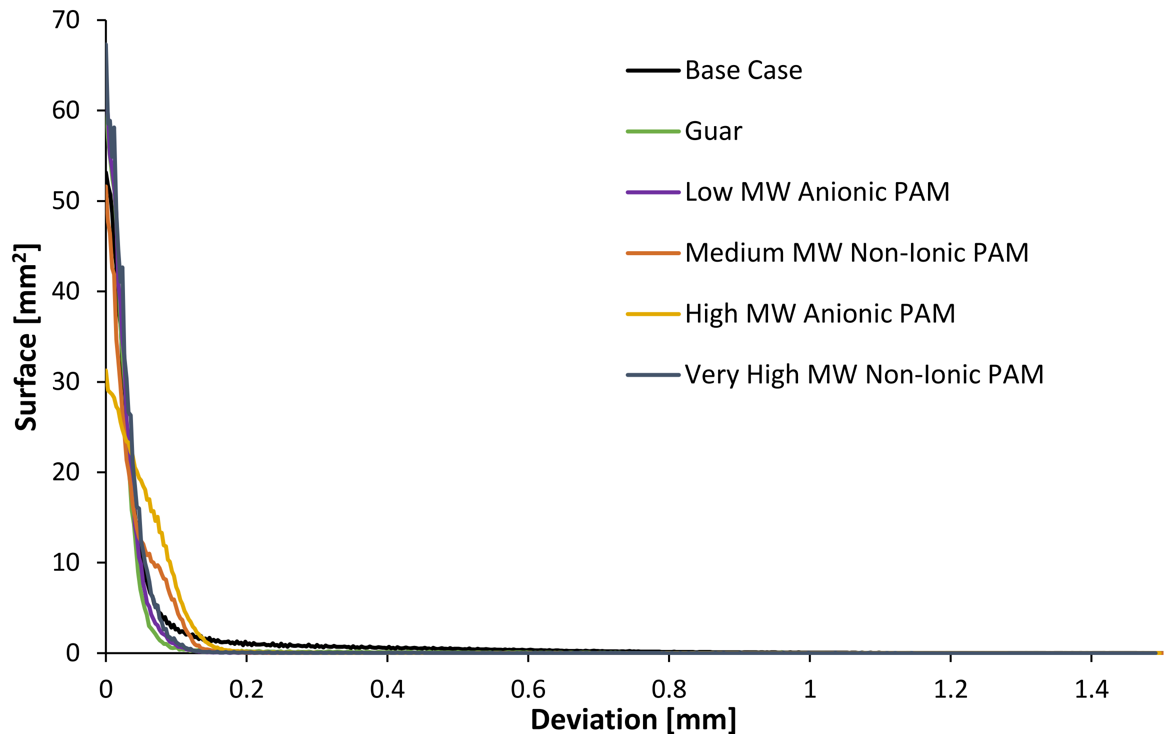

Figure 8.7: Average total surface elements (area) deviation from the flattest surface area (normalized) for each plate achieved in the presence of its unique.

It is however very difficult on this magnification in Figure 8.7 to visually see variance in the spread of surface elements (area) with increasing positive deviation from the flattest surface of each deposit. Since spread of area further down the x-axis (localized growth) is much more dangerous and important to visualize, a zoomed in Figure 8.8 was developed to see the x-axis area deviations more clearly. In Figure 8.8 it can clearly be seen that the Base Case scenario has the highest total surface area present at greater positive deviation values, followed in second place by the copper plate developed in the presence of Guar. This is comparable with the conclusions made in the qualitative analysis presented in Section 5.3.1 of this report. It is however still difficult to visually evaluate the rest of the plates. For this reason, the S_a values, which encapsulates all these data in one numerical value, were calculated and plotted compared to each other in Figure 5.13.

Stellenbosch University https://scholar.sun.ac.za

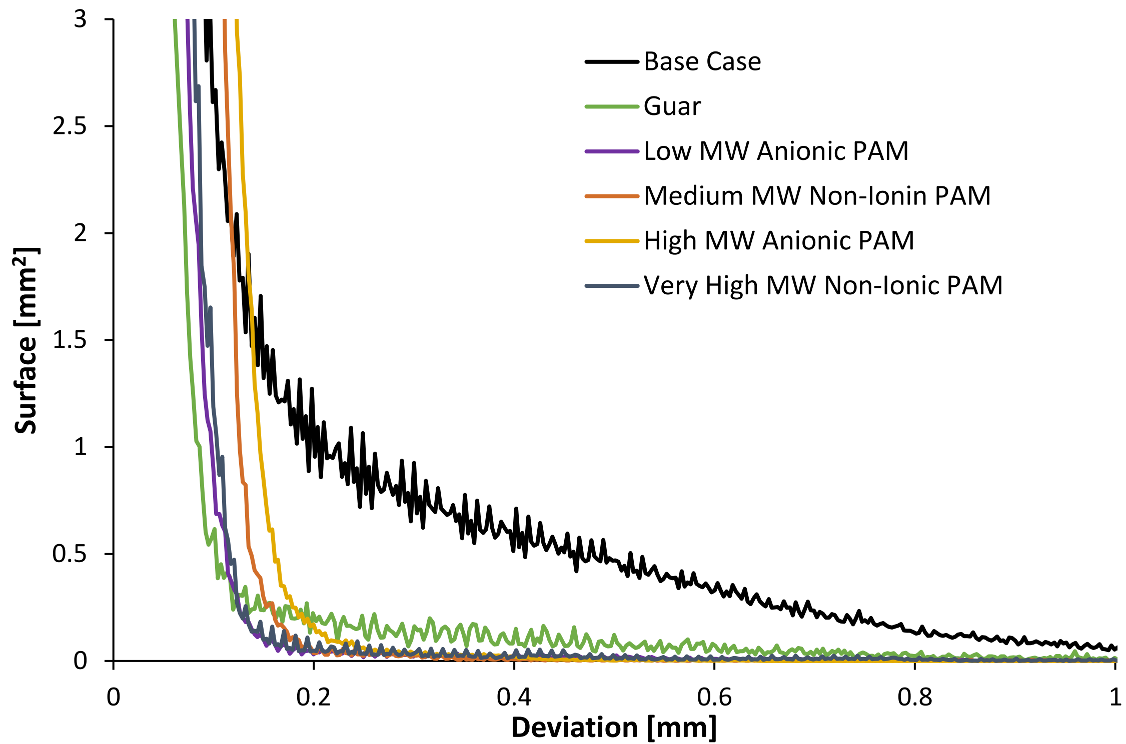

Figure 8.8: Average total surface area deviation from the flattest surface area (best fit plane) for each plate achieved in the presence of its unique additive by taking only the average positive deviation values of the 6 regions of interest for each plate into account – with focused view of total area of high positive deviation from flat surface.